Theoretical Studies of Chemical Reactivity: Some Approaches and Applications(Dissertation_全文)

AUTHOR(S):

Sakata, Ken

Theoretical Studies of Chemical Reactivity: Some Approaches and Applications

Ken Sakata

Department of Molecular Engineering,
Kyoto University

2000

Contents

General Introduction 1

Chapter 1. Transient Bonds and Chemical Reactivity of Molecules 5

Chapter 2. Population Analysis along the Intrinsic Reaction Coordinate: Application to 1,3-Dipole Cycloaddition 21

Chapter 3. Quantum Chemical Study on Low Energy Reaction Path for $SiH_4 + O(^1D) \rightarrow SiO + 2H_2$ 53

Chapter 4. Quantum Chemical Study of the Oxidation Sites in Hydrogen- and Water- Terminated Si Dimers: Attempt to Understand the Si–Si Back-Bond Oxidation on the Si Surface 69

Chapter 5. Quantum Chemical Study on the Oxidation of Hydrogen-Terminated Silicon Surface by Oxygen Anions 91

Chapter 6. Quantum Chemical Study on Aluminum Selective CVD Reaction Mechanism 121

Chapter 7. Quantum Chemical Study on p-Doping Effect of F-Terminated Silicon Surface Reaction with Silane 137

Chapter 8. Quantum Chemical Study on the Reaction between GeF_4 and Si_2H_6 153

General Conclusion 171

Acknowledgment 175

List of Publications 176

General Introduction

The birth of quantum mechanics in physics at the beginning of the 20th century makes it possible to understand how the electrons and atomic nuclei form the chemical bonds that bind the atomic nuclei in molecules and solids. At the same time, the new field called quantum chemistry which meant applications of quantum mechanics to chemical problems was born. Although the application was mainly of qualitative nature in early days, it has been developed rapidly since the 1960s with the appearance of powerful computers. Now quantum chemistry is indispensable to studies in various fields of chemistry.

The methods to describe the electronic structure of atoms and molecules are classified into two different theories: the molecular orbital (MO) theory and the density functional theory (DFT). The MO theory that is based on the one-electron approximation has been a conventional idea for both the calculational method and the theories of reactivities of molecules. The Hartree-Fock approximation established by Roothaan and Hall, for instance, is known to be used widely as the first step in many electronic structure calculations, and the theory of orbital-symmetry conservation by Woodward and Hoffmann and the frontier orbital theory by Fukui are based on the Hückel MO theory. Moreover, there are excellent methods, such as the configuration interaction, the cluster expansion, and the perturbation theory, that estimate the electron correlation energy beyond the Hartree-Fock approximation. The growth of the MO theory has led to prosperity of quantum chemistry.

On the other hand, the DFT in which an electronic system is described by the electron density $\rho(\mathbf{r})$ instead of the wave function $\Psi(\mathbf{r})$ has also been developed recently. Although the original idea of this theory was initiated by Thomas and Fermi in 1920s, this theory was established by Hohenberg and Kohn in 1964. Hohenberg and Kohn proved that an external potential $v(\mathbf{r})$ is a unique functional of $\rho(\mathbf{r})$. That is, they showed that the ground state of many-particle system is a unique functional of $\rho(\mathbf{r})$. They also showed that the energy functional $E[\rho(\mathbf{r})]$ equals the ground-state energy E for the correct $\rho(\mathbf{r})$.

Furthermore, in 1965, Kohn and Sham introduced the idea of non-interactive reference system in which the electron density is resolved into N orbital components. This enables us to regard the many-particle problem as the one-particle problem. Although there remains a problem that the form of the exact functional is unknown, this Kohn-Sham formalism has been used widely for the electronic structure calculations of the solid-state systems, and also for the molecular systems recently.

Although the DFT is noted as a very useful method for calculations of large molecular systems, it has another possibility of describing the chemical reactivity. In the DFT, the important concept like the chemical potential μ, that is the derivative of the energy E with respect to the electron number N, is introduced. The chemical potential μ is connected with the electronegativity χ by inverting its sign. Moreover, Parr and his co-workers defined the absolute hardness and the Fukui function of the system. These terms are easy to understand intuitively for chemists, therefore the DFT may provide an intuitive picture to help understanding of chemical reactions.

The main theme of this thesis is to study the chemical reactivity of molecules along the reaction coordinate and the surface reactions in manufacturing the silicon semiconductor device by using the MO theory and the DFT. It is composed of eight chapters. In the first two chapters, the author studied the chemical reactivity of molecules along the reaction path. The next six chapters present the applications of quantum chemistry to the silicon chemistry.

In Chapter 1, the orbitals participating in electron delocalization have been investigated by taking the aromatic substitution reaction as an example. The interacting orbitals have been localized around the reaction sites. It was observed that the chemical bonds were generated and broken transiently along the reaction path. Next, the reactive orbitals that were very similar to the interacting orbital were obtained by projecting the reference orbital function to specify the bond being formed onto the MO spaces of the reactant molecules. The local potential of the reaction site for electron donation estimated for substituted benzene molecules by using these projected orbitals has been compared

with the experimental scale of electron-donating and electron-withdrawing strength of substituent groups.

In Chapter 2, the population analysis along the intrinsic reaction coordinate (IRC) has been performed in order to reveal the variation of the electronic structure along the reaction coordinate. The derivatives of the gross atomic charge by Mulliken, the bond orders and the atom valence by Mayer with respect to the nuclear motion along the IRC have been calculated analytically. This method has been applied to the 1,3–dipole cycloaddition reaction between fulminic acid and acetylene.

In Chapter 3, the gas phase reaction between singlet oxygen (^{1}D) and silane has been studied. A low energy reaction path has been found in addition to the excited-state reaction path.

In Chapter 4, a cluster model reaction of the oxidation sites in hydrogen- and water-terminated Si dimers has been investigated by means of *ab initio* molecular orbital calculations in order to obtain a chemical insight into the bond in the Si surface network which the oxidant prefers to attack.

In Chapter 5, the oxidation mechanism of hydrogen-terminated Si(111) surface by oxygen anions has been studied using the *ab initio* molecular orbital method. The author studied a silicon cluster model, which was a local model of the hydrogen-terminated Si(111) surface. The author clarified that oxygen anions were stable in a cage of silicon cluster. To ensure the result of the cluster model the author has also studied an extended model with the periodic boundary condition. The author has proposed that an oxygen anion attacks Si atoms to form a penta-coordinated complex and inserts into a Si–Si bond to form a local Si–O–Si structure.

In Chapter 6, the reaction mechanism of the aluminum deposition over the hydrogen-terminated Si surface by dimethyl aluminum hydride has been discussed. This study provides a new insight into the aluminum selective chemical vapor deposition (CVD) on the silicon surface which has received much attention as a promising technology of ULSI metallization.

In Chapter 7, the deposition of SiH_4 on the fluorine-terminated Si surface and the p-doping effect have been studied. The author clarified that in the case of p-doped system the fluorine atom immersed in the bulk inserted into a pair of Si atoms to form chemical bonds.

In Chapter 8, the gas-phase reaction mechanism of the low-temperature thermal chemical vapor deposition between GeF_4 and Si_2H_6 has been studied.

Chapter 1:

Transient Bonds and Chemical Reactivity of Molecules

1. Introduction

Reactions are essentially a series of formations and breakings of bonds between atoms. The development of the precise picture of atoms and chemical bonds has affected, therefore, the outlook of chemists.[1] The mechanisms of reactions that they propose must be in harmony with the theoretical concept of bonds. The formation of new bonds between the reagent and the reactant is brought about by mutual electron delocalization.[2] In this interaction, the highest occupied (HO) MO and the lowest unoccupied (LU) MO play usually the dominant roles.[3-5] The energy levels of the HOMO and the LUMO have been connected with some important quantities of molecules, e.g., the "electronegativity" by Mulliken[6], the "absolute hardness" and "chemical potential" by Parr *et al.*[7-9] The concept of "hard and soft acids and bases" (HSAB) proposed by Pearson is related also to the frontier orbital energy levels.[10-14] These are all molecular quantities, representing the chemical and physical properties that apply to the whole system, a molecule, an ion, or a radical. However, the reactivity of molecules should be related essentially to the power of an atom or a functional group in a molecule to attract or release electrons. Thus, in the frontier orbital approach, the amplitude on an atom and the nodal property between atoms in the HOMO and the LUMO are of crucial importance.[3-5] As the systems that we study become more and more complicated, we need a way of connecting the abilities of a molecule for electron donation and acceptance in reactions to some local quantities. In evaluating those, it is important to take the effects of the molecular periphery appropriately into account. We report here that analysis of the bonds that are being formed and broken with the progress of chemical reactions leads to a reactive scale that will be applicable to large molecular species.

2. Results and Discussion

2.1. Transient Bonds in Chemical Reactions

Electron delocalization between two molecular species is represented by a combination of the occupied MOs of one part and the unoccupied MOs of the other

part.[3-5] Though the HOMO of the electron-donor part and the LUMO of the electron-acceptor part play the dominant roles, the MOs relevant for the orbital interactions tend to increase in number, as the interacting species becomes larger in size. To evaluate the participation of other MOs in chemical interactions, it may be helpful to utilize a concept of hybridized MOs. The situation is similar to molecules in which chemical bonds are represented compactly in terms of hybrid atomic orbitals.[1] The hybridized MO should have a large amplitude in a particular region of the reactant molecule to specify the active site and should have an appropriate nodal property to indicate the bonds that are broken or strengthen in the course of the reaction.

First, we want to see the orbitals that participate in electron delocalization. Then, we carry out simultaneous transformations of the occupied MOs ϕ_i (i = 1, 2, ..., m) of the donor part and the unoccupied MOs ψ_{n+l} (l = 1, 2, ..., N-n) of the acceptor part within each of the two fragment species so as to represent the intermolecular elements of the bond-order matrix for the composite reacting system in terms of the pairs of *hybridized fragment MOs*, (ϕ'_f, ψ'_f), f being the smaller of m and N-n .[15,16] The simplest example to apply the method, with abundant experimental data, may be electrophilic substitution of aromatic molecules.[17] Figure 1 sketches the benzene molecule interacting with an attacking NO_2^+ to cause an electrophilic aromatic substitution. The transition-state structure for the system in the presence of a methyl alcohol molecule has been determined.[18] The calculated C1–N distance was reported to be 2.48 Å.[18] This C–N length may be too long to form a covalent bond. To make simpler our arguments here, we have fixed the C1–N bond at 2.5 Å and at 2.0 Å and determined the other geometrical variables disregarding the solvent molecule. The MOs of the interacting system and of the two fragment species were calculated by applying the Gaussian 92 program with the simplest STO-6G minimal basis set.[19] The pair of orbitals that plays the principal role in electron delocalization from the benzene part to the NO_2^+ part is presented in Figure 1.

At the stage shown by $R_{C1\text{-}N}$ = 2.5 Å, the orbital of the benzene part looks similar to its HOMO, but the orbital was amplified on C1, C2, and C6 and was attenuated on C3 and C5. This distortion of the orbital becomes clearer at $R_{C1\text{-}N}$ = 2.0 Å. The interaction

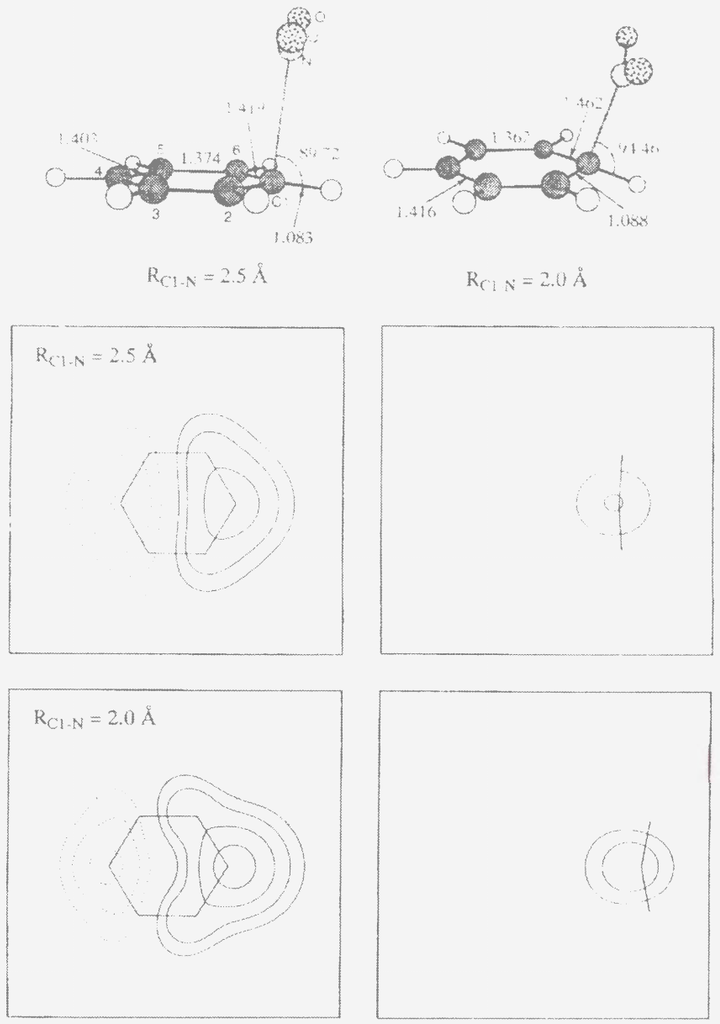

Figure 1. A sketch of the reaction model for nitration of benzene and the pair of orbitals taking part in electron delocalization from the benzene part to the NO_2^+ part. The orbital of benzene is shown on the left and that of NO_2^+ on the right. The orbitals are illustrated arbitrarily in the plane parallel to and 2.0 Å above (for $R_{C1\text{-}N}$ = 2.5 Å) and 1.0 Å above (for $R_{C1\text{-}N}$ = 2.0 Å) the plane defined by C2, C3, C5, and C6.

is three-centered in the benzene part, the carbons C2 and C6 adjacent to the reaction site C1 taking part in the electron delocalization to NO_2^+. The HOMO is the dominant component of the *interacting orbital* ϕ'_1 of the benzene part, but another π-type MO, π_1, participates significantly in the orbital ϕ'_1 to mix *in-phase* with the HOMO on the reaction site, C1. The resulting orbital is strongly bonding between C1 and C2 and between C1 and C6. This indicates that the π conjugation is weakened between the reaction site and the adjacent carbons upon electron donation to the attacking cation. This is obviously in harmony with the chemists' view of bond interchange in this reaction process that the C1–C2 and C2–C6 bonds are converted into single bonds, while the conjugation is retained in the remaining part to give a σ-complex.[17] Theoretically, an old reactivity index, "localization energy", was proposed by assuming intuitively such a change in conjugation in the reaction course.[20]

A part of the electrons donated from the orbital ϕ'_1 of the benzene part is not transferred to the paired counterpart ψ'_1 of the NO_2^+ part, but is retained in the region between the two species through the overlap between ϕ'_1 and ψ'_1 to form a loose bond between the C2–C1–C6 region of the benzene part and the nitrogen center of the electrophile.[2] As the interaction proceeds, electrons are promoted to the unoccupied MOs in the benzene part induced by electron delocalization and they participate in bonding interactions with the electrophile unoccupied orbital.[21] Then, the (C1, C2, C6)–N transient bond is converted into the C1–N bond of the sigma complex. The mixing in of the σ-type MOs of benzene is not important at the early stages of the reaction.

2.2. *Projected Reactive Orbitals*

An important aspect of electron delocalization disclosed above is that it determines the active structural units of the reagent and reactant molecules for a given reaction. It tells us what bonds are formed and what bonds are broken. The next step for us is to find a way of obtaining such orbitals without carrying out time-consuming MO calculations on the composite reacting system. In the reaction model studied above, the benzene is supposed to produce the orbital that has the maximum amplitude on the reaction center,

C1, by combining the occupied MOs. In the occupied MO space, however, the orbital cannot be localized completely on the reaction site, but is delocalized over other carbons.

Now, projection of a certain orbital function, δ_r, onto the occupied MO subspace of a molecule should give the occupied orbital, $\varphi_{oc}(\delta_r)$, that has the maximum amplitude on the function, δ_r.[22] The projected reactive occupied orbital, $\varphi_{oc}(\delta_r)$, of an isolated reactant molecule is given by

$$\varphi_{oc}(\delta_r) = \Big(\sum_{i=1}^{m} d_{i,r}\,\phi_i\Big) \Big/ \Big(\sum_{i=1}^{m} d_{i,r}^{\,2}\Big)^{1/2}, \qquad (1)$$

where $d_{i,r}$ is the coefficient of the occupied MO ϕ_i in the linear expansion of δ_r in terms of the occupied canonical MOs ϕ_i (i = 1, ..., m) and the unoccupied canonical MOs ϕ_j (j = m+1, ..., M):

$$\delta_r = \sum_{i=1}^{m} d_{i,r}\,\phi_i + \sum_{j=m+1}^{M} d_{j,r}\,\phi_j. \qquad (2)$$

To discuss the reactivity of a carbon in benzene against an electrophile, it is simplest to take the 2pπ AO of the reaction site as the reference orbital, δ_r. One may find easily that the intermixing of the one of the HOMOs, π_3, with the π_1 MO of benzene gives rise to the orbital that has the largest amplitude on C1, but is delocalized on the adjacent carbons, C2 and C6. The orbital is bonding between C1 and C2 and between C1 and C6. Actually, the orbital obtained in this manner bears a close resemblance to the *interacting orbital* ϕ'_1 derived from an analysis of electron delocalization in the reacting system, (benzene + NO_2^+), though the *projected reactive orbital* is slightly more localized. Inclusion of the 2pπ AO of C4 in δ_r makes the projected orbital closer to the interacting orbital, but we may take simply the 2pπ AO of C1 as δ_r in the present study. Application of the same procedure to substituted benzenes should lead naturally to the occupied projected orbitals that are very similar in shape to the orbital of benzene. Incidentally, the reference function δ_r is not necessarily an AO, but may be an atomic hybrid orbital or a combination of several AOs spanning a functional group, depending on the type of reaction to be studied.

Now, the *local electron donating potential* of the structural unit associated with δ_r is given by

$$\lambda_{oc}(\delta_r) = (\sum_{i=1}^{n} d_{i,r}^{2} \varepsilon_i) / (\sum_{i=1}^{m} d_{i,r}^{2}) \quad , \tag{3}$$

where ε_i signifies the energy of the MO ϕ_i. Note that the quantity defined by *eq.*(3) does not apply to the whole molecule, but represents a local property of an atom or a group. Abundant experimental results to see relative reactivities of substituted benzenes in an aromatic substitution reaction have been interpreted very compactly in terms of the Hammett σ parameter and its modified versions.[23-27] Figure 2 plots the calculated λ_{oc} values against the σ parameters for various substituent groups. One sees a good correlation between the theoretical scale and the experimental one for various electron-releasing and -withdrawing groups at different positions, *meta* and *para*. In contrast, σ^+ parameters deviate significantly from the theoretical scale for $-NH_2$, $-OH$, and $-OCH_3$ groups in the *para*-position, as illustrated in Figure 3. It has been suggested that these groups have an additional stabilizing effect: The resonance between the benzene ring and the substituent group that intervenes when an electronic charge is removed. Then, the deviation from the theoretically estimated values will make it possible to trace the effects involved in the experimental parameters into different origins. The parameters σ^0 that have been proposed so as to lift the direct resonance effect are seen to agree well with the theoretical scales for p-NH_2, p-OH, and p-OCH_3 groups, as shown in Figure 4. Unfortunately, the correlation between the theoretical scale and the σ^0 parameters is worse as a whole, relative to the original σ parameters. Adjustments within these parameters may be necessary. Now, the theoretically estimated electron-donating potential may be utilized as a reliable measure of discussing the reactivity of atoms and groups in any other type of reaction.

Projection of the reference orbital function δ_r onto the unoccupied MO subspace gives rise to the unoccupied reactive orbital that has the maximum amplitude on δ_r:[22]

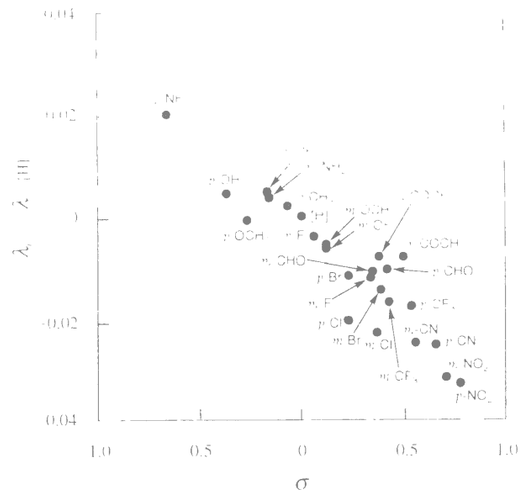

Figure 2. Correlation between the local electron-donating potential of reaction sites and the Hammett σ parameters for substituted benzenes.

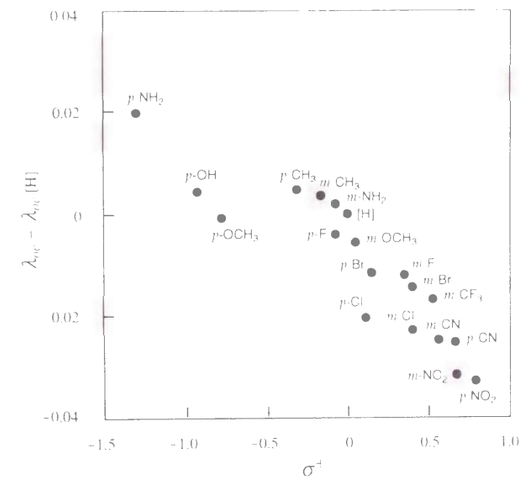

Figure 3. Correlation between the local electron-donating potential of reaction sites and the Hammett σ^+ parameters for substituted benzenes.

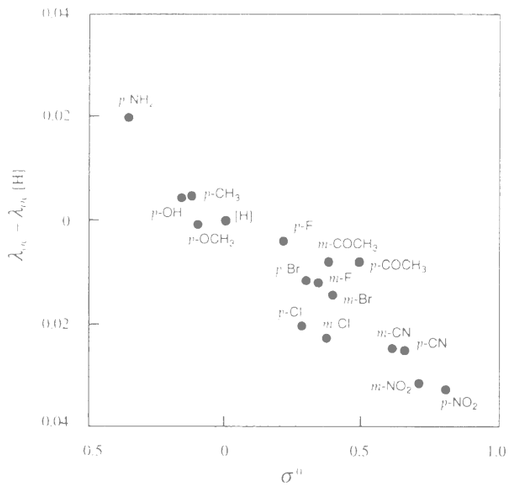

Figure 4. Correlation between the local electron-donating potential of reaction sites and the Hammett σ^0 parameters for substituted benzenes.

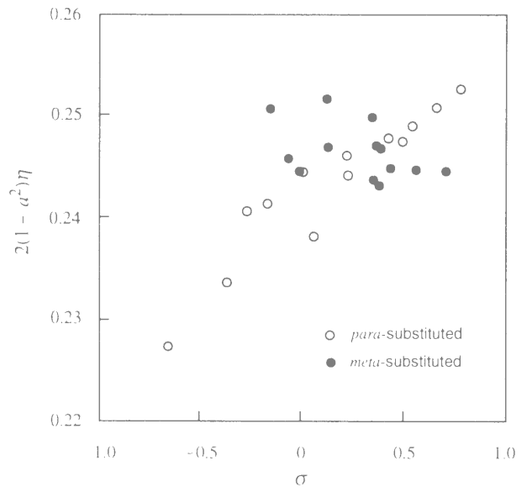

Figure 5. Correlation between the basic hardness of reaction sites and the Hammett σ parameters for substituted benzenes.

$$\phi_{unoc}(\delta_r) = \left(\sum_{j=m+1}^{M} d_{j,r}\,\phi_j\right)\Big/\left(\sum_{j=m+1}^{M} d_{j,r}^{2}\right)^{1/2}. \tag{4}$$

The *electron-accepting capacitance* of the structural unit is evaluated then by

$$\lambda_{unoc}(\delta_r) = \left(\sum_{j=m+1}^{M} d_{j,r}^{2}\,\varepsilon_j\right)\Big/\left(\sum_{j=m+1}^{M} d_{j,r}^{2}\right). \tag{5}$$

Now, the reference function is rewritten in terms of ϕ_{oc} and ϕ_{unoc} as

$$\begin{aligned}\delta_r &= \left(\sum_{i=1}^{m} d_{i,r}^{2}\right)^{1/2}\phi_{oc}(\delta_r) + \left(\sum_{j=m+1}^{M} d_{j,r}^{2}\right)^{1/2}\phi_{unoc}(\delta_r)\\ &= a\phi_{oc}(\delta_r) + (1-a^2)^{1/2}\phi_{unoc}(\delta_r) \quad (|a| \le 1).\end{aligned} \tag{6}$$

It follows then that we can evaluate the power of the reaction site to attract electrons by

$$\begin{aligned}-\lambda(\delta_r) &= -\left(\sum_{i=1}^{m} d_{i,r}^{2}\varepsilon_i\right) - \left(\sum_{j=m+1}^{M} d_{j,r}^{2}\varepsilon_j\right)\\ &= -a^2\lambda_{oc}(\delta_r) - (1-a^2)\lambda_{unoc}(\delta_r).\end{aligned} \tag{7}$$

The coefficient a^2 varies in the range between 0 and 1, depending on the reaction site or the functional group of a reactant molecule used for the reaction. If a^2 is 1, the reaction site serves only as an electron donor, whereas the reaction site serves only as an electron acceptor when a^2 is 0. Thus, a^2 and $(1 - a^2)$ measure the efficiency of a reaction site as an electron donor and as an electron acceptor, respectively. The efficiency is related obviously to the *localizability* of the projected occupied and unoccupied orbitals, ϕ_{oc} and ϕ_{unoc}, on δ_r and, hence, to the localizability of interaction on the reaction site, i.e., a^2 and $(1 - a^2)$ represent, respectively, the active part of ϕ_{oc} and of ϕ_{unoc}. In the case $a^2 = 1/2$, *eq.* (7) is formally equivalent to the Mulliken electronegativity of a molecule.[5] Thus, we can regard $-\lambda$ as giving the *local electronegativity* of the reaction site. This may be quite natural, remembering that the electronegativity indicates the power of an atom to attract electrons in a molecule in the original definition by Pauling.[28]

The electron-donating and -accepting abilities of the functional unit are defined, respectively, by[29]

$$\lambda_{oc}(\delta_r) = \lambda(\delta_r) - 2(1-a^2)\eta(\delta_r) \tag{8}$$

$$\lambda_{unoc}(\delta_r) = \lambda(\delta_r) + 2a^2\eta(\delta_r)\ , \tag{9}$$

in which

$$\eta(\delta_r) = \frac{1}{2}\{\lambda_{unoc}(\delta_r) - \lambda_{oc}(\delta_r)\}\ . \tag{10}$$

The orbital function, δ_r, has the electron-releasing or -attracting potential $\lambda(\delta_r)$. The electron-donating and -accepting potentials of the reaction site are reduced, however, by $2(1-a^2)\eta(\delta_r)$ and $2a^2\eta(\delta_r)$ from that of δ_r, respectively. The reaction site will be a good electron acceptor when both the inactive fraction $(1-a^2)$ of the orbital ϕ_{oc} and η are small. The reaction site will be a good donor when both the inactive fraction a^2 of the orbital ϕ_{unoc} and η are small. Thus, $2(1-a^2)\eta(\delta_r)$ and $2a^2\eta(\delta_r)$ are regarded as indicating the *basic hardness* and *acidic hardness of a reaction site or a functional group* specified by δ_r in a reactant molecule, respectively. Note that *eq.*(10) will give the chemical hardness of a molecule, when λ_{oc} and λ_{unoc} are replaced by $\varepsilon_{\mathrm{HOMO}}$ and $\varepsilon_{\mathrm{LUMO}}$, respectively:[7,30]

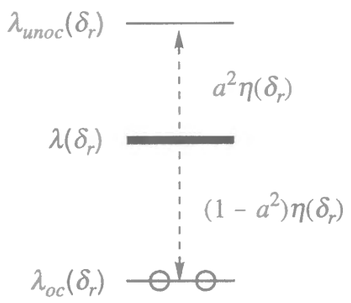

Figure 5 shows the relation between the basic hardness and the Hammett σ parameters for substituted benzenes. Though a linear correlation is found for the *para*-substituted benzenes, the *meta*-substituted benzenes show a different trend. This indicates clearly that the reactivity of atoms in a molecule is determined by a balance between its electronegativity and chemical hardness. It is natural that substituent groups affect both of them. The change in the sigma-electronic part is reflected in the reactivity by raising or lowering the value of λ.

The function δ_r may be chosen as the orbital that is likely to be utilized in the formation of new bonds with the reagent. It may be an AO or a hybrid AO in a single-centered reaction and a linear combination of several AOs in multicentered reactions. In contrast, the orbitals $\phi_{oc}(\delta_r)$ and $\phi_{unoc}(\delta_r)$ have the largest amplitude on δ_r, but are delocalized over a bond or over a few atoms. The mode and extent of delocalization of these orbitals provide us a clue to reveal the molecular mechanism of a reaction. An analysis of transient bonds in terms of paired interacting orbitals for the smallest reaction model and the evaluation of local electron-donating and -accepting potentials of atoms and groups in large molecules by projecting a reference orbital will be of use in discussing the reactivity of complicated molecules treated in modern chemistry. The reference orbital should be chosen to be appropriate for representing those bonds, since the transient bonds guide the reacting system to the transition state and to the product. To make this approach more general and practical, we may adopt the frontier MO of the smallest molecule or its principal component as the reference orbital function for larger reactant molecules that undergo the same type of reaction.

Finally, Politzer and collaborators proposed a few years ago a reactivity scale: "the average local ionization potential".[31] If we assume here that a reactant molecule provides the occupied orbital that has the maximum electron density on a point $\boldsymbol{r}$ in the molecular space when it donates an electronic charge to an electrophilic reagent, such an orbital ϕ_f is given by

$$\phi_f = \{\sum_{i=1}^{m} \phi_i(\boldsymbol{r})\phi_i\} \,/\, \{\sum_{i=1}^{m} \phi_i(\boldsymbol{r})^2\}^{1/2}\ . \tag{11}$$

The electron-donating potential of this orbital in terms of orthonormal MOs should be

$$\varepsilon_f = \{\sum_{i=1}^{m} \rho_i(\boldsymbol{r})\varepsilon_i\} \,/\, \rho(\boldsymbol{r})\ . \tag{12}$$

This is nothing but the definition of the average local ionization potential (the sign inverted). It is clear, therefore, that they are concerned with a point in the space around the reactant molecule, whereas we focus our attention on the orbitals of reaction sites. This makes a big difference, however, when we try to discuss multicentered reactions, e.g., cycloadditions, in which orbital symmetry plays a crucial role.[32]

3. Conclusion

Electron delocalization is the major driving force of chemical reactions. An analysis of electron delocalization has disclosed an attracting behavior of molecules in reactions that they recombine their MOs to give the orbitals that are localized specifically around the reaction site. They tell us what bonds are formed and what bonds are loosened in the course of reactions. By taking the interaction between benzene and NO_2^+ as an example, it has been illustrated that these interacting orbitals are reproduced approximately by projecting a certain reference function onto the MO subspaces. This finding is connected intimately with the fact that chemical interactions are local by nature: Various reactants different in size and structure undergo the same type of reaction if they have the same functional group, while a compound undergoes a variety of reactions against different kinds of reagents, as has been observed in experiments. We can thus estimate local electron-donating and -accepting abilities of an atom or a functional group in large molecules by MO calculations and interpret them in terms of local electronegativity and chemical hardness of reaction sites.

References

(1) McWeeny, R. *Coulson's Valence*, 3rd. ed.; Oxford Univeristy Press: London, 1979.

(2) Fujimoto, H.; Inagaki, S.; Fukui, K. *J. Am. Chem. Soc.* **1976**, *98*, 2670.

(3) Fukui, K. *Theory of Orientation and Stereoselections*; Springer-Verlag: Berlin, 1975.

(4) (a) Fukui, K. *Angew. Chem., Int. Ed. Engl.* **1982**, *21*, 801. (b) Fujimoto, H. ; Fukui, K. *Chemical Reactivity and Reaction Paths*; Klopman, G., Ed.; Wiley-Interscience: New York, 1974; pp 23-54.

(5) Fukui, K.; Fujimoto, H. *Bull. Chem. Soc. Jpn.* **1968**, *41*, 1989. *ibid.* **1969**, *42*, 3399.

(6) Mulliken, R. S. *J. Chem. Phys.* **1934**, *2*, 782.

(7) Parr, R. G.; Zhou, Z. *Acc. Chem. Res.* **1993**, *26*, 256.

(8) (a) Parr, R. G.; Donnelly, R. A.; Levy, M.; Palke, W. E. *J. Chem. Phys.* **1978**, *68*, 3801. (b) Parr, R. G.; Bartolotti, L. J. *J. Am. Chem. Soc.* **1983**, *104*, 3801. (c) Parr, R. G.; Yang, W. *J. Am. Chem. Soc.* **1984**, *106*, 4049.

(9) Parr, R. G.; Pearson, R. G. *J. Am. Chem. Soc.* **1983**, *105*, 7512.

(10) Pearson, R. G. *J. Am. Chem. Soc.* **1963**, *85*, 3533. *ibid.* **1985**, *107*, 6801.

(11) Pearson, R. G. *Hard and Soft Acids and Bases;* Doweden, Hutchinson and Ross: Strousbourg, PA, 1973.

(12) Pearson, R. G. *Acc. Chem. Res.* **1993**, *26*, 250.

(13) Klopman, G. *Chemical Reactivity and Reaction Path*; Klopman, G., Ed.; Wiley-Interscience: New York, 1974; pp 55-165.

(14) Klopman, G. *J. Am. Chem. Soc.* **1968**, *90*, 223.

(15) (a) Fukui, K.; Koga, N.; Fujimoto, H. *J. Am. Chem. Soc.* **1981**, *103*, 196. (b) Fujimoto, H.; Koga, N.; Hataue, I. *J. Phys. Chem.* **1984**, *88*, 3539.

(16) Fujimoto, H. *Acc. Chem. Res.* **1987**, *20*, 448.

(17) Ingold, C. K. *Structure and Mechanism in Organic Chemistry*, 2nd ed.; Cornell University Press: Ithaca, NY, 1969; pp 264-417.

(18) (a) Szabó, K. J.; Hörnfeldt, A.-B.; Gronowitz, S. *J. Am. Chem. Soc.* **1992**, *114*, 6827. (b) Politzer, P.; Jayasuriya, K.; Sjoberg, P.; Laurence, P. R. *J. Am. Chem. Soc.* **1985**, *107*, 1174. (c) Feng, J.; Zheng, X.; Zerner, M. C. *J. Org. Chem.* **1986**, *51*, 4531. (d) Szabó, K. J. *J. Mol. Struct. (THEOCHEM)* **1988**, *181*, 1.

(19) Frisch, M. J.; Trucks, G. W.; Head-Gordon, M.; Gill, P. M. W.; Wong, M. W.; Foresman, J. B.; Johnson, B. G.; Schlegel, H. B.; Robb, M. A.; Replogle, E. S.; Gomperts, R.; Andres, J. L.; Raghavachari, K.; Binkley, J. S.; Gonzalez, C.; Martin, R. L.; Fox, D. J.; Defrees, D. J.; Baker, J.; Stewart, J. J. P.; Pople, J. A. *Gaussian 92*; Gaussian, Inc.: Pittsburgh, PA, 1992.

(20) Wheland, G. W. *J. Am. Chem. Soc.* **1942**, *64*, 900.

(21) Fujimoto, H.; Inagaki, S. *J. Am. Chem. Soc.* **1977**, *99*, 7424.

(22) Fujimoto, H.; Mizutani, Y.; Iwase, K. *J. Phys. Chem.* **1986**, *90*, 2768.

(23) Hammett, L. P. *Physical Organic Chemistry*; McGraw-Hill: New York, 1940; pp 264-417.

(24) Ritchie, C. O.; Sager, W. F. *Progress in Physical Organic Chemistry, 2*; Cohen, S. C., Streitwieser, A., Jr., Taft, R. W., Eds.; Interscience: New York, 1964; pp 323-400.

(25) Hansch, C.; Leo, A.; Taft, R. W. *Chem. Rev.* **1991**, *91*, 165.

(26) Brown, H. C.; Okamoto, Y. *J. Am. Chem. Soc.* **1958**, *80*, 4979.

(27) Yukawa, Y.; Tsuno, Y.; Sawada, M. *Bull. Chem. Soc. Jpn.* **1966**, *39*, 2274.

(28) Pauling, L. *The Nature of the Chemical Bond*; Cornell University Press: Ithaca, NY, 1960.

(29) Fujimoto, H.; Satoh, S. *J. Phys. Chem.* **1994**, *98*, 1436.

(30) Sen, K. D. *Structure and Bonding 80, Chemical Hardness*; Springer-Verlag: Berlin, 1993.

(31) (a) Sjoberg, P.; Murray, J. S.; Brinck, T.; Politzer, P. *Can. J. Chem.* **1990**, *68*, 1440. (b) Murray, J. S.; Brinck, T.; Politzer, P. *J. Mol. Struct. (THEOCHEM)* **1992**, *255*, 271.

(32) Woodward, R. B.; Hoffmann, R. *Conservation of Orbital Symmetry* ; Academic Press: New York, 1970.

Chapter 2:

Population Analysis along the Intrinsic Reaction Coordinate: Application to 1,3-Dipole Cycloaddition

1. Introduction

Quantum chemistry has developed remarkably and has become a useful method in various areas of chemistry. Not only the energies and structures of various molecular species but also the reaction paths such as the transition states can easily be calculated with high accuracy, using recent powerful computers and many excellent methods of calculation.[1] Here, we should point out some problems that remain to be solved. The first point is that we have not established yet the method for a qualitative understanding of the wave function with high accuracy. The second point is that we do not know how to connect the change in wave function along the reaction coordinate with the enhancement or depression of chemical reactivity. To clarify these subjects, some attractive attempts, such as the valence bond (VB) type approach[2-7], the density functional approach[8], and the atoms in molecules (AIM)[9], have been made.

One of these attempts is the population analysis.[10-25] This concept was originally proposed by Mulliken[10] and has been generalized and developed. Wiberg introduced the bond order[11] and Giambiagi *et al.* and Mayer have generalized this idea.[12-17] The multi-center bond indices have recently been proposed[18-21] and their physical meanings and the relations between those quantities have also been discussed.[22-24]

The population analysis has the advantage of its easy treatment. Therefore, it is often used to describe the formation or cleavage of chemical bonds and the change in the atomic charges along the reaction coordinate.[25] When a linear combination of atomic orbitals for the molecular orbital (LCAO-MO) is used, both the gross atomic charge defined by Mulliken and the bond order defined by Mayer are generally made up of the electron density matrix and the overlap matrix. The question we have to ask here is what is the cause of the change in these quantities along the reaction coordinate. The change originates from two different contributions: the change in the electron density matrix with keeping the overlap matrix unaltered and the change in the overlap matrix with keeping the electron density matrix unaltered. The change in the density matrix arises from the electron redistribution caused by the nuclear motions. On the other hand, the change in

the overlap matrix arises from the LCAO formalism. In usual quantum chemical calculations, each AO is centered on the nucleus of an atom, except for the case with the floating orbital or the plane-wave basis set. These two contributions must be classified. This kind of divisions has already been introduced in the force theory. Nakatsuji *et al.* investigated the analytical second derivative of the potential energy satisfying the Hellmann-Feynman theorem and discussed the role of each term in the second derivative of the Hartree-Fock energy.[26]

In the present study, the derivatives of the gross atomic charge, the bond order, and the atom valence with respect to the nuclear positions are calculated analytically along the intrinsic reaction coordinate (IRC). This method is applied to a simple 1,3–dipole cycloaddition reaction between fulminic acid and acetylene. The 1,3–dipole cycloaddition reactions are important not only from a synthetic viewpoint but also from theoretical interests with respect to the reactivity and the regioselectivity. Some interesting studies have recently been done using the density functional theory (DFT) and a hard and soft acids and bases principle (HSAB) model for 1,3–dipole cycloaddition reactions.[27,28] Chandra *et al.*[27] investigated the cycloaddition reactions between 1,3–dipoles and dipolarophiles and observed that the hardness went through a minimum along the reaction coordinate. Méndez *et al.*[28] have used the formalism of interaction energy and suggested that the electrophilic nature of 1,3–dipole and the nucleophilic nature of dipolarophiles were important. Furthermore, they indicated that reshuffling of the charge distribution should be more important than charge-transfer processes. On the other hand, Karadakov *et al.* studied the mechanism of 1,3–dipole cycloaddition in terms of the valence-bond theory.[29] They examined the spin-coupled wave function along the reaction coordinate around the transition state and concluded that the following description (I) should be more plausible than (II), by which the mechanism of 1,3–dipole cycloaddition was usually represented.

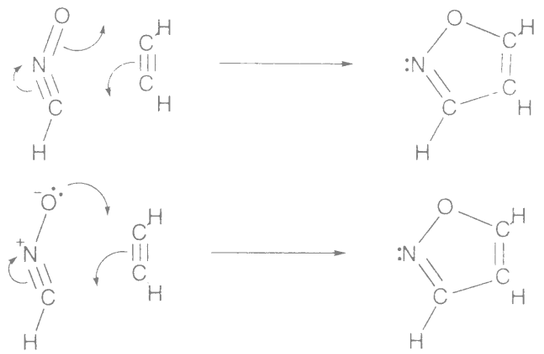

(I)

(II)

Having their discussion in mind, the reaction mechanism is investigated here by means of the population analysis using the Hartree-Fock electron density.

2. Methods of Calculation

In this study, the LCAO-MO approximation for the Roothaan-Hall equation[30] is used:

$$\phi_i(\mathbf{r}) = \sum_{\mu} c_{\mu i}\chi_{\mu}(\mathbf{r}), \tag{1}$$

where $c_{\mu i}$ is the coefficient of the AO $\chi_{\mu}(\mathbf{r})$ in the ith MO $\phi_i(\mathbf{r})$. Within this formalism, the density matrix $\boldsymbol{P}$ consists of the elements $P_{\mu\nu}$ with respect to the atomic orbital :

$$P_{\mu\nu} = 2\sum_{i}^{occ} c_{\mu i}c_{\nu i} . \tag{2}$$

According to the Mulliken's population analysis[10], the gross atomic charge of the atom A, q_A, is

$$q_A = \sum_{\mu}^{A} \left(\boldsymbol{PS}\right)_{\mu\mu} , \tag{3}$$

where $\boldsymbol{S}$ is the overlap matrix composed with the elements $S_{\mu\nu}$:

$$S_{\mu\nu} = \int \chi_{\mu}(\mathbf{r})\chi_{\nu}(\mathbf{r})d\mathbf{r}. \tag{4}$$

Therefore, the Mulliken gross atomic charge naturally corresponds to the partitioning of electron density $\rho(\mathbf{r})$ with respect to AO[22]:

$$
\begin{aligned}
N &= \int \rho(\mathbf{r})\, d\mathbf{r} \\
&= \int \sum_{\mu} \sum_{\nu} P_{\mu\nu}\chi_{\mu}(\mathbf{r})\chi_{\nu}(\mathbf{r}) d\mathbf{r} \\
&= \sum_{\mu} \sum_{\nu} P_{\mu\nu} S_{\mu\nu} \\
&= \sum_{A} q_A \ .
\end{aligned} \tag{5}
$$

Another type of analysis was originally introduced by Wiberg and generalized by Giambiagi *et al.*[12] and Mayer[13-17]. Mayer defined the bond-order index between the atom A and the atom B:

$$
I_{AB} = \sum_{\mu \in A} \sum_{\nu \in B} (\boldsymbol{PS})_{\mu\nu} (\boldsymbol{PS})_{\nu\mu} \ , \tag{6}
$$

and the total valence of the atom A:

$$
V_A = \sum_{B \neq A} I_{AB} \ . \tag{7}
$$

This corresponds to the partitioning of the exchange part of the second-order density matrix:

$$
N = \frac{1}{2} \int \rho_1(\mathbf{r}_1,\mathbf{r}_2)\rho_1(\mathbf{r}_2,\mathbf{r}_1) d\mathbf{r}_1 d\mathbf{r}_2 \ . \tag{8}
$$

Therefore, the relation between Mayer's atom valence and Mulliken's gross atomic charge is given by

$$
2q_A = V_A + \sum_{\mu \in A} \sum_{\nu \in A} (\boldsymbol{PS})_{\mu\nu} (\boldsymbol{PS})_{\nu\mu} \ . \tag{9}
$$

Although the population analysis by the partitioning of higher-order density matrices has been proposed[18-23], it is beyond the scope of this paper.

Now, the derivatives of the Mulliken gross atomic charge, the Mayer bond order and the atom valence with respect to the Cartesian coordinates of nucleus (X_i, Y_i, Z_i) (i = 1, 2,..., N) are given by

$$
\frac{\partial q_A}{\partial X_i} = \sum_{\mu}^{A} \left(\left(\frac{\partial \boldsymbol{P}}{\partial X_i} \boldsymbol{S} \right)_{\mu\mu} + \left(\boldsymbol{P} \frac{\partial \boldsymbol{S}}{\partial X_i} \right)_{\mu\mu} \right) , \tag{10}
$$

$$
\begin{aligned}
\frac{\partial I_{AB}}{\partial X_i} = & \sum_{\mu \in A} \sum_{\nu \in B} \left(\left(\frac{\partial \boldsymbol{P}}{\partial X_i} \boldsymbol{S} \right)_{\mu\nu} (\boldsymbol{PS})_{\nu\mu} + (\boldsymbol{PS})_{\mu\nu} \left(\frac{\partial \boldsymbol{P}}{\partial X_i} \boldsymbol{S} \right)_{\nu\mu} \right) \\
& + \sum_{\mu \in A} \sum_{\nu \in B} \left(\left(\boldsymbol{P} \frac{\partial \boldsymbol{S}}{\partial X_i} \right)_{\mu\nu} (\boldsymbol{PS})_{\nu\mu} + (\boldsymbol{PS})_{\mu\nu} \left(\boldsymbol{P} \frac{\partial \boldsymbol{S}}{\partial X_i} \right)_{\nu\mu} \right) .
\end{aligned} \tag{11}
$$

The term which contains the derivative $\frac{\partial \boldsymbol{P}}{\partial X_i}$ is called the density derivative term, while the contribution from $\frac{\partial \boldsymbol{S}}{\partial X_i}$ is called the overlap derivative term. Moreover, we have

$$
\frac{\partial V_A}{\partial X_i} = \sum_{B \neq A} \frac{\partial I_{AB}}{\partial X_i} \ . \tag{12}
$$

The derivative of the overlap matrix $\frac{\partial \boldsymbol{S}}{\partial X_i}$ consists of the elements $\frac{\partial S_{\mu\nu}}{\partial X_i}$:

$$
\frac{\partial S_{\mu\nu}}{\partial X_i} = \frac{\partial}{\partial X_i} \int \chi_{\mu}(\mathbf{r})\chi_{\nu}(\mathbf{r}) d\mathbf{r} , \tag{13}
$$

and the derivative of the density matrix $\frac{\partial \boldsymbol{P}}{\partial X_i}$ consists of the elements $\frac{\partial P_{\mu\nu}}{\partial X_i}$, which can be solved analytically:

$$
\frac{\partial P_{\mu\nu}}{\partial X_i} = -2 \sum_{l,m}^{occ} c_{\mu l} c_{\nu m} S_{ml}^{(1)} + 2 \sum_{l}^{occ} \sum_{a}^{unocc} u_{al}^{(1)} \left(c_{\mu l} c_{\nu a} + c_{\mu a} c_{\nu l} \right) , \tag{14}
$$

where $S_{ml}^{(1)}$ is the derivative of the MO overlap integral between the MOs ϕ_l and ϕ_m, and $u_{al}^{(1)}$ is a mixing coefficient between the occupied and unoccupied MOs. The value $u_{al}^{(1)}$ is solved by the coupled-perturbed Hartree-Fock (CPHF) equation.[31-33] Nakatsuji *et al.* interpreted the physical meanings of each term in *eq.*(14) as the renormalization term and the relaxation term in their force theory.[26] The first term on the right-hand side in *eq.*(14) which is called the renormalization term works to keep the total wave function normalized. The second term which is called the relaxation term shows the rearrangement of the charge distribution in the reaction system by mixing the occupied and unoccupied orbitals.

It should be noted that the total of Mulliken gross atomic charges must be conserved,

$$
\sum_{A}^{all} \frac{\partial q_A}{\partial X_i} = 0 . \tag{15}
$$

As shown in *eq.* (10), the derivative of the Mulliken gross atomic charge is given by two different contributions. The first term on the right-hand side represents the contribution from the change in the density matrix without the change in the overlap matrix, that is to say, the redistribution of electrons due to the nuclear motion. This term is called the density derivative term. What is more, this term is able to be divided into two terms: the renormalization term and the relaxation term. On the other hand, the second term represents the contribution from the change in the overlap without the change in AO coefficients, and hence, this is called the overlap derivative term.

By transforming the derivatives with respect to the $3N$ Cartesian coordinates into those with respect to the $3N$ mass-weighted Cartesian coordinates x_i (i =1, 2,..., $3N$), the derivative of the Mulliken gross atomic charge with respect to the intrinsic reaction coordinate (IRC) is given by

$$\frac{dq_A}{ds} = \sum_{i=1}^{3N} \frac{\partial q_A}{\partial x_i}\frac{dx_i}{ds} = \sum_{i=1}^{3N} \frac{\partial q_A}{\partial x_i}\frac{\partial V}{dV}\frac{\partial V}{\partial x_i}, \qquad (16)$$

where V is the adiabatic potential of the reaction system and where the IRC-equation[34]

$$\frac{dx_i}{ds} = \frac{\dfrac{\partial V}{\partial x_i}}{\dfrac{dV}{ds}} \quad (i = 1,2,...,3N) \qquad (17)$$

has also been used. In the same way, the derivative of the bond order is given by

$$\frac{dI_{AB}}{ds} = \sum_{i=1}^{3N} \frac{\partial I_{AB}}{\partial x_i}\frac{\partial V}{dV}\frac{\partial V}{\partial x_i}. \qquad (18)$$

The derivatives of the atom valences are also defined in a similar fashion. These derivatives are divided into the redistribution part of the electron density $\rho(\mathbf{r})$ and the exchange part of the second-order density matrix along the IRC.

The restricted Hartree-Fock scheme with Pople's 6-31G** basis set[35] was used for calculations. The 6-31G** basis set is known to give reliable results for the population

analysis. The geometry optimization and analytical frequency analysis with CPHF calculations were performed with the *Gaussian94* program package.[36] The IRC calculations by the Gonzalez-Schlegel algorithm[37] with the step size 0.01 amu$^{+1/2}$-bohr were done with the *GAMESS* program.[38]

3. Results and Discussion

Concerning the 1,3–dipole cycloaddition reaction, Huisgen[39] proposed the concerted single step reaction mechanism, while Firestone[40] proposed that this reaction should take place in two steps *via* a biradical intermediate. Schlegel *et al.*[41] performed the MC–SCF study of three different 1,3–dipole cycloaddition reactions and concluded that the concerted single step pathway was preferred to the biradical path. Therefore, the concerted single step reaction is considered here in our study.

3.1. Energy and Geometries

The optimized structures of the reactants, which are fulminic acid **1** and acetylne **2**, the transition state **TS**, and the product, isoxazole **3**, are shown in Figure 1. The total energies are presented in Table 1. The activation energy of this reaction is 35.50 kcal/mol and the reaction energy is exothermic by 81.65 kcal/mol (including zero-point energy correction). In literature, it has been reported that the activation energy is 26.0 kcal/mol and the reaction energy is 66.9 kcal/mol (exothermic) at the MRCI //MCSCF/4-31G level.[41] Another study[42] has shown that the activation energy is 11.0 kcal/mol and the reaction energy is 77.7 kcal/mol (exothermic) at the MP4(SDTQ)/6-311G(d,p)//HF/6-311G(d,p) level. More recently, it has been reported that the activation energy is 12.2 kcal/mol at the CASPT2//CAS(6,6)/6-31G* level.[29]

Figure 2 shows the potential energy profile along the IRC. At the point s = 5.9, the IRC connects practically to the product. The changes in bond lengths and bond angles along the IRC are shown in Figures 3 (a) and (b), respectively. Here, the numbering of the

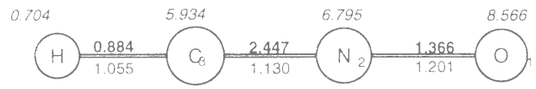

1

2

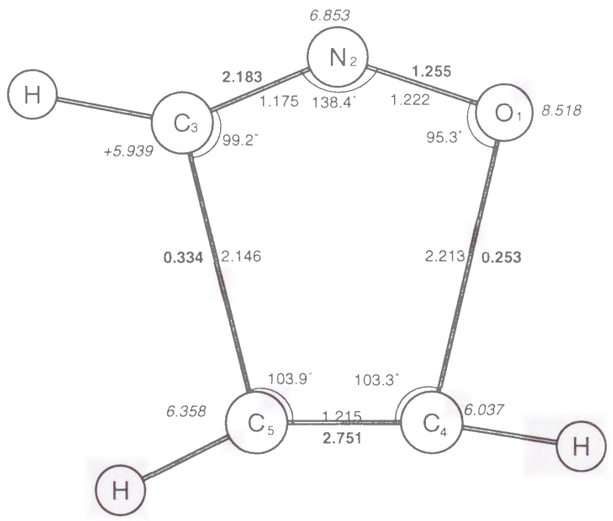

TS

Figure 1. Optimized geometries. Bond lengths and bond angles are given in angstroms and degrees, respectively. The bond orders are represented in gothic and the gross atomic charges in italic.

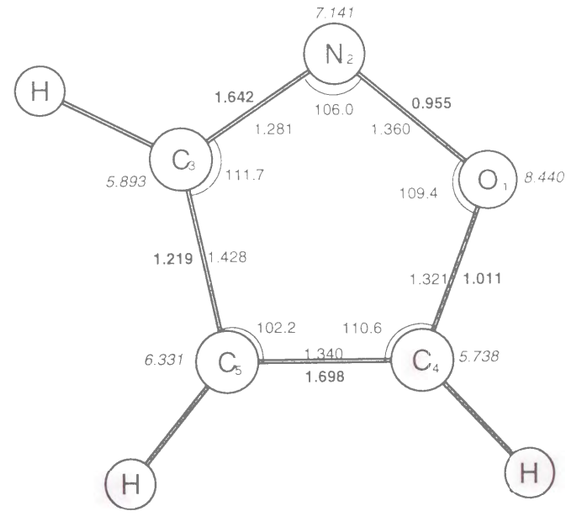

3

Figure 1. *(Continued from the previous page.)*

Table 1: Total Energies at the HF/6-31G** Level

species		total energy(au)	ZPE(kcal/mol)[a]
1 HCNO	($C_{\infty v}$)	-76.82184	12.77
2 C_2H_2	($D_{\infty h}$)	-167.63260	16.39
TS	(C_s)	-244.39925	29.84
3 isoxazole	(C_s)	-244.59419	35.20

[a]Zero-point energy (ZPE) scaled by a factor of 0.89.

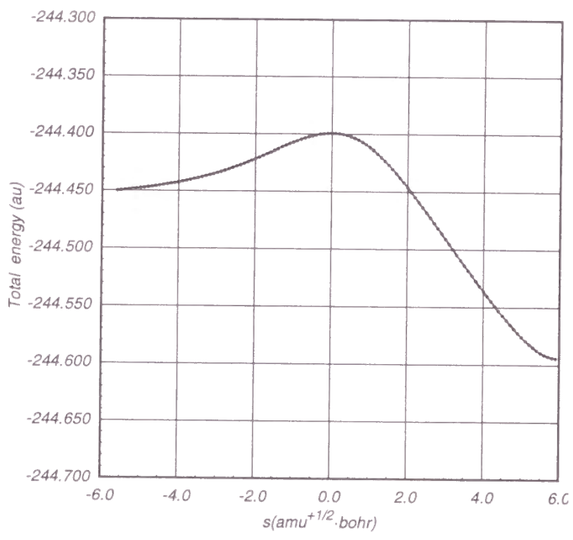

Figure 2. The potential energy curve along the IRC.

(a)

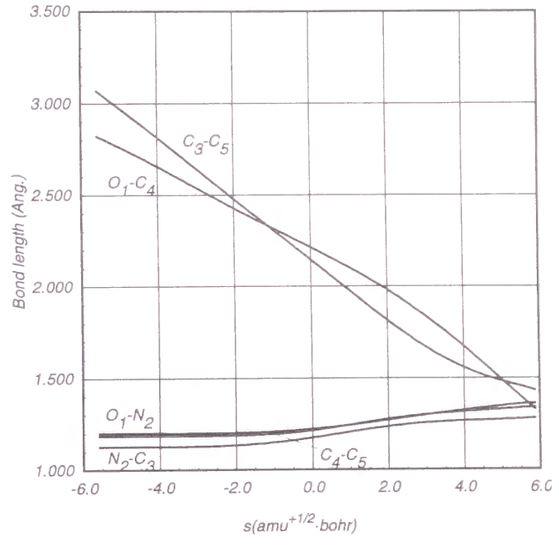

(b)

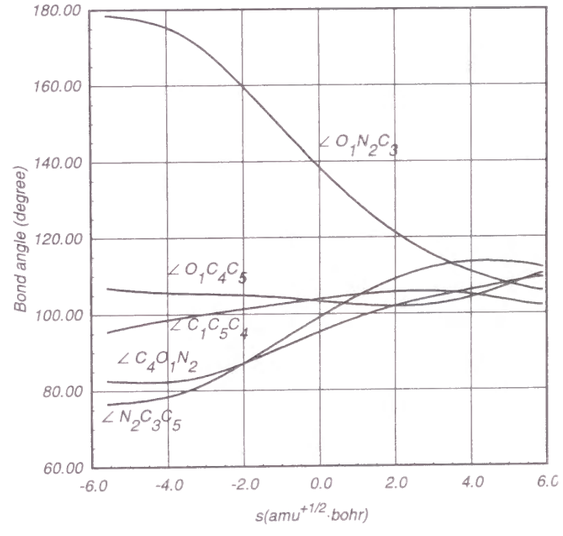

Figure 3. The geometrical changes along the IRC. The numbering of the atoms corresponds to those in Figure 1. The bond lengths are given in angstroms and the bond angles in degrees.

atoms is the same as in Figure 1. Although the bond length of O_1–C_4 is shorter than that of C_3–C_5 in the initial reaction coordinate ($s < -1.5$), the bond length of C_3–C_5 is shortened rapidly, while the O_1–C_4 bond length does not become shorter rapidly until the coordinate reaches the transition state ($s > 2.0$). These different shapes reflect non-synchronous bond formations. The bond angles of $\angle C_3C_5C_4$ and $\angle O_1C_4C_5$ do not change much along the IRC. Therefore, O_1 and C_3 atoms of fulminic acid attack the carbon atoms of the acetylene from the same directions, bending the $\angle O_1N_2C_3$ angle of the fulminic acid along the IRC, as shown in Figure 3(b). On the other hand, the C_4–C_5 bond in acetylene and the O_1–N_2 and N_2–C_3 bonds in fulminic acid are lengthened slightly after the transition state is reached.

3.2. Mulliken Charges

Figure 4 shows the gross atomic charges calculated along the IRC. The gross charge of the O_1 atom, q_{O1}, does not change so much except for the final stage on the reaction coordinate ($s > 5.0$). The gross charge of the C_3 atom does not change much either. The largest change in the gross charge in the fulminic acid part is seen on the N_2 atom. The charge q_{N2} of the N_2 atom is 6.795 in fulminic acid and becomes 7.141 in the product. The C_4 and C_5 atoms of acetylene show different charge profiles. The charge q_{C4} of the C_4 atom decreases monotonically. In contrast, the charge q_{C5} of the C_5 atom increases both at the initial stage and at the final stage on the reaction coordinate.

In order to investigate the change in the gross charges of each atom in detail, the derivatives of these gross charges, q_{O1}, q_{N2}, q_{C3}, q_{C4}, and q_{C5}, with respect to the IRC are shown in Figures 5(a)-(e), respectively. In case of the Mulliken gross charge, it is shown that the total derivative values behave in a similar way to the density derivative term. Moreover, it is seen that the two components of the density derivative term in the atomic charges exhibit different patterns. In the density derivative term of the N_2 atomic charge, both the relaxation term and the renormalization term make the N_2 atomic charge increase. On the other hand, the decrease in the density derivative term of the O_1 atom is dominated by the renormalization term. In case of the density derivative term of the C_4 atomic

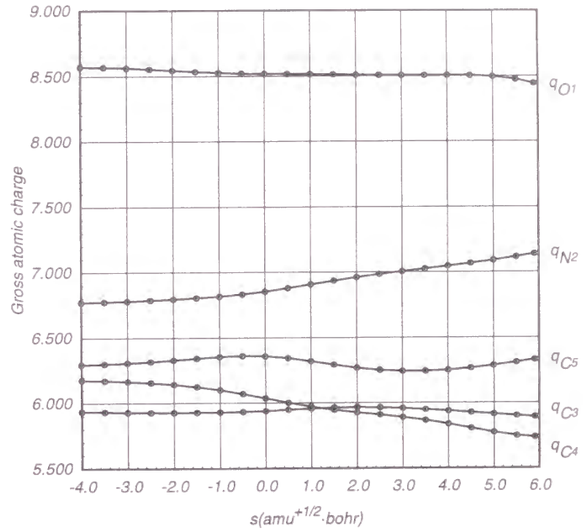

Figure 4. The gross atomic charge profile along the IRC.

(a)

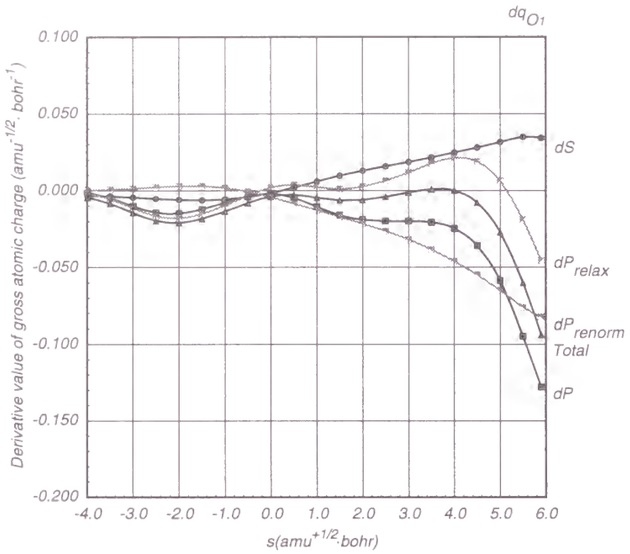

(b)

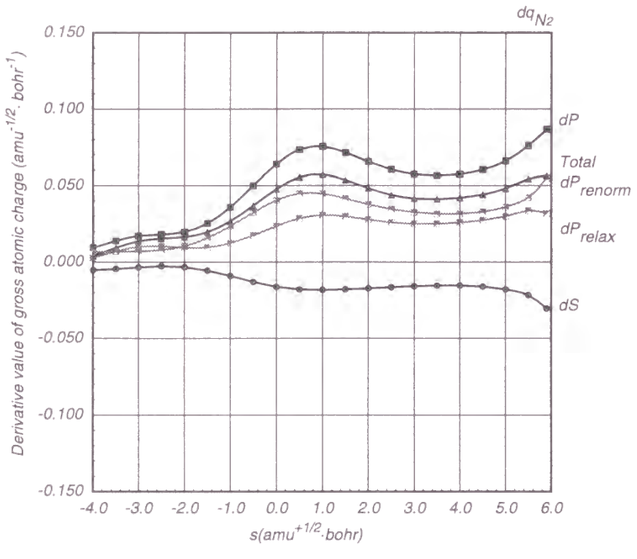

Figure 5. The derivatives of gross atomic charges (a)q_{O1}, (b)q_{N2}, (c)q_{C3}, (d)q_{C4}, and (e)q_{C5} with respect to the IRC, respectively. The density derivative term, which consisits of the renormalization term (dP_{renorm}) and the relaxation term (dP_{relax}), is plotted in the symbol (■). The overlap derivative term is plotted in the symbol (●), and the total derivative values in (▲).

(c)

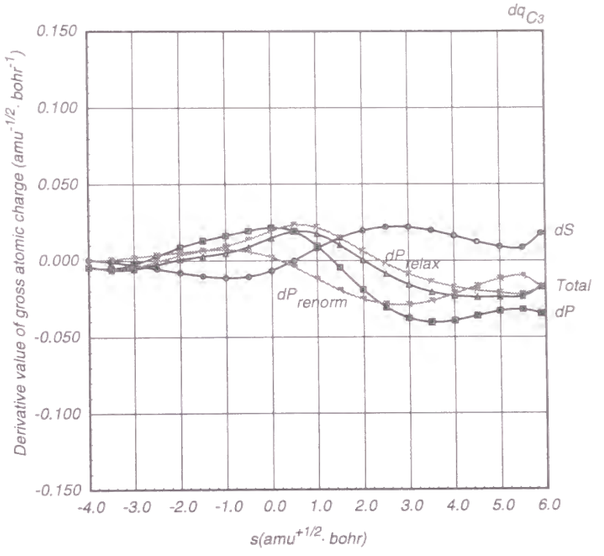

(d)

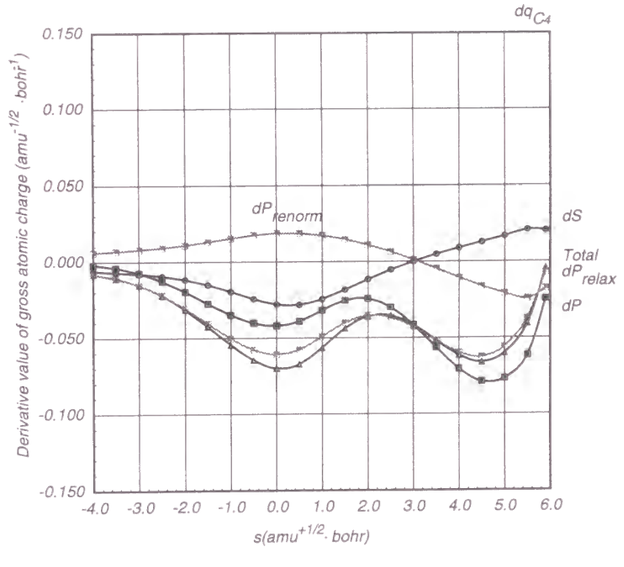

Figure 5. (*Continued from the previous page.*)

(e)

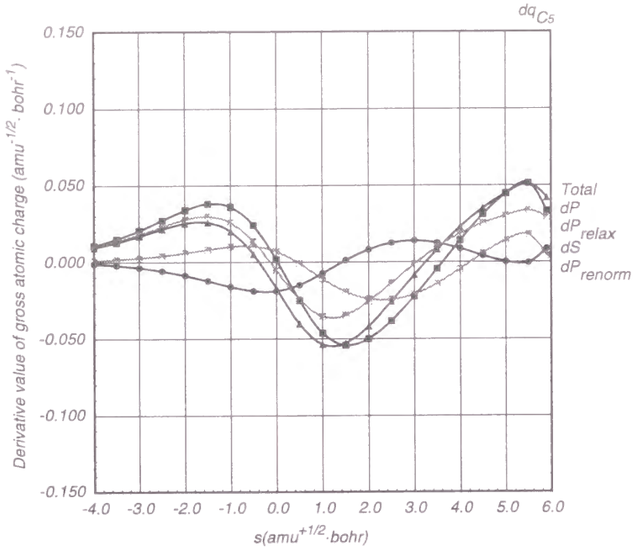

Figure 5. (*Continued from the previous page.*)

charge, the renormalization term and the relaxation term have different effects from each other. That is to say, the relaxation term reduces the atomic charge, while the renormalization term increases slightly the atomic charge around the transition state. In addition, it should be noted that the trend of the charge redistribution in the final coordinate region is different from that around the transition state.

3.3. Bond Orders and Atom Valences

Figure 6 shows the bond order profile along the IRC. In the fulminic acid part, the bond order between the O_1 atom and the N_2 atom, I_{O1N2}, is 1.366 and the bond order between the N_2 atom and the C_3 atom, I_{N2O3}, is 2.447. These values decrease gradually as the reaction proceeds and the bond orders I_{O1N2} and I_{N2C3} become 0.955 and 1.642 in the product, respectively. The bond order I_{C4C5}, which represents the triple bond in acetylene, is 3.190 initially and is 1.698 in the product. On the other hand, the bond orders I_{O1C4} and I_{C3C5}, which show the formation of new chemical bonds, increase along the IRC. It is found that I_{C3C5} increases more steeply than I_{O1C4}. As a result, the bond order I_{C3C5} is larger than I_{O1C4} in the product.

The derivatives of the bond orders, I_{O1N2}, I_{N2C3}, I_{C4C5}, I_{O1C4}, and I_{C3C5}, with respect to the IRC are shown in Figures 7(a)-(e), respectively. First, we examine the derivatives of bond orders I_{O1N2}, I_{N2C3}, and I_{C4C5}, all of which decrease along the IRC. In these, the overlap derivative term dS contributes to the decrease in bond orders, while the density derivative term dP contributes to the increase, although the two terms, dP_{renorm} and dP_{relax}, show different contributions. The renormalization term increases the bond orders slightly, while the relaxation term contributes intensely to a decrease in the bond orders. The derivative value of I_{O1N2} decreases and reaches the minimum at s = 1.0. On the other hand, the derivative of I_{N2C3} decreases more steeply than that of I_{O1N2} till the reacting system comes to the transition state and reaches the minimum at s = 0.5, since the large negative contribution of the relaxation term dominates the density derivative term. Consequently, the N_2–C_3 bond is more sensitive to the nuclear motion than the O_1–N_2 bond is around the transition state. This is connected with the π-electron

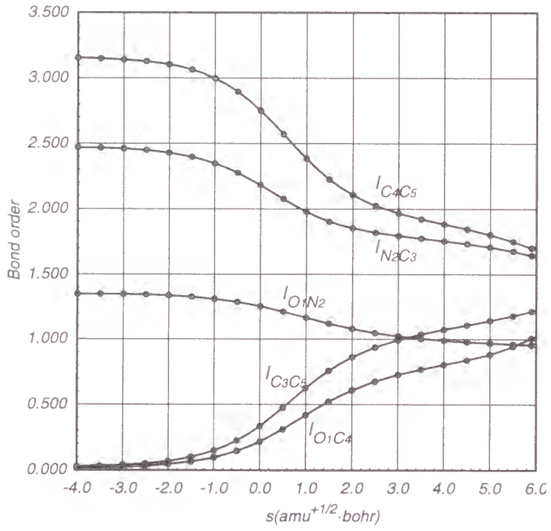

Figure 6. The bond order profile along the IRC.

(a)

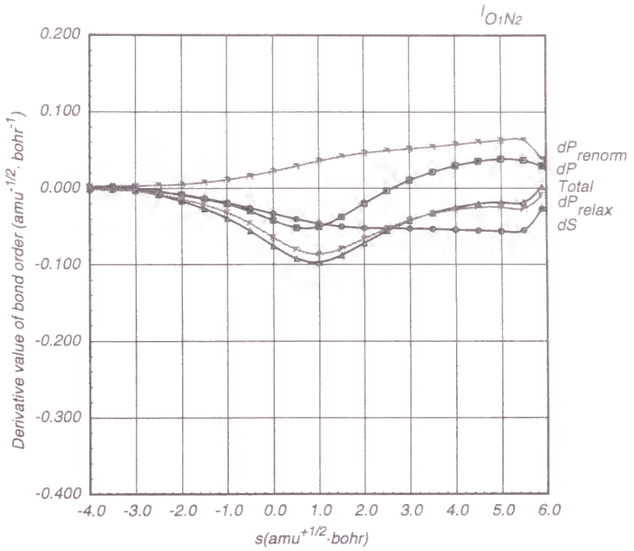

(b)

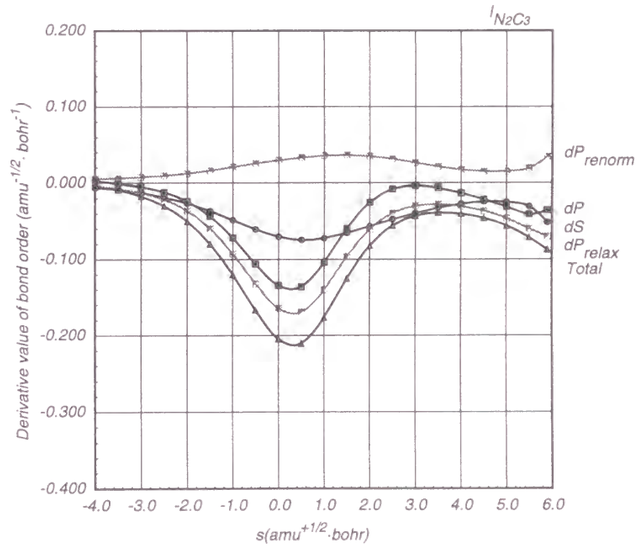

Figure 7. The derivatives of bond orders (a) I_{O1N2}, (b) I_{N2C3}, (c) I_{C4C5}, (d) I_{O1C4}, and (e) I_{C3C5} with respect to the IRC, respectively.

(c)

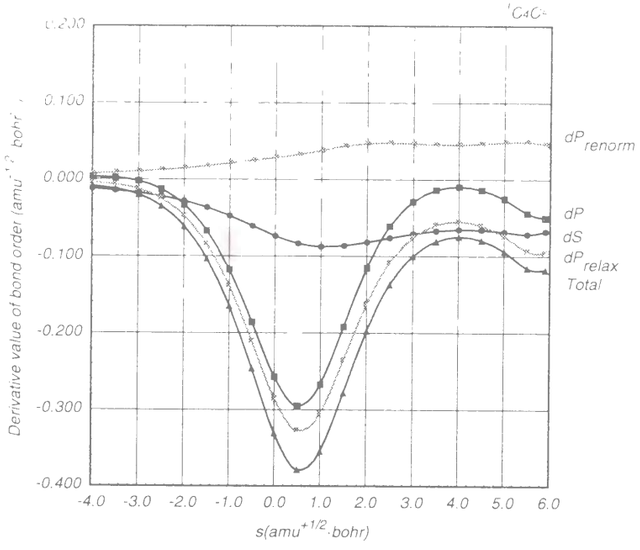

(d)

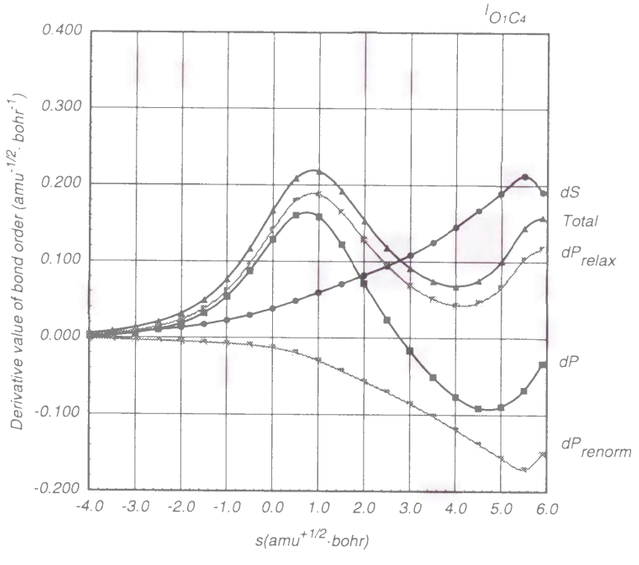

Figure 7. (*Continued from the previous page.*)

(e)

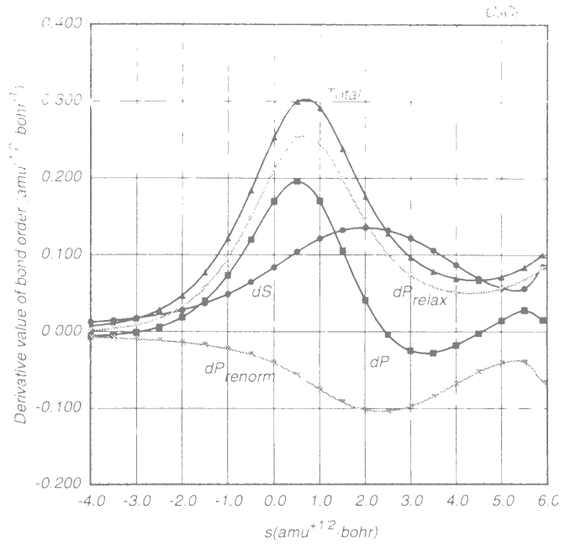

Figure 7. (*Continued from the previous page.*)

state of the fulminic acid in the initial reaction coordinate. Namely, a part of electrons utilized to form the N_2–C_3 triple bond in the initial state should be converted to the lone pair of electrons on the N_2 atom in the product. After passing the minimum point, the derivative of I_{O1N2} comes close to zero in the product region, while that of I_{N2C3} comes close to zero at s = 3.0 and decreases again by the effect of the relaxation term dP_{relax}. The derivative of I_{C4C5} does not become zero in the final stage on the reaction coordinate either.

We compare next the derivatives of I_{C3C5} and I_{O1C4}. In both of the two terms, the overlap derivative term dS contributes to the increase in bond orders. As to the density derivative term, the relaxation term dP_{relax} increases these bond orders, while the renormalization term dP_{renorm} decreases these bond orders. As a result, the density derivative term dP causes these bond orders to increase. Before the transition state, the derivative of I_{C3C5} is larger than that of I_{O1C4} and I_{C3C5} increases more steeply than I_{O1C4} as noted above. Moreover, it is found that the maximum points in each derivative value differ from each other, though not large in extent. In the final stage, both of the derivatives also increase. It is interesting to note that the trend is different from that around the transition state. That is, although the density derivative term is a main component till the reacting system reaches the transition state, showing that the electron redistribution forms new bonds, the overlap derivative term is found to be the main part at the final stage. This shows that the nuclear motion is forced to complete the bond formation at the final stage.

We have analyzed the derivatives of the bond order by dividing them into the overlap derivative term and the density derivative term as mentioned above. We can discuss the bond formation also from another point of view. For the derivatives of bond orders presented in Figure 7, the overlap derivative term dS and the renormalization term dP_{relax} of the density derivative term exhibit the opposite behaviors and they are nearly counterbalanced with each other along the IRC. Therefore, the total derivative value depends on the relaxation term of the density derivative term. That is, the change in bond orders originates from the relaxation of electron density.

The atom valences are shown in Figure 8. While the gross charge of the N_2 atom increases gradually with the progress of the reaction as shown in Figure 4, the atom valence, V_{N2}, decreases around the transition state. This indicates that the second term of the right-hand side in *eq.* (9) changes dynamically to break the N_2–C_3 triple bond and place a lone pair of electrons on N_2. The decrease in V_{N2} is caused both by the density derivative term and by the overlap derivative term, as shown in Figure 9(b). The O_1 atom valence, V_{O1}, increases gradually along the IRC. Because the gross charge of this atom changes little, the electron population of the lone-pair orbital decreases only slightly. This gives rise to the electronic mechanism as described by (II) of the transition state, within the Hartree-Fock scheme of electron density.

The derivative of the O_1 atom valence is dominated by the density derivative term around the transition state. On the contrary, the overlap derivative term becomes the main contributor at the final stage. The density derivative term is counterbalanced by the renormalization term and the relaxation term. Thus, the change in the O_1 atom valence V_{O1} in the final stage is not positive owing to the electron redistribution. In Figures 10 (a) and (b), the contour maps of the density differential with respect to the IRC at TS and at s = 5.5 are shown, respectively. In the final stage around s = 5.5, the density changes represent the formation of the σ-bonds.

Finally we refer to the other relevant study and mention a limitation of the method used in this study. Balawender *et al.*[43] have studied the derivatives of the molecular valence in order to measure the aromaticity of five-membered heterocycles recently. They treated the derivatives of the molecular valence, which consists of the sum of each atom valences, with respect to the electron number N. The derivatives with respect to the IRC are investigated in the present study. We believed that analysis of the variation in the electronic structure along the reaction coordinate is also important.[44,45] It is known well that Mulliken's population analysis gives strange results when diffuse functions are applied in the calculation of the wave function. Some useful localization methods have been introduced to overcome this problem.[46-48] These localization methods may describe the variation of bonds along the reaction coordinate suitably. Our calculation was

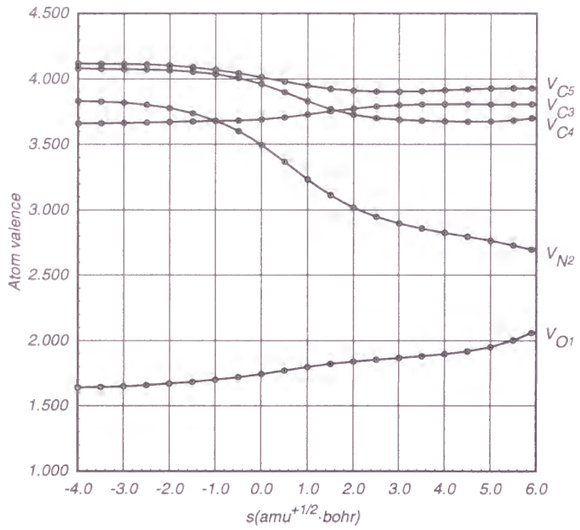

Figure 8. The atom valence profile along the IRC.

(a)

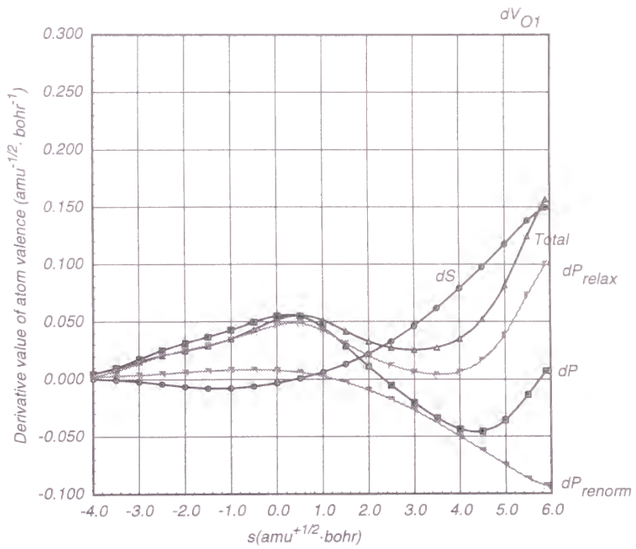

(b)

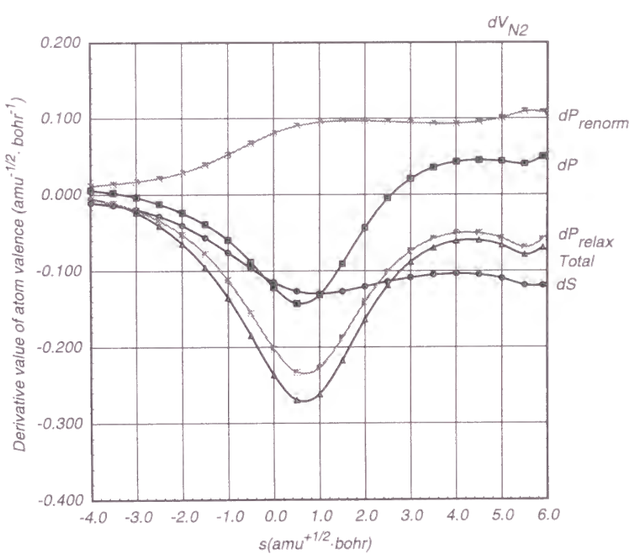

Figure 9. The derivatives of (a) O_1 atom valence and (b) N_2 atom valence with respect to the IRC, respectively.

(a)

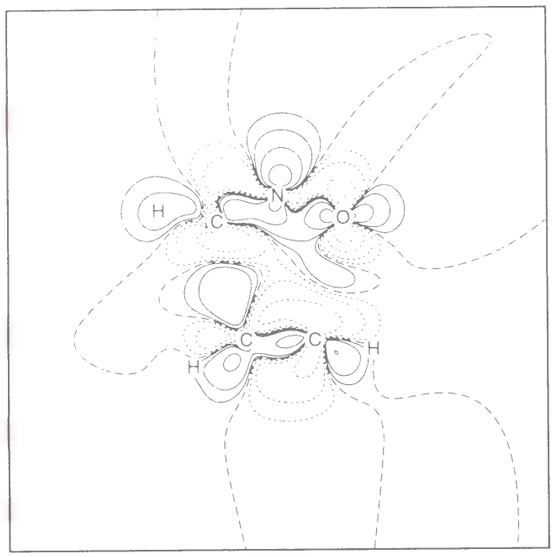

(b)

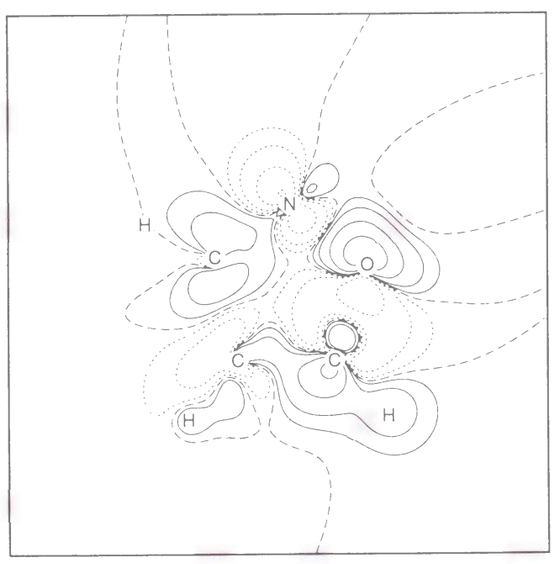

Figure 10. Contour maps of the density differential with respect to the IRC in (a) TS and (b) s=5.5 on the Cs plane. Contours are drawn by solid lines: 0.3, 0.1, 0.03, 0.01, 0.003, and 0.001; dashed line: 0.0; broken lines: -0.001, -0.003, -0.01, -0.03, -0.1, and -0.3.

performed within the Hartree-Fock formalism. It is possible to extend this study, by using wave functions of higher accuracy.[16]

4. Conclusion

The population analysis along the IRC has been investigated. The derivatives of the Mulliken atomic gross charge and the Mayer's bond order with respect to the nuclear motion along the IRC have been calculated analytically. These derivatives have been divided into two components: the derivative term of the density matrix and the derivative term of the overlap matrix. Furthermore, the density derivative term has been shown to be divided into two parts, namely, the renormalization term and the relaxation term. The method has been applied to the 1,3–dipole cycloaddition reaction between fulminic acid and acetylene using the Hartree-Fock electron density. Concerted but non-synchronous bond formation has been described clearly in this analysis.

References

(1) Hehre, W. J.; Radom, L.; Schleyer, P. v. R.; Pople, J. A. *Ab initio Molecular Orbital Theory* ; Wiley: New York, 1986.

(2) Hiberty, P. C.; Leforestier, C. *J. Am. Chem. Soc.* **1978**, *100*, 2012.

(3) Shaik, S. S.; Hiberty, P. C. *Theoretical Models of Chemical Bonding, Part 4,* Maksič, Z. B., Ed.; Springer-Verlag, 1991.

(4) Cooper, D. L.; Gerratt, J.; Raimondi, M. *Chem. Rev.* **1992**, *91*, 929.

(5) Hirao, K.; Nakano, H.; Nakayama, K.; Dupuis, M. *J. Chem. Phys.* **1996**, *105*, 9227.

(6) Thorsteinsson, T.; Cooper, D. L.; Gerrat, J.; Karadakov, P. B.; Raimondi, M. *Theor. Chim. Acta* **1996**, *93*, 343.

(7) Goddard, W. A., III; Dunning, T. H., Jr.; Hunt, W. J.; Hay, P. J. *Acc. Chem. Res.* **1973**, *6*, 368.

(8) Parr, R. G.; Yang, W. *Density Functional Theory of Atoms and Molecules*; Oxford University Press: New York, 1989.

(9) Bader, R. F. W. *Atoms in Molecules–A Quantum Theory*; Oxford University Press: New York, 1990.

(10) Mulliken, R. S. *J. Chem. Phys.* **1955**, *23*, 1833.

(11) Wiberg, K. B. *Tetrahedron* **1968**, *24*,1083.

(12) Giambiagi, M.; de Giambiagi, M. S.; Filho, W. B. *Chem. Phys. Lett.* **1981**, *78*, 541.

(13) Mayer, I. *Chem. Phys. Lett.* **1983**, *97*, 270.

(14) Mayer, I. *Chem. Phys. Lett.* **1984**, *110*, 440.

(15) Mayer, I. *Theor. Chim. Acta* **1985**, *67*, 315.

(16) Mayer, I. *Int. J. Quantum Chem.* **1986**, *29*, 73.

(17) Mayer, I. *Int. J. Quantum Chem.* **1986**, *29*, 477.

(18) Giambiagi, M.; Giambiagi, M. S.; Mundim, K. C. *Struct. Chem.* **1990**, *1*, 123.

(19) Sannigrahi, A. B.; Kar, T. *Chem. Phys. Lett.* **1990**, *173*, 569.

(20) Kar, T.; Marcos, E. S. *Chem. Phys. Lett.* **1992**, *192*, 14.

(21) Giambiagi, M. S.; Giambiagi, M.; Frotes, M. S. *J. Mol. Struct. (THEOCHEM)* **1997**, *391*, 141.

(22) Bochicchio, R. B.; Ponec, R.; Lain, L.; Torre, A. *J. Phys. Chem. A* **1998**, *102*, 7176.

(23) Ponec, R.; Mayer, I. *J. Phys. Chem. A* **1997**, *101*, 1738.

(24) Ángyán, J. G.; Loos, M.; Mayer, I. *J. Phys. Chem.* **1994**, *98*, 5244.

(25) Lendvay, G. *J. Mol. Struct. (THEOCHEM)* **1988**, *167*, 331.

(26) Nakatsuji, H.; Kanda, K.; Yonezawa, T. *J. Chem. Phys.* **1982**, *77*, 1961.

(27) Chandra, A. K.; Nguyen, M. T. *J. Phys. Chem. A* **1998**, *102*, 6181.

(28) Méndez, F.; Tamariz, J.; Geerlings, P. *J. Phys. Chem. A* **1998**, *102*, 6292.

(29) Karadakov, P. B.; Cooper, D. L.; Gerratt, J. *Theor. Chem. Acc.* **1998**, *100*, 222.

(30) (a) Roothaan, C. C. J. *Rev. Mod. Phys.* **1951**, *23*, 69. (b) Hall, G. G. *Proc. Roy. Soc. (London)* **1951**, *A205*, 541.

(31) Pople, J. A.; Krishnam, R.; Schlegel, H. B.: Binkley, J. S. *Int. J. Quantum Chem.* **1979**, *13*, 225.

(32) Gerrat, J.; Mills, I. M. *J. Chem. Phys.* **1968**, *49*, 1719.

(33) Gerrat, J.; Mills, I. M. *J. Chem. Phys.* **1968**, *49*, 1730.

(34) Fukui, K. *Acc. Chem. Res.* **1981**, *14*, 363.

(35) Francl, M. M.; Pietro, W. J.; Hehre, W. J.; Binkley, J. S.; Gordon, M. S.; Defrees, D. J.; Pople, J. A. *J. Chem. Phys.* **1982**, *77*, 3654.

(36) Frisch, M. J.; Trucks, G. W.; Schlegel, H. B.; Gill, P. M. W.; Johnson, B. G.; Robb, M. A.; Cheeseman, J. R.; Keith, T.; Petersson, G. A.; Montgomery, J. A.; Raghavachari, K.; Al-Laham, M. A.; Zakrzewski, V. G.; Ortiz, J. V.; Foresman, J. B.; Cioslowski, J.; Stefanov, B. B.; Nanayakkara, A.; Challacombe, M.; Peng, C. Y.; Ayala, P. Y.; Chen, W.; Wong, M. W.; Andres, J. L.; Replogle, E. S.; Gomperts, R.; Martin, R. L.; Fox, D. J.; Binkley, J. S.; Defrees, D. J.; Baker, J.; Stewart, J. P.; Head-Gordon, M.; Gonzalez, C.; Pople, J. A. *Gaussian 94, Revision D.4*; Gaussian, Inc.: Pittsburgh, PA, 1995.

(37) Gonzalez, C.; Schlegel, H. B. *J. Chem. Phys.* **1989**, *90*, 2154.

(38) Schmidt, M. W.; Baldridge, K. K.; Boatz, J. A.; Elbert, S. T.; Gordon, M. S.; Jensen, J. H.; Koseki, S.; Matsunaga, N.; Nguyen, K. A.; Su, S. J.; Windus, T. L.; Dupuis, M.; Montgomery, J. A. *J. Comput. Chem.* **1993**, *14*, 1347.

(39) Huisgen R. *Angew. Chem.* **1963**, *2*, 565.

(40) Firestone, R. A. *J. Org. Chem.* **1968**, *33*, 2285.

(41) McDouall, J. J.; Robb, M. A.; Niazi, U.; Bernardi, F.; Schlegel, H. B. *J. Am. Chem. Soc.* **1987**, *109*, 4642.

(42) Sosa, C.; Andzelm, J.; Lee, C.; Blake, J. F.; Chenard, B. L.; Butler, T. W. *Int. J. Quantum Chem.* **1994**, *49*, 511.

(43) Balawender, R.; Komorowski, L.; DeProft, F.; Geerlings, P. *J. Phys. Chem. A* **1998**, *102*, 9912.

(44) Tachibana, A.; Parr, R. G. *Int. J. Quantum Chem.* **1992**, *41*, 527.

(45) Tachibana, A.; Nakamura, K.; Sakata, K.; Morisaki, T. *Int. J. Quantum Chem.* **1999**, *74*, 669.

(46) Reed, A. E.; Curtiss, L. A.; Weinhold, F. *Chem. Rev.* **1988**, *88*, 899.

(47) Mayer, I. *Chem. Phys. Lett.* **1995**, *242*, 499.

(48) Mayer, I. *J. Phys. Chem.* **1996**, *100*, 6249.

Chapter 3:

Quantum Chemical Study on Low Energy Reaction Path for $SiH_4 + O(^1D) \rightarrow SiO + 2H_2$

1. Introduction

One of the methods to produce SiO_2 layer over the Si surface is the chemical vapor deposition (CVD) by using oxygen gas and silane gas.[1] A number of relevant reactions have been examined[2-12] and some interesting studies have been published recently.[13-16] But little is known about the mechanism of this oxidation reaction not only on the surface but also in the gas phase. Therefore, we have been applying quantum chemical methods to study these problems. At the first step of a series of these studies, we take up the gas phase reaction between singlet oxygen(^1D) and silane (SiH_4).[17-24] This is because excited oxygen species are considered to be important in the CVD reaction, especially plasma CVD reaction, while the detailed reaction mechanism is not well established. For this reaction, Koda *et al.* observed SiH_3 and OH as the reaction products by means of infrared diode laser kinetic spectroscopy.[25] Recently, Tezaki *et al.* have studied this reaction in more detail by laser-induced fluorescence (LIF):[26]

(1) The overall observed rate constant is $3\times10^{-10}cm^3molecule^{-1}s^{-1}$, which is three times faster than that of methane.

(2) A H atom was detected as one of the products.

(3) A vibrationally excited (to v=11) SiO molecule was detected as a product species, and the rate constant agrees with the pseudo-first order rate constant of O atom decay.

Moreover, vibrational distribution of product SiO in low v regime is distinct from that in high v regime as compared with prior distribution of surprisal analysis.[26] This suggests that a low energy reaction path does exists and plays an important role in addition to the excited state reaction path. We have therefore examined this interesting reaction system $SiH_4 + O(^1D) \rightarrow SiO + 2H_2$ using MP2(fc)/6-31G** level *ab initio* molecular orbital calculations.

2. Methods of Calculation

The calculations were performed with the GAUSSIAN-92[27], -94[28] program packages. Geometries of minima and saddle points have been optimized at the Hartree-Fock level and the second-order Møller-Plesset level (frozen cored)[29-30] with 6-31G** basis set (denoted as HF/6-31G** and MP2(fc)/6-31G**). For all species except for triplet and singlet oxygen atoms, restricted Hartree-Fock (RHF) calculations were performed. And for triplet oxygen atoms, unrestricted Hartree-Fock (UHF) calculations were performed.

For the calculation for singlet oxygen atoms, complex orbitals were used in order to describe a closed-shell singlet atom. Electron correlation calculations were also carried out at the MP2 level.

Harmonic vibrational frequencies and zero-point energies were obtained at the MP2 level for each stationary point. Zero-point energies were scaled by the factor 0.94.[31,32]

3. Results and Discussion

Total energies of all species are listed in Table 1. **TS** denotes transition state of the reaction path as defined in Figure 1. Reaction energies are summarized in Table 2 and the energy diagram in Figure 1. Vibrational frequencies are listed in Table 3.

3.1. $SiH_4 + O(^1D) \rightarrow SiH_3OH$

The title species O(^{1}D) is well known to insert into X–H bonds, such as H–H, C–H, and N–H. Theoretically, the following insertion reactions have been studied: H_2 + O (^{1}D)[33], CH_4 + O(^{1}D).[34,35] In the present reaction system also, we assume that the insertion reaction of O(^{1}D) into Si–H bond occurs and the potential surface for SiH_4 + O (^{1}D) connects to the most stable species silanol (SiH_3OH) with no reaction barrier. Indeed, the reaction is extremely exothermic with reaction energy -175.79kcal/mol, as shown in Figure 1. To check the accuracy of our estimation of reaction energy, we

Table 1: Total Energies, Zero-Point Energies at the HF/6-31G** and the MP2/6-31G** Levels

species		HF/6-31G**	MP2/6-31G**	ZPE
H	(K_h)	-0.49823	–	–
O (^{3}P)	(K_h)	-74.78393	-74.88004	–
O (^{1}D)[a]	(K_h)	-74.69685	-74.80072	–
1 H_2	($D_{\infty h}$)	-1.13133	-1.15766	6.21
2 SiO ($^1\Sigma_g$)	($C_{\infty v}$)	-363.77884	-364.04581	1.58
3 OH	($C_{\infty v}$)	-75.38833	-75.53209	5.18
4 H_2O	(C_{2v})	-76.02362	-76.21979	12.94
5 SiH_2	(C_{2v})	-290.00263	-290.08339	7.30
6 SiH_3	(C_{3v})	-290.61058	-290.69825	13.22
7 SiH_4	(T_d)	-291.23084	-291.33900	19.33
8 SiH_3OH	(C_s)	-366.14192	-366.42677	23.66
9 SiH_2-H_2O	(C_1)	-366.05050	-366.33540	24.14
10 SiH_3O (^{2}A')	(C_s)	-365.50186	-365.73461	16.22
11 SiH_2OH	(C_1)	-365.51709	-365.78281	17.73
12 H_2SiO	(C_{2v})	-364.91752	-365.19933	11.35
13 *cis* -HSiOH	(C_s)	-364.93006	-365.19430	12.54
14 *trans*-HSiOH	(C_s)	-364.93042	-365.19543	12.79
TS-1	(C_1)	-365.98510	-366.29546	21.16
TS-2	(C_1)	-366.00397	-366.30880	21.24
TS-3	(C_s)	-366.00188	-366.31283	21.04
TS-4	(C_s)	-364.75298	-365.05383	8.83
TS-5	(C_1)[b]	-364.79062	-365.10063	8.50
TS-6	(C_1)	-364.91567	-365.17690	11.13
TS-7	(C_s)	-364.83007	-365.12457	9.62
TS-8	(C_1)	-365.99206	-366.29759	22.11
TS-9	(C_1)	-365.99108	-366.29632	21.94
TS-10	(C_1)	-366.00461	-366.30866	21.12

Total energies are in au, and zero-point energies are in kcal/mol. Zero-point energies are computed at the MP2/6-31G** level and scaled by 0.94.

[a] Using complex orbitals.

[b] C_1 symmetry at HF/6-31G**, C_s at MP2/6-31G**.

Table 2: Reaction Energies(kcal/mol)[a]

reaction	activation energy	heat of reaction
$SiH_4 + O(^1D) \rightarrow SiH_3OH$	–	-175.79
$SiH_3OH \rightarrow SiH_4 + O(^3P)$	–	126.02
$SiH_3OH \rightarrow SiH_3 + OH$	–	118.00
$SiH_3OH \rightarrow SiH_3O + H$	–	114.25
$SiH_3OH \rightarrow SiH_2OH + H$	–	85.52
$SiH_3OH \rightarrow SiH_2$-$H_2O$ *complex*	79.91	57.82
$SiH_3OH \rightarrow$ *trans*-HSiOH $+H_2$	71.61	41.57
$SiH_3OH \rightarrow$ *cis*-HSiOH $+H_2$	71.58	42.03
$SiH_3OH \rightarrow H_2SiO + H_2$	68.88	37.69
SiH_2-H_2O *complex* $\rightarrow$ *trans*-HSiOH $+H_2$	21.59	-16.25
SiH_2-H_2O *complex* $\rightarrow$ *cis*-HSiOH $+H_2$	22.22	-15.79
$H_2SiO \rightarrow SiO + H_2$	88.78	-6.16
$H_2SiO \rightarrow$ *trans*-HSiOH	59.08	-3.88
trans-HSiOH $\rightarrow$ *cis*-HSiOH	9.97	0.46
cis-HSiOH $\rightarrow SiO + H_2$	40.84	10.50

[a]At the MP2(fc)/6-31G** level including ZPE(scaled) corrections.

Table 3: Vibrational Frequencies[a]

species	harmonic vibrational frequencies
H_2	4608(σ_g)
SiO	1176(σ_g)
OH	3844(σ_g)
H_2O	1682(a_1), 3892(a_1), 4030(b_2)
SiH_2	1078(a_1), 2168(a_1), 2169(b_2)
SiH_3	821(a_1), 984(e), 984(e), 2317(a_1), 2352(e), 2352(e)
SiH_4	974(t_2), 974(t_2), 974(t_2), 1018(e), 1018(e), 2339(a_1), 2350(t_2), 2350(t_2), 2350(t_2)
SiH_3OH	225(a''), 713(a'), 756(a''),856(a'), 930(a'), 998(a''), 1027(a'), 1073(a'), 2318(a''), 2324(a'), 2375(a'), 3964(a')
SiH_2-H_2O	158, 333, 475, 559, 720, 856,1061,1659,2113,2164,3841,3974
SiH_3O	475(a''), 637(a'), 834(a'), 971(a''), 1002(a'), 1058(a'), 2343(a'), 2357(a''), 2357(a')
SiH_2OH	276, 711, 812, 874, 925, 987, 2274, 2343, 3953
H_2SiO	728(b_1), 728(b_2), 1080(a_1), 1188(a_1), 2341(a_1), 2354(b_2)
cis- HSiOH	687(a''), 761(a'), 872(a'), 1018(a'), 2059(a'), 3909(a')
trans- HSiOH	728(a''), 831(a'), 870(a'), 1004(a'), 2153(a'), 3903(a')
TS-1	1480i, 364, 524, 606, 792, 879, 1043, 1168, 1963, 2270, 2300, 3797
TS-2	1360i, 345, 632, 759, 806, 853, 998, 1136, 1652, 2265, 2369, 3944
TS-3	1524i(a'), 575(a''), 729(a''), 856(a'), 980(a'), 1073(a'), 1182(a'), 1234(a''), 2053(a'), 2232(a'), 2348(a''), 2350(a')
TS-4	2116i(a'), 534(a''), 664(a'), 1118(a'), 1510(a'), 2359(a')
TS-5	1125i(a'), 202(a''), 817(a'), 979(a'), 2090(a'), 2217(a')
TS-6	791i, 308, 904, 918, 2055, 4077
TS-7	1953i(a'), 946(a'), 1028(a'), 1241(a''), 1850(a'), 2071(a')
TS-8	1443i, 578, 626, 744, 916, 984, 1151, 1397, 1938, 1997, 2207, 3864
TS-9	1402i, 551, 623,698, 928, 961, 1125, 1413, 1964, 2000, 2137, 3878
TS-10	1338i, 396, 607, 727, 805, 848, 999,1132,1613, 2274, 2336, 3937

[a]At the MP2/6-31G** level; in cm^{-1}.

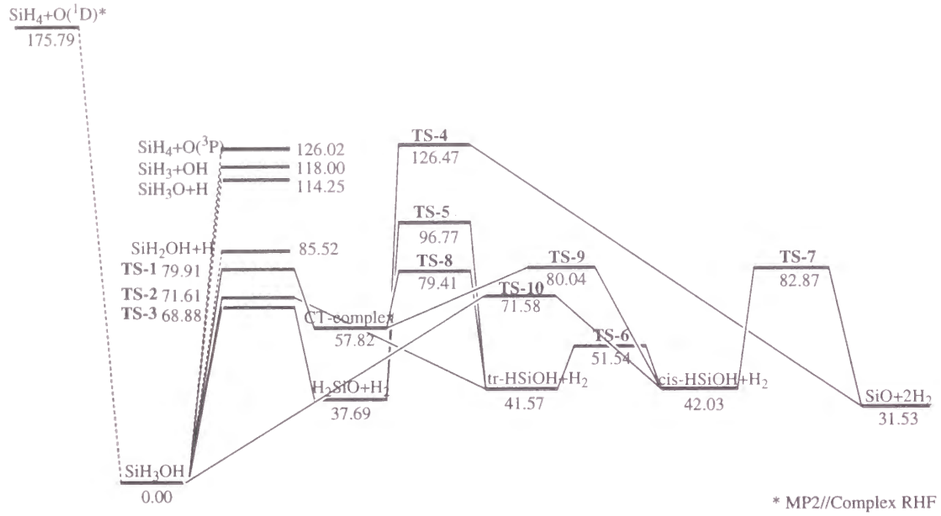

Figure 1. Energy diagram at the MP2(fc)/6-31G** level including ZPE(scaled).

examined the $O(^3P) \leftrightarrow O(^1D)$ splitting energy: our estimate is 49.76kcal/mol at the MP2 level, and the experimental value is 45.37 kcal/mol[36]. both being in good agreement.

We further assume that this silanol is decomposed into many species, as described below.

3.2. SiH_3OH Decomposition

Thermal decomposition reaction paths of SiH_3OH are considered as follows:

$$SiH_3OH \rightarrow SiH_3 + OH \quad (1)$$

$$SiH_3OH \rightarrow SiH_3O + H \quad (2)$$

$$SiH_3OH \rightarrow SiH_2OH + H \quad (3)$$

$$SiH_3OH \rightarrow \textbf{TS-1} \rightarrow SiH_2\text{-}H_2O \text{ complex} \quad (4)$$

$$SiH_3OH \rightarrow \textbf{TS-2} \rightarrow \textit{trans}\text{-}HSiOH + H_2 \quad (5)$$

$$SiH_3OH \rightarrow \textbf{TS-3} \rightarrow H_2SiO + H_2 \quad (6)$$

SiH_3 and OH were detected by Koda and Suga by the time-resolved infrared-diode laser absorption technique.[25] H atoms were detected by Tezaki *et al.* by laser-induced fluorescence.[26] These species are considered to be decomposed from SiH_3OH as in reactions (1), (2), and (3). Energy diagrams of Figure 1 show that the reactions of SiH_4 + $O(^1D)$ leading to these products are exothermic, so that these homolytic reaction paths are considered main reaction channels. The barrier height of the reactions (4), (5), and (6) is 79.91kcal/mol (**TS-1**), 71.10 kcal/mol(**TS-2**), and 68.88 kcal/mol(**TS-3**), respectively, in agreement with higher level calculations by MP4/MC-311G(d,p)//MP2/6-31G(d,p).[2]

3.3. $H_2SiO \rightarrow SiO + 2H_2$

The unimolecular decomposition of silanone H_2SiO has been investigated by Kudo and Nagase[3] and our group.[4] A series of reaction pathways are as follows:

$$H_2SiO \rightarrow \textbf{TS-4} \rightarrow SiO + H_2 \quad (7)$$

$$H_2SiO \rightarrow \textbf{TS-5} \rightarrow \textit{trans}\text{-}HSiOH + H_2 \quad (8)$$

$$\textit{trans}\text{-}HSiOH \rightarrow \textbf{TS-6} \rightarrow \textit{cis}\text{-}HSiOH \quad (9)$$

$$\textit{cis}\text{-}HSiOH \rightarrow \textbf{TS-7} \rightarrow SiO + H_2 \quad (10)$$

One channel is direct decomposition (7) through **TS-4** and another channel is via rearrangement channel (8)→(9)→(10) through **TS-5**, **TS-6** and **TS-7**. Reaction (7) has high energy barrier of 88.78 kcal/mol and hence is of little importance. While the rearrangement channel (8)→(9)→(10) proceeds easily as found in Figure 1. In reaction (9), **TS-6** was found to have C_1 symmetry at the HF/6-31G** level, while C_s symmetry at the MP2/6-31G** level.[37]

3.4. H_2Si-H_2O Complex→ cis- or trans- HSiOH

Although the favorable reaction path of SiH_3OH is H_2 elimination leading to *trans*-HSiOH or H_2SiO, yet we propose the path to the SiH_2-H_2O complex is considerably important. The H_2Si-H_2O complex has been considered a precursor of the reaction of $SiH_2 + H_2O$ leading to SiH_3OH so far.[8-10] Zachariah and Thang considered that in the $SiH_2 + H_2O$ reaction this CT complex forms at first, and then rearrangement of H atom to silanol occurs.[16] In case of singlet carben, this kind of CT complex is not on the reaction coordinate of $CH_2 + H_2O$[38-41], so it is considered important in case of silicon compounds. Indeed, in our present study, it is confirmed to stay on the reaction surface by HF/6-31G** level calculations of the intrinsic reaction coordinate (IRC) starting from **TS-1**, as shown in Figure 1.

We propose a new reaction path of this CT complex leading directly to *cis*- or *trans*- HSiOH, not via formation of H_2SiO:

$$H_2Si\text{-}H_2O \text{ complex} \rightarrow \textbf{TS-8} \rightarrow \textit{trans}\text{- HSiOH} + H_2 \qquad (11)$$

$$H_2Si\text{-}H_2O \text{ complex} \rightarrow \textbf{TS-9} \rightarrow \textit{cis}\text{- HSiOH} + H_2 \qquad (12)$$

The products *trans*-HSiOH + H_2 and *cis*-HSiOH + H_2 are 41.57, 42.03 kcal/mol higher in energy than silanol, but the barriers of these reactions are considerably lower: 21.59 kcal/mol for **TS-8**, 22.22 kcal/mol for **TS-9**. As shown in Figure 1, these reactions are likely to occur. Figure 2 shows the structure of **TS-9** for the transition state of the reaction (12). The imaginary frequency of this transition state is $1443i$ cm^{-1} as shown in Table 3. The imaginary vibrational mode corresponds to H_2 elimination. The reaction paths are interpreted in terms of classical valence bond theory as follows.

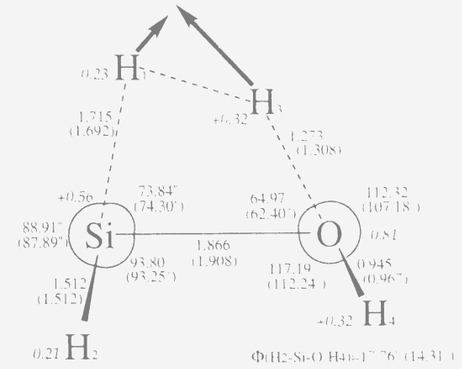

TS-9

Figure 2. Optimized geometry of **TS-9** at the HF/6-31G** level. Bond lengths are in angstroms and bond angles and dihedral angles are in degrees. MP2 level optimized data are in parentheses. The atomic charges are in italics. Arrows show the imaginary vibrational mode.

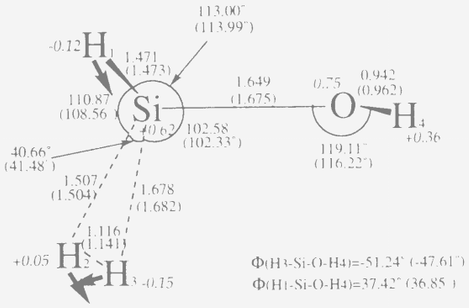

TS-10

Figure 3. Optimized geometry of **TS-10** at the HF/6-31G** level. For details, see caption of Figure 2.

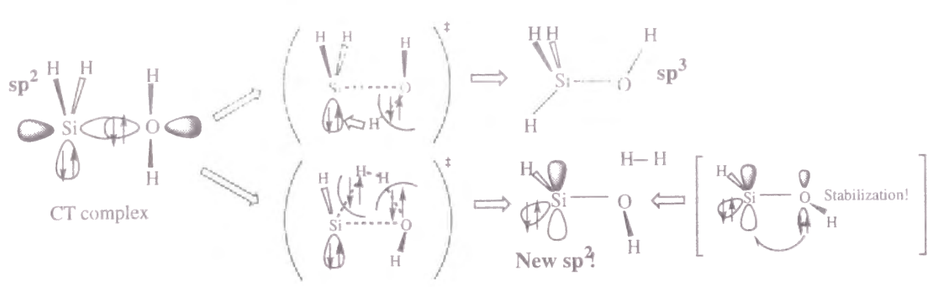

The H_2Si-H_2O complex forms through a donor-acceptor CT interaction between a lone–pair orbital in H_2O and an empty p orbital in SiH_2. In this complex, the H atom bonded to the Si atom has a hydride-ion-like character (whose atomic charge is calculated to be -0.215 on the average), while a H atom bonded to the O atom has a proton-like character (whose atomic charge is calculated to be +0.39). Here, if the proton-like H moves over to the silylene lone–pair orbital, then new sp^3 bond is formed. This is the 1,2-hydrogen shift reaction like the reaction path of silylene derivatives, such as dimethyl silylene. On the other hand, if the proton-like H attacks the hydride-ion-like H, then a H_2 molecule is formed. The resulting new sp^2 type vacant orbital of Si is stabilized by hyperconjugation of the oxygen lone–pair orbital.[42] It is interesting to observe that the barrier heights for these two reaction paths are comparable.

The additional reaction path that directly leads to *cis*-HSiOH is found as follows:

$$SiH_3OH \rightarrow \textbf{TS-10} \rightarrow \textit{cis}\text{-HSiOH} + H_2 \qquad (13)$$

Figure 3 shows the structure of **TS-10** for transition state of the reaction (13).

3.5. General View

The low energy reaction paths examined in this paper are here summarized. Silanol proceeds to $SiO + 2H_2$ through the following reaction channels:

(6) **TS-3** → (8) **TS-5** → (9) **TS-6** → (10) **TS-7** (Channel 1)

(5) **TS-2** → (9) **TS-6** → (10) **TS-7** (Channel 2)

(4) **TS-1** → (12) **TS-9** → (10) **TS-7** (Channel 3)

(13) **TS-10** → (10) **TS-7** (Channel 4)

All channels are possible candidates as low energy processes as shown in Figure 1. Channel 4 is probably the easiest to occur. Elimination reaction of two H_2 molecules can occur through these low energy processes.

4. Conclusion

We studied the reaction mechanism of $SiH_4 + O(^1D)$. Applying a quantum chemical method, a low energy reaction path is found in addition to the excited state reaction path. This agrees well with the experimental observation on the vibrational energy distribution of product SiO by laser-induced fluorescence (LIF).

References

(1) Jasinski, J. M.; Gates, S. M. *Acc. Chem. Res.* **1991**, *24*, 9.

(2) Gordon, M. S.; Pederson, L. A. *J. Phys. Chem.* **1990**, *94*, 5527.

(3) Kudo, T.; Nagase, S. *J. Phys. Chem.* **1984**, *88*, 2833.

(4) Tachibana, A.; Fueno, H.; Yamabe, T. *J. Am. Chem. Soc.* **1986**, *108*, 4346.

(5) Ma, B.; Schaefer, H. F., III *J. Chem. Phys.* **1994**, *101*, 2734.

(6) Tachibana, A.; Koizumi, M.; Teramae, H.; Yamabe, T. *J. Am. Chem. Soc.* **1987**, *109*, 1383.

(7) Sakai, S.; Gordon, M. S.; Jordan, K. *J. Phys. Chem.* **1988**, *92*, 7053.

(8) Raghavachari, K.; Chandrasekhar, J.; Frisch, M. J. *J. Am. Chem. Soc.* **1982**, *104*, 3779.

(9) Raghavachari, K.; Chandrasekhar, J.; Gordon, M. S.; Dykema, K. *J. Am. Chem. Soc.* **1984**, *106*, 5853.

(10) Su, S.; Gordon, M. S. *Chem. Phys. Lett.* **1993**, *204*, 306.

(11) Nagase, S.; Kudo, T.; Akasaka, T.; Ando, W. *Chem. Phys. Lett.* **1989**, *163*, 23.

(12) Akasaka, T.; Nagase, S.; Yabe, A.; Ando, W. *J. Am. Chem. Soc.* **1988**, *110*, 6270.

(13) Lucas, D. J.; Curtiss, L.; Pople, J. A. *J. Chem. Phys.* **1993**, *99*, 6697.

(14) Darling, C. L.; Schlegel, H. B. *J. Phys. Chem.* **1993**, *97*, 8207.

(15) Darling, C. L.; Schlegel, H. B. *J. Phys. Chem.* **1994**, *98*, 8910.

(16) Zachariah, M. R.; Thang, W. *J. Phys. Chem.* **1995**, *99*, 5308.

(17) Ding, L.; Marshall, P. *J. Chem. Phys.* **1993**, *98*, 8545.

(18) Park, C. R.; White, G. D.; Wiesenfeld, J. R. *J. Phys. Chem.* **1988**, *92*, 152.

(19) Agrawalla, B. S.; Setser, D. W. *J. Chem. Phys.* **1987**, *86*, 5421.

(20) Horrie, O.; Taega, R.; Riemann, B.; Arthur, N. L.; Potzinger, P. *J. Phys. Chem.* **1991**, *95*, 4393.

(21) Sugawara, K.; Nakanaga, T.; Takeo, H.; Matsumura, C. *Chem. Phys. Lett.* **1989**, *157*, 309.

(22) Slagle, I. R.; Bernhardt, J. R.; Gutman, D. *Chem. Phys. Lett.* **1988**, *149*, 180.

(23) Koshi, M.; Miyoshi, A.; Matsui, H. *J. Phys. Chem.* **1991**, *95*, 9869.

(24) Koda, S. *Prog. Energy Comust. Sci.* **1992**, *18*, 513.

(25) Koda, S.; Suga, S. *Chem. Phys. Lett.* **1989**, *161*, 35.

(26) Tezaki, A. *et al.*, private communication.

(27) Frisch, M. J.; Trucks, G. W.; Head-Gordon, M.; Gill, P. M. W.; Wong, M. W.; Foresman, J. B.; Johnson, B. G.; Schlegel, H. B.; Robb, M. A.; Replogle, E. S.; Gomperts, R.; Andres, J. L.; Raghavachari, K.; Binkley, J. S.; Gonzalez, C.; Martin, R. L.; Fox, D. J.; Defrees, D. J.; Baker, J.; Stewart, J. J. P.; Pople, J. A. *Gaussian 92*; Gaussian, Inc.: Pittsburgh, PA, 1992.

(28) Frisch, M. J.; Trucks, G. W.; Schlegel, H. B.; Gill, P. M. W.; Johnson, B. G.; Robb, M. A.; Cheeseman, J. R.; Keith, T.; Petersson, G. A.; Montgomery, J. A.; Raghavachari, K.; Al-Laham, M. A.; Zakrzewski, V. G.; Ortiz, J. V.; Foresman, J. B.; Peng, C. Y.; Ayala, P. A.; Chen, W.; Wong, M. W.; Andres, J. L.; Replogle, E. S.; Gomperts, R.; Martin, R. L.; Fox, D. J.; Binkley, J. S.; Defrees, D. J.; Baker, J.; Stewart, J. P.; Head-Gordon, M.; Gonzalez, C.; Pople, J. A. *Gaussian 94, Revision B.3*; Gaussian, Inc.: Pittsburgh, PA, 1995.

(29) Møller, C.; Plesset, M. S. *Phys. Rev.* **1934**, *46*, 618.

(30) Binkley, J. S.; Pople, J. A. *Int. J. Quantum Chem.* **1975**, *9*, 229.

(31) Hehre, W.; Radom, L.; Schleyer, P. v. R.; Pople, J. A. *Ab initio Molecular Orbital Theory*; Wiley: New York, 1986.

(32) Pople, J. A.; Scott, A. P.; Wong, M. W.; Radom, L. *Israel J. Chem.* **1993**, *33*, 345.

(33) Fitzcharles, M. S.; Schatz, G. C. *J. Phys. Chem.* **1986**, *90*, 3634.

(34) Nakajima, M.; Tsuda, M.; Oikawa, S. *Chem. Pharm. Bull.* **1987**, *35*, 941.

(35) Arai, H.; Kato, S.; Koda, S. *J. Phys. Chem.* **1994**, *98*, 12.

(36) Baskin, S.; Stroner, J. O., Jr. *Atomic Energy Levels and Grotrian Diagrams Vol. 1*; North Holland, 1975.

(37) Taketsugu, T.; Hirano, T. *J. Chem. Phys.* **1993**, *99* , 9806.

(38) Pople, J. A.; Raghavachari, K.; Frisch, M. J.; Binkley, J. S.; Schleyer, P. v. R. *J. Am. Chem. Soc.* **1983**, *105*, 6389.

(39) Harding, L. B.; Schlegel, H. B.; Krishnan, R.; Pople, J. A. *J. Phys. Chem.* **1980**, *84*, 3394.

(40) Eades, R. A.; Gassman, P. G. ; Dixon, D. A. *J. Am. Chem. Soc.* **1981**, *103*, 1066.

(41) Walch, S. P. *J. Chem. Phys.* **1993**, *98*, 3163.

(42) Luke, B. T.; Pople, J. A.; Krogh-Jespersen, M.-B.; Apeloig, Y.; Karni, M.; Chandrasekhar, J.; Schleyer, P. v. R. *J. Am. Chem. Soc.* **1986**, *108*, 270.

Chapter 4:

Quantum Chemical Study of the Oxidation Sites in Hydrogen- and Water- Terminated Si Dimers: Attempt to Understand the Si–Si Back-Bond Oxidation on the Si Surface

1. Introduction

A thorough understanding of the silicon surface oxidation processes both scientifically and technologically is significant because of the necessity to control the formation of atomic-scale structures at the Si/SiO_2 interface for application to ultralarge-scale integrated circuits. As a matter of fact, fine control of Si/SiO_2 interface electronic characteristics has become a crucial problem since the oxide layer thickness must be reduced due to the demand of further reduction of the device size. The attempt to have an appropriate understanding of silicon surface oxidation in order to control atomic-scale structures at the interface has just begun.

From a historical point of view, not only experimental studies[1,2] but also many interesting theoretical studies were made.[3-14] For example, Goddard III *et al.* studied the chemisorption of an oxygen molecule on a silicon surface using the generalized valence bond (GVB) method.[3] They treated a $Si_3H_6O_2$ complex, which was used to describe the O_2 molecule chemisorbed on a Si_3H_6 surface cluster model. They concluded that the chemisorbed O_2 in the initial stage is a peroxy radical. Moreover, they postulated that a local electronic excitation would lead to the subsequent formation of normal SiO_2-like structure.

Schubert *et al.* studied the initial stages of oxidation of the Si(111)-7×7 surface using extended Hückel tight-binding calculations.[4,5] They noted that the most reactive site was the adatom in the Takayanagi model, or dimer adatom stacking fault (DAS) model of a Si(111)-7×7 surface when O_2 molecule interacts with a silicon surface.[4] As a result, they found that the major stable precursors were of the chemisorbed peroxy radical type attached to one Si adatom (which Goddard III *et al.* studied).

Next,[5] they studied the pathways involved in converting the initial precursors into SiO_4 units and compared the calculated density of states (DOS) with the X-ray photoemission spectroscopy (XPS) and ultraviolet photoemission spectroscopy (UPS) experimental data. Once the initial precursors are inserted into the Si–Si back bond, an

O_2 molecule can be inserted into the adjacent Si–Si back bonds to form a normal SiO_4 unit.

On the other hand, Uchiyama and Tsukada investigated the stable structures of oxygen-adsorbed Si(001) surfaces by first principles molecular dynamics and found that back-bond site adsorption was more stable than dimer bond adsorption energetically and that the band structures of surfaces were different because the electronegativity of oxygen enhanced the ionicity of the dimer bond.[12,13] Recently Kato *et al.* studied the oxidation of the Si(001) surface and clarified that the back-bond oxidation of the Si surface by O_2 proceeds with no barrier height.[14]

In this study, we investigate the stabilities of both Si–O–Si and Si–O–H bonds in molecules. First, we examine the reactions of disilane Si_2H_6 with O_2:

$$SiH_3SiH_3 + O_2(^3\Sigma_g) \rightarrow SiH_3SiH(OH)_2 \quad (1)$$

$$SiH_3SiH_3 + O_2(^3\Sigma_g) \rightarrow SiH_3\text{-}O\text{-}SiH_2(OH) \quad (2)$$

We show that the Si–O–Si bond is more stable than the Si–O–H bonds in a small molecule. Next, we note the reaction of $SiH_3SiH_2(OH)$ with H as one of the reactions involved in forming a Si–O–Si bond or a Si–O–H bond. This reaction starts with hydrogen abstraction by exposing a hydrogen atom to make an oxygen radical center:

$$SiH_3SiH_2OH + H \rightarrow SiH_3SiH_2O + H_2. \quad (3)$$

Then oxygen is inserted into a Si–Si back bond:

$$SiH_3SiH_2O \rightarrow SiH_3\text{-}O\text{-}SiH_2. \quad (4)$$

Moreover, another reaction is considered:

$$SiH_3SiH_2O \rightarrow SiH_3SiH(OH). \quad (5)$$

On the basis of these results, we discuss the surface oxidation mechanisms in relation to local reaction site character.

2. Methods of Calculation

MO calculations were performed using the GAUSSIAN94[15] program packages. The geometries were optimized by the analytical energy gradient method at the Hartree-Fock (HF) level and the second-order Møller-Plesset (MP) perturbation theory[16,17] that includes correlation for all electrons, using the standard 6-31G** basis set (denoted as HF/6-31G** and MP2(full)/6-31G**).[18] In HF calculations, the spin-restricted HF (RHF) method was used for closed-shell singlet states, and the spin-unrestricted HF (UHF) method was used for open-shell doublet states. Theoretical harmonic vibrational frequencies were obtained from analytical second derivatives calculated at the MP2(full)/6-31G** level. Zero-point vibrational energies (ZPE) were then scaled by a factor of 0.94.[19] To obtain higher correlation energies, single point calculations were made by the third-order Møller-Plesset perturbation theory (MP3) and the single and double substituted configuration interaction (CISD) method.[20] In CISD calculations, an unlinked cluster quadruple correction (QC) was added for size-consistency correction [denoted as CISD(full)+QC].[21] The Mulliken atomic charge was calculated using the self-consistent field (SCF) density at the MP2(full)/6-31G** level optimized geometry.[22]

3. Results and Discussion

The total energies of the species are listed in Table 1 and the vibrational frequencies of these, in Table 2. Figure 1 shows some of the species. **TSn** denotes the transition state of reaction(n) (n = 3, 4, 5). Reaction energies are summarized in Tables 3 and 4 and the energy diagrams in Figures 2 and 3.

3.1. Reactions of Si_2H_6 with O_2

3.1.1. Optimized Structures Before we studied $SiH_3SiH(OH)_2$ **7**, we investigated the simple dihydroxy molecule $SiH_2(OH)_2$ because dihydroxy silane $SiH_2(OH)_2$ has been studied by many researchers due to its anomeric effects[23-25] and simplicity for use as a model for silicone polymers and for silicates.[26,27] It was reported that there are less anomeric effects in silicon compounds than in carbon compounds. As demonstrated in Figure 1, we considered two structures for $SiH_2(OH)_2$. One of them, **4**, maintains C_2 symmetry and the other, **5**, has C_s symmetry. Reed *et al.*[23] reported that the C_s symmetry

Table 1: Total Energies (au)

species		HF	$\langle s^2 \rangle$	MP2(full)	$\langle s^2 \rangle^a$	MP3(full) //MP2(full)	CISD+QC(full) //MP2(full)
H		-0.49823	0.750				
1 H_2		-1.13133		-1.15766		-1.16316	-1.16514
2 $O_2(^3\Sigma_g)$		-149.61791	2.032	-149.95432	2.037	-149.94558	-149.95958
3 SiH_4		-291.23084		-291.34986		-291.37067	-291.37821
4 $SiH_2(OH)_2$	(C_2)	-441.06520		-441.54677		-441.55999	-441.57092
5 $SiH_2(OH)_2$	(C_s)	-441.06266		-441.54409		-441.55739	-441.56829
6 H_3SiSiH_3		-581.31357		-581.53462		-581.57062	-581.58311
7 $H_3SiSiH(OH)_2$	(C_s)	-731.14175		-731.72610		-731.75382	-731.76783
8 $H_3Si\text{-}O\text{-}SiH_2(OH)$		-731.18997		-731.77206		-731.79683	-731.81180
9 SiH_3SiH_2OH	(C_s)	-656.22253		-656.62421		-656.65619	-656.66967
10 $SiH_3SiH_2O(^2A')$	(C_s)	-655.58454	0.758	-655.93507	0.759	-655.97431	-655.99022
11 $SiH_3SiH_2O(^2A'')$	(C_s)	-655.58166	0.756	-655.93028	0.757	-655.97011	-655.98488
12 $SiH_3\text{-}O\text{-}SiH_2(^2A')$	(C_s)	-655.64287	0.753	-656.02252	0.753	-656.04748	-656.06186
13 $SiH_3\text{-}O\text{-}SiH_2$	(C_1)	-655.64289	0.753	-656.02277	0.753	-656.04767	-656.06212
14 $SiH_3SiH(OH)$	(C_1)	-655.60210	0.755	-655.98424	0.755	-656.01282	-656.02655
TS3$(^2A')$	(C_s)	-656.67542	0.794	-657.07602	0.781	-657.11645	-657.13580
TS4$(^2A')$	(C_s)	-655.55302	0.784	-655.93097	0.770	-655.96698	-655.98654
TS5	(C_1)	-655.50970	0.811	-655.89384	0.765	-655.92555	-655.94520

[a]Expectation values of spin-squared operater before spin-annihilation of SCF.

Table 2: Vibrational Frequencies at the MP2(full)/6-31G** Level[a]

species	harmonic vibrational frequency (cm^{-1})	ZPE[a]
1	4609(σ_g)	6.21
2	1412(σ_g)	1.90
3	974(t_2), 1018(e), 2347(a_1), 2360(t_2)	19.39
4	257(a), 314(b), 391(a), 638(b), 787(a), 837(a), 902(b), 920(a), 958(b), 1020(a), 1023(b), 2377(a), 2383(b), 3955(b), 3957(a)	27.92
5	91(a''), 285(a'), 349(a'), 624(a'), 762(a''), 830(a'), 894(a''), 937(a'), 945(a''), 1012(a'), 1030(a''), 2318(a'), 2429(a'), 3971(a''), 3972(a')	27.56
6	146(a_{1u}), 384(e_u), 460(a_{1g}), 667(e_g), 901(a_{2u}), 980(a_{1g}), 985(e_g), 1002(e_u), 2318(a_{2u}), 2327(a_{1g}), 2333(e_g), 2341(e_u)	30.40
7	102(a''), 110(a''), 172(a''), 199(a'), 279(a'), 361(a'), 455(a'), 556(a'), 560(a''), 761(a'), 798(a''), 814(a'), 900(a''), 926(a'), 977(a''), 994(a'), 999(a'), 1000(a''), 2284(a'), 2325(a'), 2336(a''), 2343(a'), 3946(a''), 3947(a')	37.93
8	35, 69, 97, 269, 363, 616, 670, 760, 766, 816, 869, 930, 987, 1011, 1019, 1031, 1070, 1111, 2344, 2350, 2365, 2370, 2391, 3958	38.09
9	117(a''), 164(a'), 228(a''), 393(a''), 450(a'), 549(a'), 659(a''), 772(a''), 825(a'), 856(a'), 924(a'), 988(a'), 990(a''), 1014(a'), 1041(a'), 2302(a'), 2304(a''), 2322(a'), 2335(a'), 2342(a''), 3943(a')	34.39
10	112(a''), 144(a'), 377(a''), 441(a'), 515(a'), 631(a''), 680(a''), 817(a'), 847(a'), 931(a'), 989(a'), 989(a''), 1045(a'), 2325(a'), 2337(a'), 2341(a''), 2349(a'), 2359(a'')	27.26
11	113(a''), 163(a'), 378(a''), 444(a'), 545(a'), 662(a''), 798(a'), 841(a''), 891(a'), 932(a'), 983(a'), 989(a''), 991(a'), 2315(a'), 2327(a'), 2330(a''), 2338(a'), 2344(a'')	27.47
12	52i(a''), 37(a''), 89(a'), 590(a'), 741(a''), 759(a''), 760(a'), 850(a'), 991(a'), 1013(a''), 1017(a'), 1060(a'), 1135(a'), 2303(a'), 2332(a''), 2343(a'), 2359(a'), 2359(a'')	27.95
13	49, 68, 102, 606, 734, 759, 772, 846, 984, 1011, 1016, 1054, 1113, 2294, 2336, 2344, 2346, 2372	28.04
14	110, 157, 203, 432, 454, 552, 685, 791, 836, 915, 953, 986, 994, 2261, 2318, 2332, 2344, 3938	28.66
TS3	1859i(a'), 115(a''), 136(a'), 141(a''), 331(a'), 403(a''), 450(a'), 542(a'), 646(a''), 658(a''), 752(a''), 802(a'), 840(a'), 887(a'), 947(a'), 989(a''), 989(a'), 1041(a'), 2319(a'), 2327(a'), 2330(a''), 2344(a'), 2354(a''), 2504(a')	33.49
TS4	282i(a'), 127(a''), 393(a''), 393(a'), 457(a'), 615(a''), 686(a'), 706(a''), 887(a'), 946(a'), 984(a'), 1000(a''), 1061(a'), 2298(a'), 2340(a'), 2352(a''), 2368(a'), 2389(a'')	26.96
TS5	1747i, 84, 179, 359, 436, 545, 577, 703, 866, 916, 949, 985, 989, 2033, 2310, 2328, 2341, 2360	25.55

[a]ZPE (kcal/mol) scaled by 0.94.

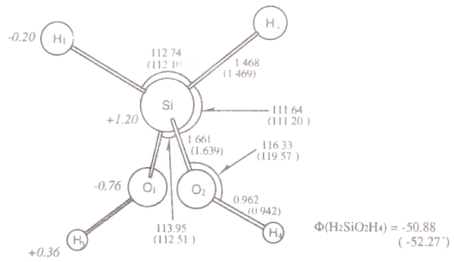

4 (C_2)

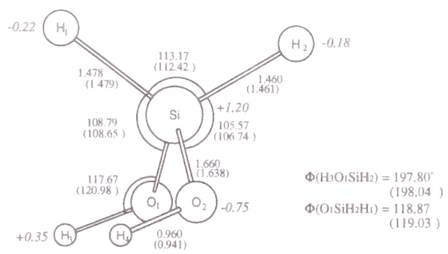

5 (C_s)

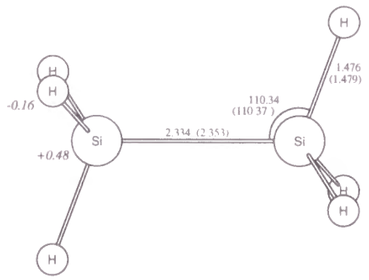

6 (D_{3d})

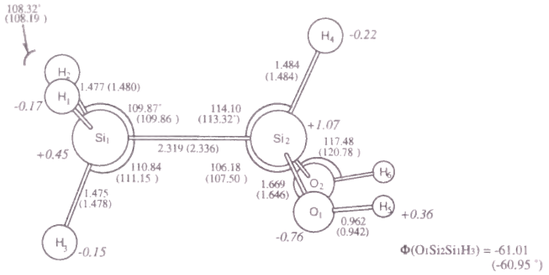

7 (C_s)

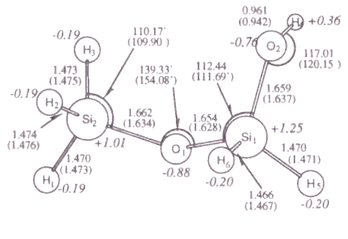

8 (C_1)

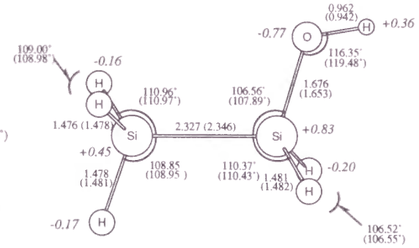

9 (C_s)

Figure 1. Optimized geometries of some species at the MP2(full)/6-31G** level. Bond lengths are in angstroms and bond angles and dihedral angles are in degrees. HF level optimized data are in parentheses. The Mulliken atomic charges are in italics. The spin densities are in gothic. Arrows in **TSn** show movement of nuclei along the imaginary vibrational mode.

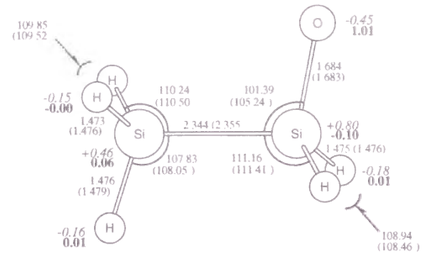

10(^{2}A') (C_s)

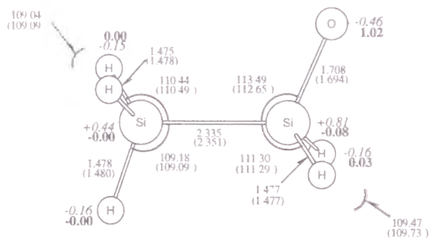

11 (^{2}A") (C_s)

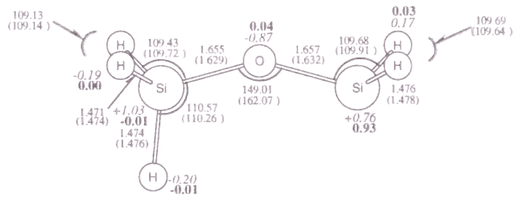

12 (C_s)

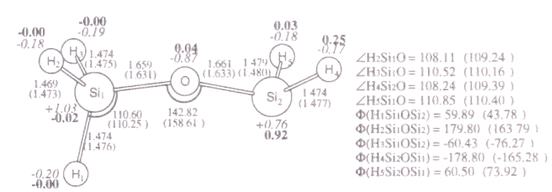

13 (C_1)

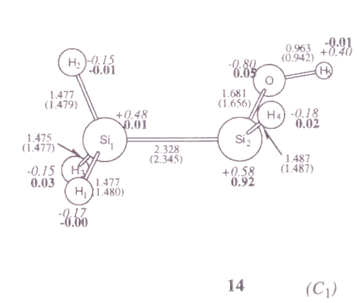

14 (C_1)

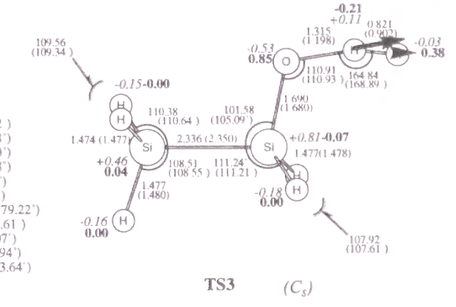

TS3 (C_s)

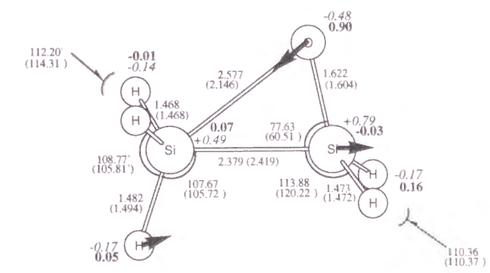

TS4 (C_s)

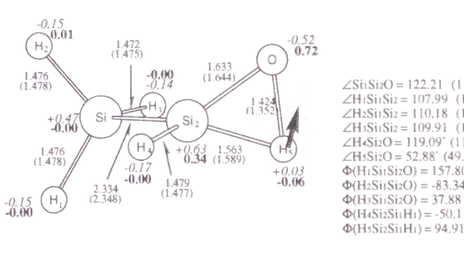

TS5 (C_1)

Figure 1. *(Continued from the previous page.)*

Table 3: Reaction Energies

reaction		heat of reaction in kcal/mol[a] (eV)		
		MP2(full)	MP3(full)	CISD(full)+QC
$SiH_3SiH_3 + O_2(^3\Sigma_g) \rightarrow SiH_3SiH(OH)_2$	(1)	-143.19 (-6.21)	-143.48 (-6.22)	-135.65 (-5.88)
$SiH_3SiH_3 + O_2(^3\Sigma_g) \rightarrow SiH_3\text{-}O\text{-}SiH_2(OH)$	(2)	-171.87 (-7.45)	-170.31 (-7.39)	-163.08 (-7.07)

[a]Including ZPE(scaled) at the MP2(full)/6-31G** level.

Table 4: Reaction Energies in kcal/mol (eV in parentheses)

reaction		activation energy[a] /heat of reaction[a]		
		MP2(full)	MP3(full)	CISD(full)+QC
$SiH_3SiH_2OH + H \rightarrow SiH_3SiH_2O(^2A') + H_2$	(3)	28.23 (1.22)	22.93 (0.99)	19.24 (0.83)
		/17.72 (0.77)	/9.72 (0.42)	/6.95 (0.30)
$SiH_3SiH_2O(^2A') \rightarrow SiH_3OSiH_2(C_1)$	(4)	2.27 (0.10)	4.30 (0.19)	2.01 (0.09)
		/-54.25 (-2.35)	/-45.25 (-1.96)	/-44.34 (-1.92)
$SiH_3SiH_2O(^2A') \rightarrow SiH_3SiH(OH)(C_1)$	(5)	24.16 (1.05)	28.89 (1.25)	26.54 (1.16)
		/-29.45 (-1.28)	/-22.77 (-0.99)	/-21.40 (-0.93)

[a]Including ZPE(scaled) at the MP2(full)/6-31G** level.

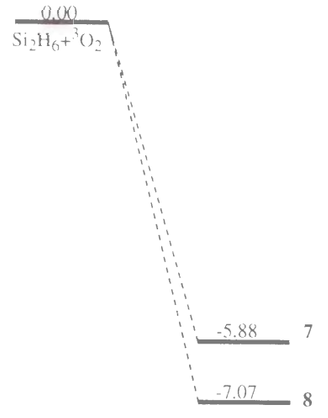

Figure 2. Energy diagram (in eV) at the CISD(full)/6-31G** level including ZPE (scaled by 0.94).

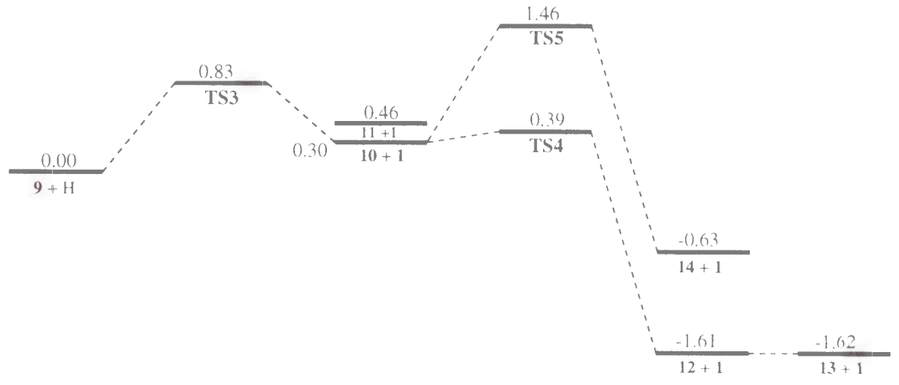

Figure 3. Energy diagram (in eV) at the CISD(full)/6-31G** level including ZPE (scaled by 0.94).

structure is 2.16 kcal/mol more stable than the C_2 symmetry structure in MP2/6-31G*//HF/3-21G(*) level calculation. However, **4** is 1.29 kcal/mol more stable than **5** in our CISD/6-31G**//MP2/6-31G** level(+ZPE) calculation. This energy difference is so small that the H atom of the hydroxy group is easy to move.

$SiH_3SiH(OH)_2$ **7** has C_S symmetry as depicted in Figure 1. It corresponds to **5** in $SiH_2(OH)_2$ with respect to the hydroxyl combination. Another structure corresponding to **4** could not be optimized at the HF/6-31G** level, although it was optimized at the HF/STO-3G level. Comparing $SiH_3SiH(OH)_2$ **7** with SiH_3SiH_3 **6**, the Si–Si bond length is shorter in **7** due to hydroxyl groups, whereas the Si–H bond length is longer.

SiH_3-O-SiH_2(OH) **8** has C_1 symmetry as shown in Figure 1, due to the repulsive O–O interaction induced by polarization effects. It was reported that the Si–O–Si bond is very flexible and has a shallow potential surface in SiH_3-O-SiH_3.[28-33] Moreover, **4** and **7** show that their Si–O–H bonds have the same character. In the same manner, **8** has a very shallow potential surface, which is proved by the low vibrational frequencies listed in Table 2.

3.1.2. Reaction Energies We consider the reaction energies of (1) and (2). From Table 3, we find that these reactions are highly exothermic. The oxidized layer on the silicon surface is strongly stabilized if lattice strain is fully relaxed. Moreover, we compare the reaction energy of (1) with that of (2). The difference is 27.43kcal/mol and is very large. It shows that the Si–O–Si bond is more stable than the Si–O–H bond.

3.2. Mechanism Involved in the Reaction between $SiH_3SiH_2(OH)$ and Hydrogen Atom

3.2.1. $SiH_3SiH_2OH + H \rightarrow SiH_3SiH_2O + H_2$ Figure 1 shows that the reactant $SiH_3SiH_2(OH)$ **9** has C_S symmetry and its structural character is the same as **7** found in previous section. The Si–Si bond length is larger than that of SiH_3SiH_3 while the Si–H bond length is smaller, although the effect of the hydroxyl group is weaker.

The transition state of this reaction is **TS3**, as shown in Figure 1. The structure of **TS3** and the vector of its imaginary frequency vibrational mode show hydrogen abstraction by a hydrogen atom from the hydroxyl group. The activation energy is

19.24kcal/mol at the CISD//MP2(+ZPE) level and is almost the same as that for the reaction $SiH_3OH + H \rightarrow SiH_3O + H_2$ by Zachariah and Tsang.[34] They studied the reaction using the bond additivity correction (BAC) procedure and estimated an activation energy of about 18 kcal/mol.

The reaction energy is 6.95kcal/mol (endothermic) at the CISD+QC//MP2(+ZPE) level, which is a small value. Thus, this reaction is not markedly inhibited, and leads to the second stage as found in subsection 3.2.2.

3.2.2. $SiH_3SiH_2O \rightarrow SiH_3$-O-$SiH_2$ The reactant SiH_3SiH_2O has C_S symmetry; therefore, two electronic states, **10** for $^2A'$ and **11** for $^2A''$, are considered as depicted in Figure 1. There are few differences in these optimized structures except for the Si–O bonds. Optimized structure **10** is more stable than **11** by 3.56kcal/mol (CISD(full) //MP2(full) +ZPE level). Spin densities of oxygen are +1.01 for **10** and +1.02 for **11**, and the singly occupied molecular orbital (SOMO) of each structure is localized at the oxygen atom.

As shown in Figure 1, the product SiH_3-O-SiH_2 has C_1 symmetry. In **12**, which has C_S symmetry, low imaginary frequency ($52i$ cm^{-1}(a'')) exists. Indeed, **13**, which is an optimized structure with C_1 symmetry, exhibits a tendency of excluding the oxygen atom from the symmetry plane. However, the energy difference is very small and the Si–O–Si bond has a very flexible structure. The SOMO is localized at the Si atom (the spin densities are +0.93 for **12** and +0.92 for **13**).

The reaction path $CH_3O \rightarrow CH_2(OH)$ was studied by many researchers.[35-41] In particular, this reaction path is considered to be a bifurcating one.[35,39,40] Considering an intrinsic reaction coordinate (IRC) path, the bifurcating point that breaks the symmetry retention of the reaction path exists in the reaction path from the transition state to the product CH_2OH. Reaction (4) has the same character as this reaction. Therefore, we consider the reaction path of (4) with $^2A'$ potential surface of C_S symmetry. The structure of the transition state **TS4** shows an early transition trend, as demonstrated in Figure 1. The activation barrier is 2.01kcal/mol at the CISD(full)//MP2(full)(+ZPE) level, which is a very small value. Moreover, the reaction energy is 44.34 kcal/mol (exothermic).

Therefore, although structure **10** is a local minimum structure (having all real vibrational frequencies), **10** reacts to **12** and **13** with almost no barrier and the product is much more stable than the reactant.

The SOMO of SiH_3SiH_2O is localized at oxygen 2p orbital as shown in Figure 4. On the other hand, the highest occupied molecular orbital (HOMO) is the Si–Si σ–bond (Figure 4). These HOMO-SOMO interactions result in a low activation energy of the reaction because SOMO energy level is lower than HOMO energy level in alpha space.

3.2.3. $SiH_3SiH_2O \rightarrow SiH_3SiH(OH)$ Reaction (5) is an alternative to reaction (4) except for the difference of oxygen insertion into Si–H bond. The transition state structure is shown in Figure 1. Its imaginary frequency is $1747i cm^{-1}$; thus, the potential energy surface is very sharp along this reaction path. The activation energy is 26.54 kcal/mol, which is higher by 24.53 kcal/mol than that of reaction (4). The reaction energy is 21.40 kcal/mol (exothermic). Comparing reaction (4) with reaction (5), it is found that the Si–Si bond is more easily broken than the Si–H bond and the Si–O–Si bond is definitely more stable than the Si–O–H bond.

3.3. Local Oxidation Character of Hydrogen-Terminated Si Surface

In section 3.1, it is shown that the Si–O–Si bond is more stable than the Si–O–H bond in molecular structure. This corresponds to the preference of back-bond oxidation of H-Si(111), which was observed experimentally by Hattori *et al.*[42-46] Recently, Hattori investigated the oxidation of a hydrogen-terminated Si(111) surface, that is, the H-Si(111)-1×1 surface[42] at 300 °C in dry O_2 under a pressure of 1 Torr up to a thickness of 0.5 nm. Oxidation-induced changes in Si 2p and Si $2p_{3/2}$ photoelectron spectra and infrared absorption spectra were observed. As a result, he concluded that no desorption of H occurs and no Si–OH bonds are formed, but oxygen is inserted into the Si–Si back bonds. Similar results were reported for the oxidation of a hydrogen-terminated Si(100) surface by Nagasawa *et al.*[47] They prepared a hydrogen-terminated Si(100) surface and investigated the change in FT-IR-ATR (Fourier-transform infrared attenuated total

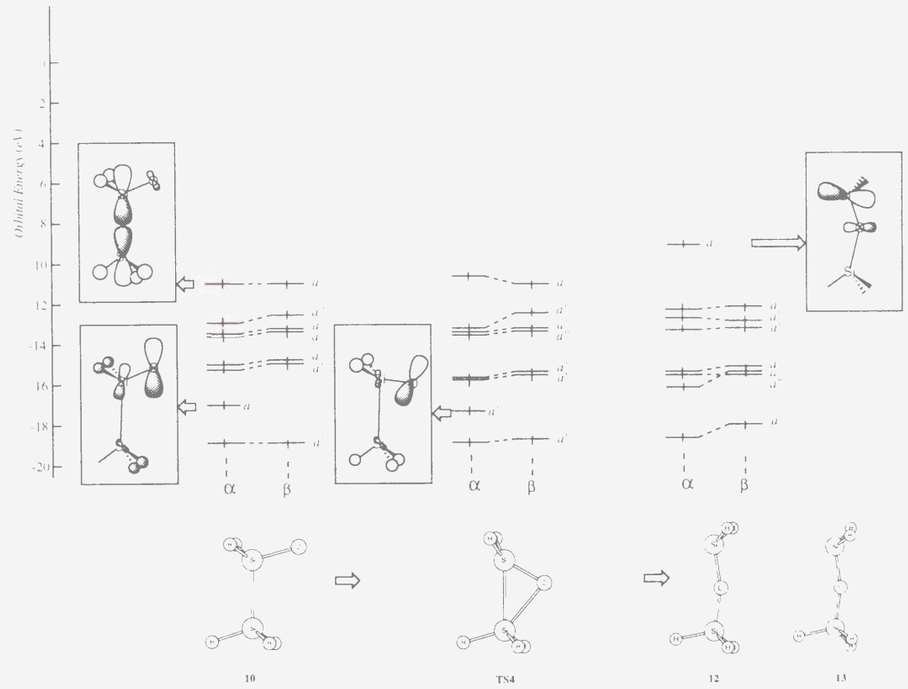

Figure 4. MO energy diagrams of **10**, **TS4** and **12** at the UHF/6-31G** level on the MP2(full)/6-31G** level geometries.

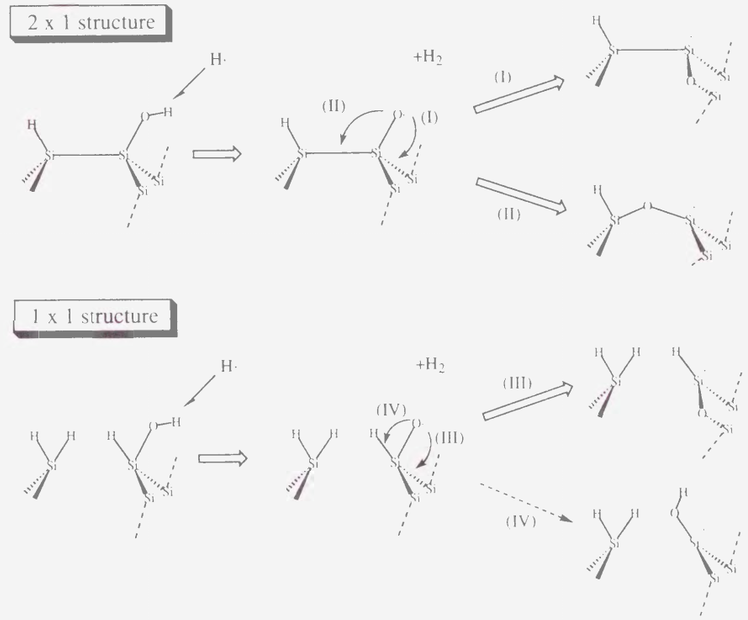

Figure 5. Oxygen insertion reactions.

reflection) spectra of the surface exposed to air at room temperature. As a result, they observed a new peak at 2215cm^{-1} after 12 days, which was attributed to the SiH_2 stretching mode where two oxygen atoms combine with Si. They also indicated that oxygen breaks the Si–Si back bond first rather than the Si–H bond in the initial oxidation stage. If indeed chemical bond character affects the reaction site of the Si surface, then their results are completely consistent with ours.

3.4. Mechanisms Involved in the Reaction of H_2O-Terminated Si Surface

Here we discuss the oxygen insertion reaction pertinent to the experiment conducted by Ikeda *et al.*,[48] on the basis of our results regarding molecular reactions. They studied the reaction between a H_2O-terminated Si(100) surface and a hydrogen atom by high-resolution electron energy loss spectroscopy (HREELS) for the purpose of understanding the initial oxidation process. H_2O molecules adsorb dissociatively on dangling bonds of Si dimers on Si(100) and form Si–H and Si–OH bonds that have the 2×1 structure.[49-56] While this H_2O-adsorbed Si(100) surface was exposed to hydrogen atoms at room temperature, they investigated the intensity changes of the energy loss peaks for Si–O–Si, Si–OH and Si–H species. It was conjectured that the following reactions are involved in the oxygen uptake into the Si–Si back bond, upon observing that the intensity of Si–OH peaks decreases and that of Si–O–Si and Si–H peaks increases with increasing amount of hydrogen exposure:

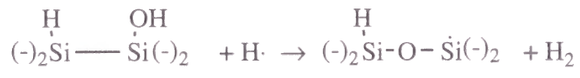

$$(-)_2\mathrm{Si}(\mathrm{H})-\mathrm{Si}(\mathrm{OH})(-)_2 + \mathrm{H}\cdot \rightarrow (-)_2\mathrm{Si}(\mathrm{H})-\mathrm{O}-\mathrm{Si}(-)_2 + \mathrm{H}_2 \quad \text{(i)}$$

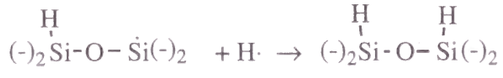

$$(-)_2\mathrm{Si}(\mathrm{H})-\mathrm{O}-\mathrm{Si}(-)_2 + \mathrm{H}\cdot \rightarrow (-)_2\mathrm{Si}(\mathrm{H})-\mathrm{O}-\mathrm{Si}(\mathrm{H})(-)_2 \quad \text{(ii)}$$

By analyzing the Langmuir plot for the peak intensity, however, it was found that the reduction rate of Si–OH bonds was higher than the formation rate of Si–O–Si bonds at small amounts of hydrogen exposure. Therefore, the following reactions were also considered to occur:

$$(-)_2\mathrm{Si}(\mathrm{H})-\mathrm{Si}(\mathrm{OH})(-)_2 + \mathrm{H}\cdot \rightarrow (-)_2\mathrm{Si}(\mathrm{H})-\mathrm{Si}(-)_2 + \mathrm{H}_2\mathrm{O} \quad \text{(iii)}$$

$$(-)_2\mathrm{Si}(\mathrm{H})-\mathrm{Si}(-)_2 + \mathrm{H}\cdot \rightarrow (-)_2\mathrm{Si}(\mathrm{H})-\mathrm{Si}(\mathrm{H})(-)_2 \quad \text{(iv)}$$

Analysis of the LEED pattern revealed that surface structure changed from a monohydride layer that has the 2×1 structure to a dihydride layer that has the 1×1 structure, depending on the amount of hydrogen exposure. This leads to the following reaction:

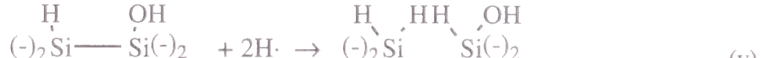

$$(-)_2\mathrm{Si}(\mathrm{H})-\mathrm{Si}(\mathrm{OH})(-)_2 + 2\mathrm{H}\cdot \rightarrow (-)_2\mathrm{Si}(\mathrm{HH})-\mathrm{Si}(\mathrm{OH})(-)_2 \quad \text{(v)}$$

On the basis of these results, at small amounts of hydrogen exposure, reactions (i)-(v) were considered to occur simultaneously, while at large amounts, (i) and (ii) were dominant over (iii) and (iv). This result indicates that external atomic hydrogen can control the oxidation of Si surfaces. Moreover, of note is that the oxygen atom insertion into the Si–Si back bond (i) occurred on both monohydride and dihydride Si surfaces.

We discuss the oxygen insertion reaction pertinent to this experiment. In this experiment, H_2O-terminated Si(100) surface that was terminated by a hydrogen or a hydroxyl group was exposed to hydrogen atoms. As a starting point, reaction (3) was considered to be the cluster model of hydrogen abstraction from the OH group by hydrogen atom. An oxygen atom radical center was found to remain after abstraction of the hydrogen atom from the hydroxyl group by reaction with a hydrogen atom. We need to find out how the oxygen atom radical penetrates into the Si–Si back bond.

The possibilities of the reactions that lead to the insertion of oxygen are shown in Figure 5. In the 2×1 structure, oxygen atom has two possibilities of inserting either into the Si–Si back-bond (I) or the Si–Si dimer bond (II). We assume reaction (4) to be the cluster model of both (I) and (II). From the character of reaction (4), which has a smaller activation energy than reaction (3) with high exothermicity, both (I) and (II) are considered to occur. However, only (I) was observed experimentally. Although this experimental result is not resolved at the present stage of calculation, it is considered that

the study by Uchiyama and Tsukada gave a way of explanation.[12,13] Further work should be done in order to fully understand the selectivity of (I) over (II).

In the 1×1 structure, two reactions, oxygen insertion into the Si–Si back bond (III) and oxygen insertion into the Si–H bond (IV), are considered. Assuming reaction (4) as the model of (III) and reaction (5) as the model of (IV), the former is much more favorable than the latter from the viewpoint of both activation energy and reaction energy. Therefore, only (III) can occur.

If we interpret the local electronic character of the cluster reactions to the surface reactions, HOMO of **10** is regarded as the Si–Si valence band. The oxygen radical is more stable than the Si–Si valence band because it is localized in the oxygen 2p orbital, so it easily inserts into the Si bond and has a strong interaction with the Si valence band.

Consequently, in either the 2×1 or the 1×1 surface structure of H_2O-terminated Si(100), the oxygen atom inserts into the Si–Si bond rapidly after an oxygen atom radical center is formed by the reaction of hydrogen atom with the hydroxyl group.

The attacking hydrogen atoms are considered to react in many other ways. For example, Ikeda *et al.* [43] considered that reaction (iii) is the reason for the inconsistency between the increase in Si–O–H peak and the decrease in Si–O–Si peak at small amounts of hydrogen exposure. They suggested that this reaction did not occur in the 1×1 structure because of steric hindrance. Other experiments[49] indicated that oxygen species were lost from the silicon surface. Therefore, we must consider the various possibilities of reactions in further experimental and theoretical studies.

4. Conclusion

We studied the local electronic property of Si–Si bond oxidation using *ab initio* molecular orbital calculation and discussed Si–Si back-bond oxidation in the hydrogen-terminated silicon surface.

First, we investigated Si–O–H bond and Si–O–Si bond stability. The cluster model SiH_3-O-SiH_2(OH) is 27.43kcal/mol more stable than $SiH_3SiH(OH)_2$ at the CISD(full)/6-31G**//MP2(full)/6-31G** level(+ZPE). Therefore, the Si–O–Si bond is more stable than the Si–O–H bond. Adapting this result to the local electronic property of the hydrogen-terminated Si surface, we found that the oxygen atom prefers Si–Si back-bond insertion rather than terminating Si–H bond insertion when oxygen molecules oxidize the silicon surface. This result agrees with that from the experimental study by Hattori *et al.*[42] that not the Si–O–H bond but the Si–O–Si bond is formed upon oxidation of the hydrogen-terminated Si(111) surface.

Second, we investigated oxygen insertion reaction in terms of radical reaction by considering the molecular reaction $SiH_3SiH_2O \rightarrow SiH_3$-O-$SiH_2$ (4). The reaction barrier height is 2.01kcal/mol and the reaction energy is 44.34kcal/mol (exothermic) at the CISD(full)/6-31G**//MP2(full)/6-31G**(+ZPE) level. Therefore, this reaction easily occurs. Another reaction, which is insertion of oxygen into the Si–H bond, has a possibility but its corresponding reaction $SiH_3SiH_2O \rightarrow SiH_3SiH(OH)$ (5) has higher activation energy and lower reaction energy than reaction (4). Therefore, once a hydrogen atom attacks the hydrogen of the OH group and makes an oxygen atom radical center, as assumed in the model reaction (3), reaction (4) should occur rapidly. This agrees well with the results of an experimental study on surface reaction processes of hydrogen atoms with H_2O-terminated Si(100) by Ikeda *et al.*[48]

References

(1) Cabrera, N.; Mott, N. F. *Rept. Prog. Phys.* **1949**, *12*, 163.

(2) Deal, B. E.; Grove, A. S. *J. Appl. Phys.* **1965**, *36*, 3770.

(3) Goddard, W. A., III; Redondo, A.; McGill, T. C. *Solid State Commun.* **1976**, *16*, 981.

(4) Schubert, B.; Avouris, P.; Hoffmann, R. *J. Chem. Phys.* **1993**, *98*, 7593.

(5) Schubert, B.; Avouris, P.; Hoffmann, R. *J. Chem. Phys.* **1993**, *98*, 7606.

(6) Stoneham, A. M.; Grovenor, C. R.; Cerezo, A. *Philos. Mag. B* **1987**, *55*, 201.

(7) Hagon, J. P.; Stoneham, A. M.; Jaros, M. *Philos. Mag. B* **1987**, *55*, 211.

(8) Hasegawa, E.; Ishitani, A.; Akimoto, K.; Tsukiji, M.; Ohta, N. *J. Electrochem. Soc.* **1995**, *142*, 273.

(9) Miyamoto, Y.; Oshiyama, A. *Phys. Rev. B* **1990**, *41*, 12680.

(10) Hoshino, T.; Tsuda, M.; Oikawa, S.; Ohdomari, I. *Surf. Sci.* **1993**, *291*, L763.

(11) Hoshino, T.; Tsuda, M.; Oikawa, S.; Ohdomari, I. *Phys. Rev. B* **1994**, *50*, 14999.

(12) Uchiyama, T.; Tsukada, M. *Surf. Sci.* **1996**, *357-358*, 509.

(13) Uchiyama, T.; Tsukada, M. *Phys. Rev. B* **1996**, *53*, 7917.

(14) Kato, K.; Uda, T.; Terakura, K. *Phys. Rev. Lett.* **1998**, *80*, 2000.

(15) Frisch, M. J.; Trucks, G. W.; Schlegel, H. B.; Gill, P. M. W.; Johnson, B. G.; Robb, M. A.; Cheeseman, J. R.; Keith, T.; Petersson, G. A.; Montgomery, J. A.; Raghavachari, K.; Al-Laham, M. A.; Zakrzewski, V. G.; Ortiz, J. V.; Foresman, J. B.; Peng, C. Y.; Ayala, P. A.; Chen, W.; Wong, M. W.; Andres, J. L.; Replogle, E. S.; Gomperts, R.; Martin, R. L.; Fox, D. J.; Binkley, J. S.; Defrees, D. J.; Baker, J.; Stewart, J. P.; Head-Gordon, M.; Gonzalez, C.; Pople, J. A. *Gaussian 94, Revision B.3*; Gaussian, Inc.: Pittsburgh, PA, 1995.

(16) Møller, C.; Plesset, M. S. *Phys. Rev.* **1934**, *46*, 618.

(17) Binkey, J. S.; Pople, J. A. *Int. J. Quantum Chem.* **1975**, *9*, 229.

(18) Hehre, W. J.; Radom, L.; Schleyer, P. v. R.; Pople, J. A. *Ab initio Molecular Orbital Theory*; Wiley: New York, 1986.

(19) Pople, J. A.; Scott, A. P.; Wong, M. W.; Radom, L. *Israel J. Chem.* **1993**, *33*, 345.

(20) Pople, J. A.; Binkley, J. S.; Seeger, R. *Int. J. Quantum Chem. Symp.* **1976**, *10*, 1.

(21) Pople, J. A.; Binkley, J. S.; Krishnan, R. *Int. J. Quantum Chem. Symp.* **1977**, *11*, 149.

(22) Mulliken, R. S. *J. Chem. Phys.* **1955**, *23*, 1833.

(23) Reed, A. E.; Schade, C.; Schleyer, P. v. R.; Kamath, P. V.; Chandrasekhar, J. *J. Chem. Soc., Chem. Commun.* **1988**, 67.

(24) Apeloig, Y. *The Chemistry of Organic Silicon Compounds*, Patai, S., Rappoport, Z., Eds.; Wiley: New York, 1989.

(25) Apeloig, Y.; Stanger, A. *J. Organomet. Chem.* **1988**, *346*, 305.

(26) O'Keeffe, M.; Gibbs, G. V. *J. Chem. Phys.* **1984**, *81*, 876.

(27) Ferrari, A. M.; Ugliengo, P.; Garrone, E. *J. Phys. Chem.* **1993**, *97*, 2671.

(28) Csonka, G. I.; Réffy, J. *Chem. Phys. Lett.* **1994**, *229* , 191.

(29) Luke, B. T. *J. Phys. Chem.* **1993**, *97*, 7505.

(30) Nicholas, J. B.; Winans, R. E.; Harrison, R. J.; Iton, L. E.; Curtiss, L. A.; Hopfinger, J. *J. Phys. Chem.* **1992**, *96*, 7958.

(31) Shambayati, S.; Blake, J. F.; Wierschke, S. G.; Jorgensen, W. L.; Schreiber, S. L. *J. Am. Chem. Soc.* **1990**, *112*, 691.

(32) Grigoras, S.; Lane, T. H. *J. Comput. Chem.* **1987**, *8*, 84.

(33) Teppen, B. J.; Miller, D. M.; Newton, S. Q.; Schäfer, L. *J. Phys. Chem.* **1994**, *98*, 12545.

(34) Zachariah, M. R.; Tsang, W. *J. Phys. Chem.* **1995**, *99*, 5308.

(35) Taketsugu, T.; Tajima, N.; Hirao, K. *J. Chem. Phys.* **1996**, *105*, 1933.

(36) Tachikawa, H. *Chem. Phys. Lett.* **1993**, *212*, 27.

(37) Walch, S. P. *J. Chem. Phys.* **1993**, *98*, 3076.

(38) Page, M.; Lin, M. C.; He, Y.; Choudhury, T. K. *J. Phys. Chem.* **1989**, *93*, 4404.

(39) Colwell, S. M.; Handy, N. C. *J. Chem. Phys.* **1985**, *82* , 1981.

(40) Colwell, S. M. *Mol. Phys.* **1984**, *51*, 1217.

(41) Saebø, S.; Radom, L.; Schaefer, H. F., III *J. Chem. Phys.* **1983**, *78*, 845.

(42) Hattori, T. *CRC Crit. Rev. Solid State Mater. Sci.* **1995**, *20*, 339.

(43) Hattori, T.; Nohira, H.; Tamura, Y.; Ogawa, H. *Jpn. J. Appl. Phys.* **1992**, *31*, L638.

(44) Nohira, H.; Tamura, Y.; Ogawa, H.; Hattori. T. *IEICE Trans. Electron.* **1992**, *E75-C*, 757.

(45) Hattori, T.; Nohira, H.; Ohishi, K.; Shimizu, Y.; Tamura, Y. *Mater. Res. Soc. Symp. Proc.* **1993**, *315*, 387.

(46) Hattori, T. *J. Vac. Sci. Technol. B* **1993**, *11*, 528.

(47) Nagasawa, Y.; Ishida, H.; Takahagi, T.; Ishitani, A.; Kuroda, H. *Solid State Electron.* **1990**, *33*, 129.

(48) Ikeda, H.; Hotta, K.; Yamada, T.; Zaima, S.; Yasuda, Y. *Jpn. J. Appl. Phys.* **1995**, *34*, 2191.

(49) Flowers, M. C.; Jonathan, N. B. H.; Morris, A.; Wright, S. *Surf. Sci.* **1996**, *351*, 87.

(50) Himpsel, F. J.; McFeely, F. R.; Taleb-Ibrahimi, A.; Yarmoff, J. A. *Phys. Rev. B*, **1988**, *38*, 6084.

(51) Avouris, P.; Lyo, I.-W. *Surf. Sci.* **1991**, *242*, 1.

(52) Edamoto, K.; Kubota, Y.; Kobayashi, H.; Onchi, M.; Nishijima, M. *J. Chem. Phys.* **1985**, *83*, 428.

(53) Lyo, I.-W.; Avouris, P.; Schubert, B.; Hoffmann, R. *J. Phys. Chem.* **1990**, *94*, 4400.

(54) Chander, M.; Li, Y. Z.; Patrin, J. C.; Weaver, J. H. *Phys. Rev. B* **1993**, *48*, 2493.

(55) Chabal, Y. J. *Phys. Rev. B* **1984**, *29*, 3677.

(56) Oellig, E. M.; Butz, R.; Wagner, H.; Ibach, H. *Solid State Commun.* **1984**, *51*, 7.

Chapter 5:

Quantum Chemical Study on the Oxidation of Hydrogen-Terminated Silicon Surface by Oxygen Anions

1. Introduction

The crucial demand for reduction in the design rule of ultralarge-scale integrated circuit (ULSI) technology will soon lead us to a new era of future metal-oxide-semiconductor (MOS) devices with minimum feature sizes below 0.1μm. The electrical properties of MOS devices are strongly correlated with structural characteristics at the SiO_2/Si interface. It now appears that atomic-scale control of ultrathin SiO_2 film formation to only 5-6 atomic layers should play an important role in order to obtain an SiO_2/Si interface of the highest-quality.

Surface cleaning is the primordial process of preparing a tailor-made surface of a Si single crystal clean enough to enable fabrication of a well-designed SiO_2 film on it. Hydrocarbon contamination or native oxide that covers the surface of pristine Si single crystal can be removed by hydrogen fluoride (HF) etching whereby an atomically flat hydrogen-terminated Si surface (abbreviated as H-Si surface hereafter) is obtained.[1,2] A novel method of preparing the atomically flat H-Si(111) surface was found via 40% NH_4F solution [3,4] or boiling water [5,6,7] treatment. The H-Si surface is chemically passivated against oxidation even if it is exposed to air at room temperature. Hattori performed the oxidation of the H-Si(111) surface at 300°C in dry O_2 under a pressure of 1 torr up to a thickness of 0.5nm, whereby further heating resulted in layer-by-layer oxidation at the SiO_2/Si interface.[8] The oxidation process and the role of hydrogen atoms in the surface reaction remain to be clarified.

In the present paper, the chemical reactivity of an oxygen anion O^- with the H-Si(111) surface is studied using *ab initio* molecular orbital method of quantum chemistry. The oxygen anion O^- has milder reactivity with Si than the oxygen atom O [9]; moreover, if it were included in the Si bulk, it would become a major diffusing species.[10] However, the formation of O^- from O_2 gas is inhibited on the H-Si(111) surface since the route of charge transfer from the surface to O_2 is blocked by hydrogen termination. Our idea is to supply O^- efficiently.[11] This can be done by carefully choosing plasma processes, such as a variation of the remote plasma method, although we do not intend to restrict

ourselves to a particular technique of O^- supply. Instead, we would like to demonstrate the hypervalency of Si that stabilizes five (penta)-coordinated anionic species.

Theoretical studies have proved that the penta-coordinated Si plays an important role in the hydroxide-containing reactions of Si.[12-16] Gordon *et al.* [15] studied the penta-coordinated silicon anionic species $H_3(CH_3)SiOH^-$ and $(CH_3)Si(OH)_4^-$ in the experiments by DePuy *et al.*[12] on the reactions of OH^- with methylsilane or tetramethylsilane. They identified the penta-coordinated intermediates in a series of pseudo-rotation reaction pathways. Gordon *et al.* noted the formation of the penta-coordinated intermediate $Si(OH)_5^-$ along the reaction pathway:

$$Si(OH)_4 + OH^- \rightarrow \text{penta-coordinated } Si(OH)_5^- \rightarrow Si(OH)_3O^- + H_2O$$

for polymerization and sol-gel processes.[16] In the case of O^- with Si, the hypervalency of Si works in a similar manner to stabilize the penta-coordinated complex.

2. Methods of Calculation

Molecular orbital calculations were performed using the GAUSSIAN 94 program package.[17] The geometry of the cage model $Si_{10}H_{16}$ was optimized by the analytical energy gradient method using the spin-restricted Hartree-Fock (RHF) procedure with 6-31G* basis sets.[18] Vibrational frequencies were then obtained analytically. The geometry of this cage model was reoptimized with O^- in it under the constraint of C_{3v} symmetry and Si–O bond length of 2.3Å, where we added a diffuse orbital for O^- (6-31+G*) using the spin-unrestricted HF (UHF) method. Electron correlation energies were estimated by the second-order Møller-Plesset perturbation theory that includes correlation of valence electrons (MP2(fc)).[19,20]

The geometries of all other cluster models were optimized using the HF procedure with 6-31+G** basis set (denoted as HF/6-31+G**). In HF calculations, the RHF method was used for closed-shell singlet states, and the UHF method for open-shell doublet and triplet states. Vibrational frequencies were then obtained analytically at the HF/6-31+G** level. Electron correlation energies were estimated by the second-order

and third-order Møller-Plesset perturbation theory (MP2 and MP3) and single and double substituted configuration interaction (CISD)[21] that includes correlation for all electrons with 6-31+G** basis sets at the HF/6-31+G** optimized geometries (denoted as MPn(full)/6-31+G**//HF/6-31+G** (n=2,3) or CISD(full)/6-31+G**//HF/6-31+G**). In CISD calculations, unlinked cluster quadruple correction (QC) was added to enable size-consistency correction (denoted as CISD(full)+QC).[22] To estimate the effects of higher spin contaminations, spin-projected MP2 calculations were also made.[23] The Mulliken atomic charge[24] and spin densities were calculated using SCF density.

Surface model calculations discussed in section 3.6 were performed in CASTEP[25] code. We used LSDA as parameterized by Perdew and Zunger[26] and non-local pseudo-potentials with the plane wave basis set of the Kleinman-Bylander type.[27,28]

3. Results and Discussion

3.1. Reaction Pathways

The possible reaction pathways (I), (II), and (III) of O^- on H-Si(111) surface are schematically shown in Figure 1. The energy diagrams along the reaction coordinates are shown in Figure 2, where the local cluster models **1**-**12** adopted are shown in Figure 3. Total energies of **1**-**12** are shown in Table 1 and vibrational frequencies, in Table 2. Relative energies of reaction pathways (I)-(III) are given in Tables 3 and 4. The presence of the penta-coordinated anionic species **7** at the beginning of all the reaction pathways strongly supports the hypervalency of Si that initiates the reactions, where the stabilization energy of **7** is 41.31 kcal/mol at CISD(full)+QC/6-31+G**. An oxygen anion can therefore be inserted into a Si–Si bond to form a local Si–O–Si structure. The stabilization energy is enhanced if the deformation energy in the local Si–O–Si structure is released from **10** to **9** via **11** or **5** to **4** via **6**, as shown in Figure 2. At the final stage of each reaction pathway, the escaping tendency of an excess electron is estimated as follows.

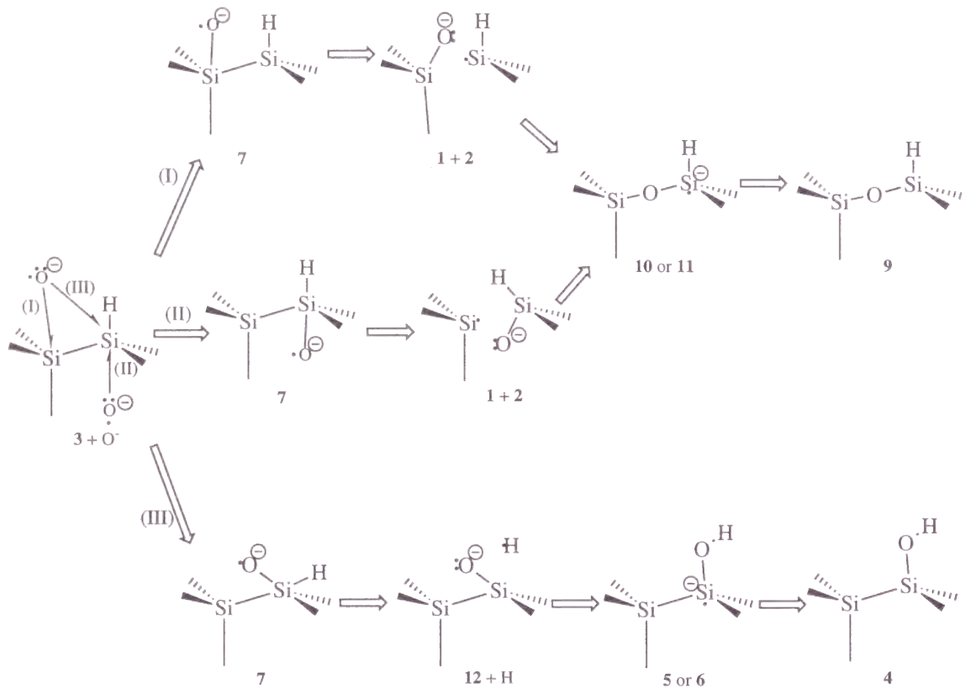

Figure 1. Reaction pathways (I), (II), and (III) of O^- on H-Si(111) surface.

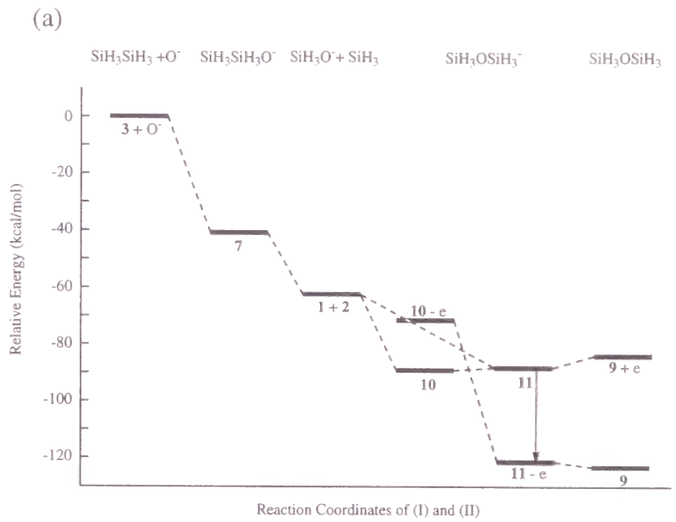

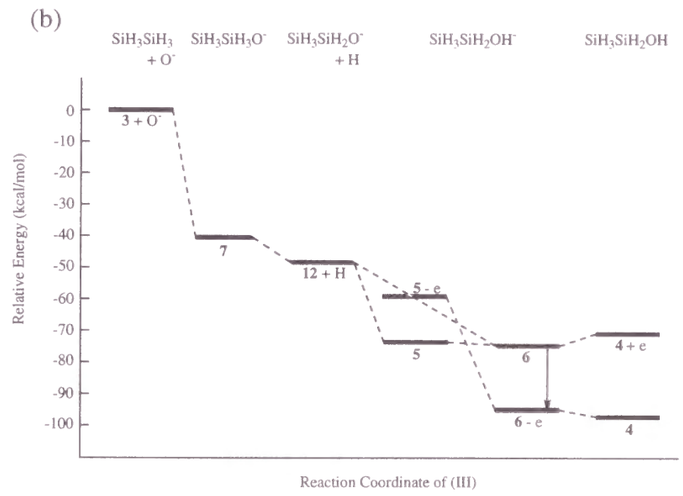

Figure 2. Relative energy diagrams at the CISD(full)+QC//HF level (kcal/mol) for the reaction pathways of (a) (I) and (II), and (b) (III).

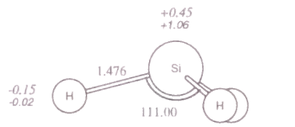

1 (C_{3v})

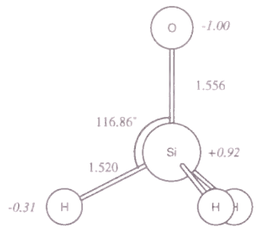

2 (C_{3v})

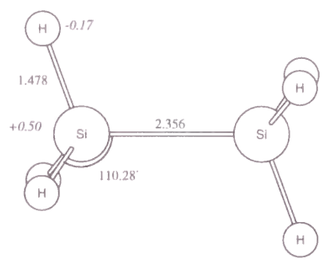

3 (D_{3d})

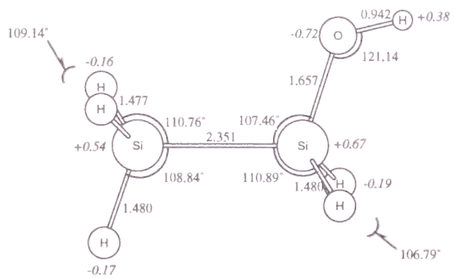

4 (C_s)

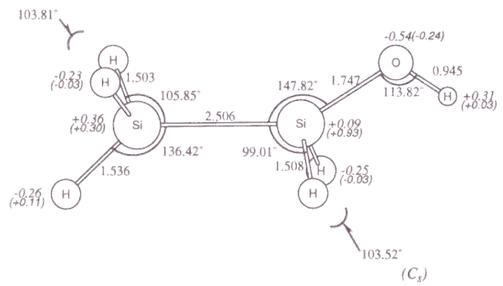

5 (C_s)

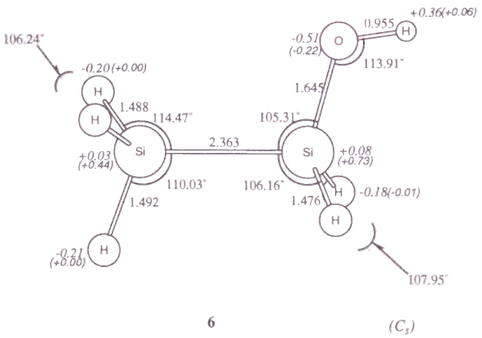

6 (C_s)

Figure 3. Optimized geometries of the species **1-12** at the HF/6-31+G** level. Bond lengths are in Å and bond angles in degrees. The Mulliken atomic charges are in italics. The spin densities are in parentheses.

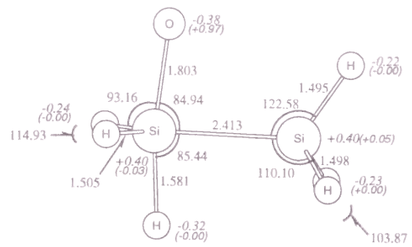

7 $(C_s)\ ^2A'$

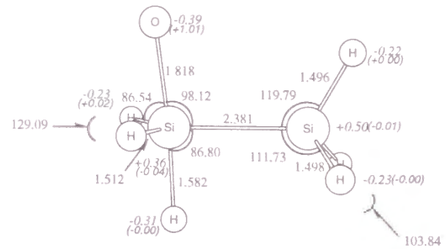

8 $(C_s)\ ^2A''$

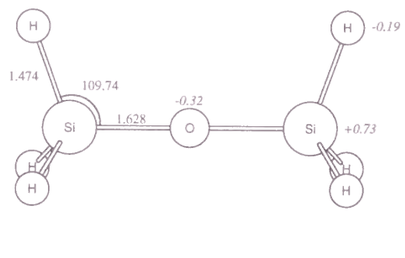

9 (D_{3h})

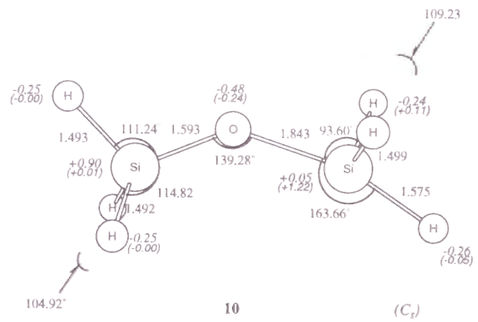

10 (C_s)

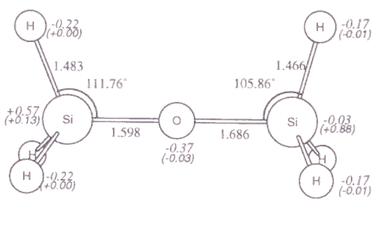

11 (C_{3v})

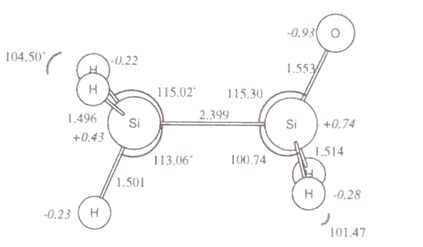

12 (C_s)

Figure 3. *(continued from the previous page.)*

Table 1: Total Energies at the HF/6-31+G** Optimized Geometries in au

species	HF/6-31+G**	$\langle S^2 \rangle$	MP2(full) /6-31+G**	PMP2(full) /6-31+G**	MP3(full) /6-31+G**	CISD(full)+QC /6-31+G**
H	-0.49823	0.750	–	–	–	–
$O(^3\Sigma_g)$	-74.78676	2.008	-74.88750	-74.88911	-74.90059	-74.90464
O^-	-74.76662	0.764	-74.92760	-74.92984	-74.93293	-74.93903
1SiH_3 (C_{3v})	-290.61162	0.754	-290.71145	-290.71197	-290.72917	-290.73632
2SiH_3O^- (C_{3v})	-365.55198		-365.87115		-365.87750	-365.89031
3SiH_3SiH_3 (D_{3d})	-581.31584		-581.54022		-581.57631	-581.58887
4$SiH_3SiH_2(OH)$ (C_s)	-656.22886		-656.63805		-656.66956	-656.68327
4+e ($^2A'$)	-656.17812	0.751	-656.59717	-656.59725	-656.62809	-656.64228
5$SiH_3SiH_2(OH)^-$ ($^2A'$) (C_s)	-656.17338	0.775	-656.59916	-656.60126	-656.63055	-656.64507
5-e	-656.16139		-656.57573		-656.60755	-656.62228
6$SiH_3SiH_2(OH)$($^2A'$) (C_s)	-656.18210	0.751	-656.60158	-656.60165	-656.63221	-656.64655
6-e	-656.22419		-656.63435		-656.66568	-656.67956
7$SiH_3SiH_3O^-$ ($^2A'$) (C_s)	-656.14137	0.761	-656.53444	-656.53656	-656.57639	-656.59340
8$SiH_3SiH_3O^-$ ($^2A''$) (C_s)	-656.14085	0.758				
9SiH_3-O-SiH_3 (D_{3h})	-656.27338		-656.68102		-656.70988	-656.72400
9+e	-656.20531	0.750	-656.61844	-656.61845	-656.64805	-656.66250
10SiH_3-O-SiH_3^- ($^2A'$) (C_s)	-656.20140	0.754	-656.62739	-656.62829	-656.65411	-656.67033
10-e	-656.18051		-656.59910		-656.62599	-656.64282
11SiH_3-O-SiH_3^- (C_{3v})	-656.21196	0.750	-656.62594	-656.62598	-656.65455	-656.66939
11-e	-656.26924		-656.67763		-656.70625	-656.72073
12 $SiH_3SiH_2O^-$ (C_s)	-655.65304		-656.06782		-656.08875	-656.10567

Table 2: Vibrational Frequencies at the HF/6-31+G** Level

species	harmonic vibrational frequencies (cm^{-1})	ZPE
1SiH_3	874(a_1), 1018(e), 2343(a_1), 2361(e)	14.26
2SiH_3O^-	804(e), 1058(e), 1089(a_1), 1180(a_1), 2043(e), 2154(a_1)	17.49
3SiH_3SiH_3	136(a_{1u}), 418(e_u), 461(a_{1g}), 696(e_g), 948(a_{2u}), 1028(e_g), 1031(a_{1g}), 1044(e_u), 2338(a_{2u}), 2338(e_g), 2347(e_u),2354(a_{1g})	32.90
4$SiH_3SiH_2(OH)$	95(a''), 181(a'), 397(a''), 438(a'), 450(a''), 563(a'), 670(a''), 714(a''), 800(a'), 902(a'), 984(a'), 1029(a'), 1036(a'), 1044(a''), 1048(a'), 2253(a'), 2276(a''), 2290(a'), 2325(a''), 2339(a'), 3937(a')	37.41
5$SiH_3SiH_2(OH)^-$	53(a''), 124(a'), 175(a''), 248(a'), 300(a''), 497(a'), 543(a''), 686(a'), 845(a'), 907(a''), 955(a'), 970(a'), 1015(a'), 1052(a''), 1061(a'), 1961(a'), 2128(a''), 2152(a'), 2181(a''), 2194(a'), 4139(a')	34.58
6$SiH_3SiH_2(OH)^-$	104(a''), 180(a'), 210(a''), 416(a''), 454(a'), 578(a'), 680(a''), 803(a''), 817(a'), 890(a'), 959(a'), 1022(a'), 1033(a''), 1040(a'), 1070(a'), 2318(a''), 2325(a'), 2338(a'), 2351(a''), 2353(a'), 4223(a')	36.84
7$SiH_3SiH_3O^-$ ($^2A'$)	24(a''), 178(a'), 202(a''), 354(a'), 443(a'), 480(a''), 607(a'), 738(a''), 772(a'), 905(a'), 999(a'), 1043(a'), 1053(a''), 1179(a'), 1181(a''), 1716(a'), 2145(a''), 2161(a'), 2216(a''), 2222(a'), 2249(a')	32.69
8$SiH_3SiH_3O^-$ ($^2A''$)	29i(a''), 176(a'), 262(a''), 401(a'), 410(a'), 414(a''), 552(a'), 619(a''), 669(a'), 931(a'), 1017(a'), 1044(a'), 1053(a''), 1164(a'), 1202(a''), 1712(a'), 2117(a'), 2122(a''), 2214(a''), 2217(a'), 2248(a')	32.23
9SiH_3-O-SiH_3	27(a_1''), 122(e'), 577(a_1'), 778(e''), 818(e'), 1045(a_2''), 1053(e''), 1059(e'), 1115(a_1'), 1227(a_2''), 2358(e''), 2358(e''), 2362(e'), 2372(a_2''), 2385(a_1')	36.95
10SiH_3-O-SiH_3^-	23(a''), 76(a''), 101(a'), 378(a'), 567(a''), 578(a'), 794(a''), 802(a'), 904(a'), 1023(a'), 1060(a''), 1062(a'), 1094(a'), 1130(a''), 1148(a'), 1714(a'), 2180(a''), 2193(a'), 2225(a'), 2227(a''), 2285(a')	33.69
11SiH_3-O-SiH_3^-	32(a_2), 135(e), 529(a_1), 771(e), 815(e), 815(e), 903(a_1), 1006(e), 1061(e), 1106(a_1), 1197(a_1), 2296(e), 2333(a_1), 2379(e), 2391(a_1)	36.33
12$SiH_3SiH_2O^-$	124(a''), 190(a'), 385(a''), 397(a'), 549(a'), 678(a''), 822(a''), 943(a'), 1014(a'), 1042(a'), 1044(a''), 1065(a'), 1160(a'), 2079(a''), 2135(a'), 2203(a'), 2229(a''), 2252(a')	29.04

Table 3: Relative Energies of Reaction Pathways (I) and (II) (kcal/mol)

reactions	MP2(full)[a]	PMP2(full)[a]	MP3(full)[a]	CISD(full)+QC[a]	CISD(full)+QC[b]
$SiH_3SiH_3 + O^-$					
→ $SiH_3SiH_3O^-$ **7**	-41.80	-41.73	-42.14	-41.10	-41.31
→ SiH_3O^- **2** + SiH_3 **1**	-72.03	-70.95	-61.14	-61.95	-63.10
→SiH_3-O-SiH_3^- **10**	-100.13	-99.29	-90.91	-89.38	-88.59
→SiH_3-O-SiH_3^- **11**	-99.22	-97.84	-91.18	-88.79	-85.36
→SiH_3-O-SiH_3 **9**	-133.79	-132.38	-125.90	-123.05	-119.00

[a]Without ZPE correction.
[b]With ZPE correction.

Table 4: Relative Energies of Reaction Pathway (III) (kcal/mol)

reactions	MP2(full)[a]	PMP2(full)[a]	MP3(full)[a]	CISD(full)+QC[a]	CISD(full)+QC[b]
$SiH_3SiH_3 + O^-$					
→ $SiH_3SiH_3O^-$ **7**	-41.80	-41.73	-42.14	-41.10	-41.31
→ $SiH_3SiH_2O^-$ **12** +H	-61.64	-60.23	-48.78	-47.69	-51.65
→ $SiH_3SiH_2(OH)^-$ **5**	-82.42	-82.33	-76.12	-73.53	-71.90
→ $SiH_3SiH_2(OH)^-$ **6**	-83.94	-82.57	-77.16	-74.45	-70.51
→ $SiH_3SiH_2(OH)$ **4**	-106.82	-105.42	-100.60	-94.50	-89.99

[a]Without ZPE correction.
[b]With ZPE correction.

In Figure 2, **n**-e denotes the relative energy in the case where the anionic species **n** releases an excess electron at the same geometry of **n** (vertical electron ionization), while **m**+e denotes the relative energy in the case where the neutral species **m** gets the excess electron at the same geometry of **m** (vertical electron attachment). The excess electron can escape from **11** or **6** as shown by an arrow in Figure 2, leading to final products **9** or **4** that are realistic local cluster models of uncharged SiO_2.

3.2. Energetics

We have investigated the electron affinity of oxygen atoms in order to confirm the numerical accuracy of our calculation. Experimentally, this affinity was observed to be 33.71kcal/mol.[29] Theoretically, Curtiss *et al.* reported 31.8kcal/mol using the G2(QCI) procedure[30] and 31.1kcal/mol at G2(MP2) procedure.[31] Lauderdale *et al.* calculated it to be 30.76 kcal/mol in ROHF-based fourth-order many-body perturbation theory using Dunning's correlation consistent basis sets.[32] In our case, electron affinity is -12.64 kcal/mol at HF/6-31+G** level and 21.58kcal/mol at CISD(full)+QC/6-31+G** level.

SiH_3O^- **2** has been studied for the purpose of estimating proton affinity in the gas phase. Curtiss *et al.* studied it using Gaussian-1(G1) and Gaussian-2(G2) procedures and reported that its proton affinity is 356.0 kcal/mol at G1 and 356.2kcal/mol at G2.[33] Their optimized Si–O bond length is 1.579 Å at the MP2(full)/6-31G* level. Sauer and Ahlrichs calculated it using the coupled pair function (CPF) method with contraction basis sets from Huzinaga's primitive sets plus polarization function and reported that the Si–O bond length is 1.563 Å.[34] In our case, the Si–O bond length is 1.556 Å, which is similar to the other results, and is smaller than that in neutral SiH_3O in which the Si–O bond length is 1.676 Å at HF/6-31+G** level. This is because all degenerate Si–O π orbitals are occupied in SiH_3O^-. Similar propensity is expected for $SiH_3SiH_2O^-$ **12**.

The penta-coordinated complex $SiH_3SiH_3O^-$ **7** has C_s symmetry in the $^2A'$ electronic state. It possesses all real vibrational frequencies although the lowest one is merely 24 cm^{-1}. Another structure **8** is optimized in the $^2A''$ electronic state and has one imaginary vibrational frequency. The stable structure **7** demonstrates typical penta-

coordination at Si. Equatorial Si–Si and Si–H bonds are slightly longer than those of normal coordination. On the other hand, axial Si–H and Si–O bonds are very long, exhibiting the typical 3-centers 4-electrons bonding. The spin density of O in **7** is +0.97 as its singly occupied molecular orbital (SOMO) is localized on it.

3.3. Reaction Mechanism

We discuss the microscopic mechanism of O^- insertion into an Si–Si bond at the early stage of oxidation. We consider that O^-, which is in the gas phase or diffusing into Si crystal, attacks Si atom on the silicon surface to form the penta-coordinated complex. O^- has three possible ways of attacking Si atom, as shown in Figure 1. The initial way (I) is that the gas-phase O^- attacks the second-most Si atom of the surface. The second way (II) is that diffusing O^- attacks from the back of the topmost Si atom on the surface. The third one (III) is that the gas-phase O^- attacks from skewed-front of the topmost Si atom on the surface. All of these are supported by the hypervalency of Si that leads to the penta-coordinated structure.[35] At the early stage of the reaction, the lone-pair electrons of O^- attack the lowest unoccupied molecular orbital (LUMO) of Si that spreads to the backside of the apical bond. The unpaired electron of O^- remains intact and is situated in the radical SOMO of O^- that spreads orthogonal to the apical bond. The occupied orbital energy diagram of $SiH_3SiH_3O^-$ **7** at HF/6-31+G** level is shown in Figure 4(b). The 8*a′* highest occupied molecular orbital (HOMO) and the 5*a′* orbital are for 3c-4e bonding of apical O–Si–H bond. The 4*a′* orbital SOMO is localized in the oxygen atom because of the difference in electronegativity between Si and O, which stabilizes the orbital significantly. It is characteristic of the Si–O radical system that the energy of SOMO be stabilized. The 7*a′* orbital is for Si–Si σ bond.

The Si–Si bond in **7** is easily cleaved through the electron transfer from 7*a′* to 4*a′*, which leads to the formation of SiH_3O^- **2** and SiH_3 **1**. This is supported by a large stabilization energy of 4*a′* even after accepting an additional electron, as shown in Figure 5. In Figure 5 is also shown the residual SOMO-LUMO interaction remaining in **7**. In the separation limit, SiH_3 **1** + SiH_3O^- **2** is more stable than **7** by 21.79 kcal/mol at

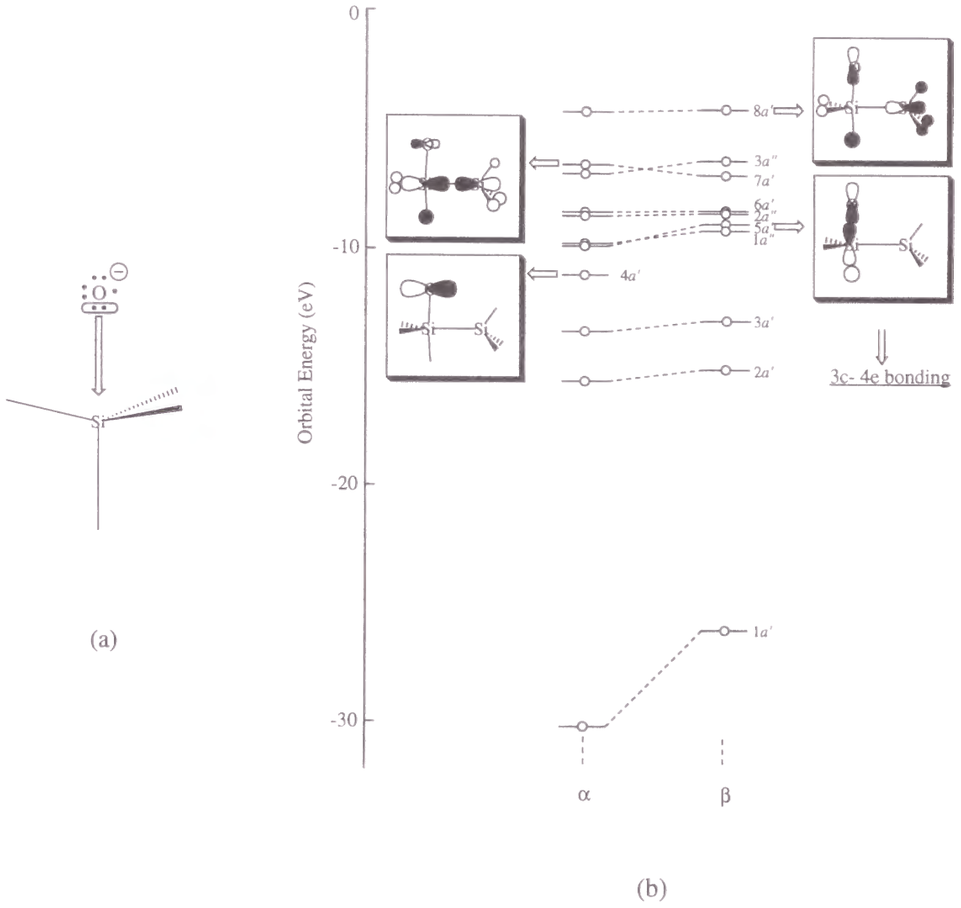

Figure 4. (a) Classical bond image of penta-cooridinated Si with O^- and (b) Occupied orbital energy diagram of $SiH_3SiH_3O^-$ **7** at the UHF/6-31+G** level for both α and β spin spaces.

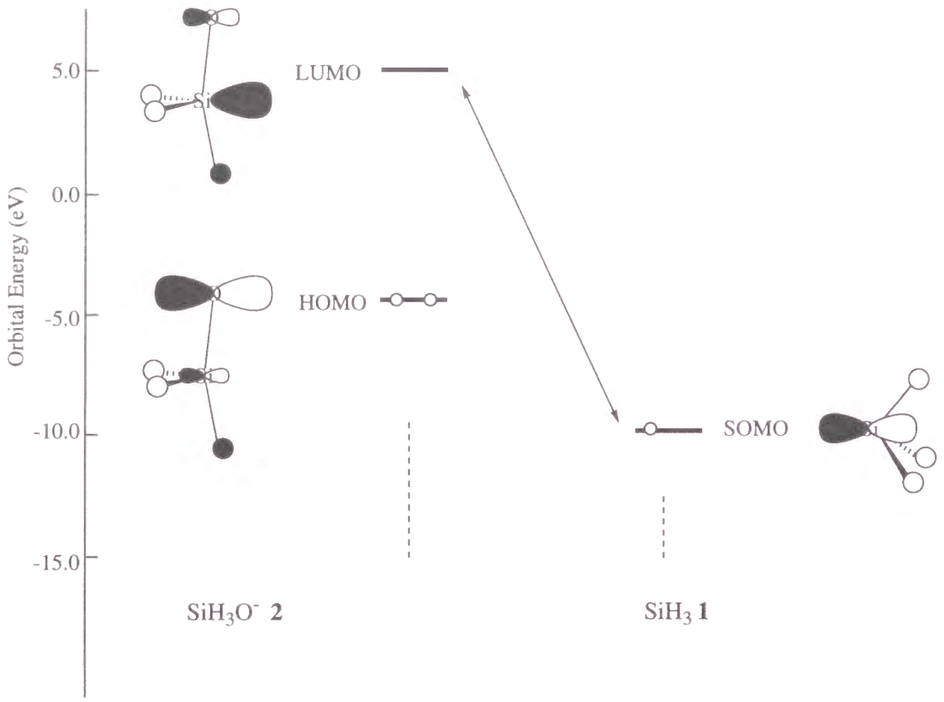

Figure 5. SOMO-LUMO interaction between SiH_3O^- **2** and SiH_3 **1** in $SiH_3SiH_2O^-$ **7**.

CISD(full) level, as shown in Figure 2(a). Analogously, $SiH_3SiH_2O^-$ **12** + H is more stable than **7** by 6.59 kcal/mol at CISD(full) level, as shown in Figure 2(b).

The separated SiH_3 **1** and SiH_3O^- **2** are again bound to form $SiH_3OSiH_3^-$ **10** or **11**. From an energetic view, **10** or **11** is more stable by about 27.43 kcal/mol than SiH_3 **1** + SiH_3O^- **2**. As discussed above, the structure **10** may have a very short lifetime or be excluded from the reaction pathway. However, an important point is that there exists a local level that affects the local electronic character of a reaction series when a lattice collapses locally. Analogously, the separated $SiH_3SiH_2O^-$ **12** and H are recombined to form $SiH_3SiH_2O^-$ **5** or **6**, the stabilization energy of which is about 25.84 kcal/mol. After releasing the excess electron, neutral species SiH_3OSiH_3 **9** in reaction pathways (I) and (II) or SiH_3SiH_2OH **4** in (III) are obtained as demonstrated in Figure 2.

It should be noted from Tables 3 and 4 as well as Figure 2 that SiH_3OSiH_3 **9** is more stable than its structural isomer SiH_3SiH_2OH **4** by 28.55 kcal/mol. This proves the preference for Si–Si bond oxidation.[36-43] Moreover, after all the back bonds are oxidized, the reaction pathway (III) is opened when the terminating H is removed en route to the recombination of $SiH_3SiH_2O^-$ **12** and H.

The discussions given above are all based on the assumption of a localized electron in the domain of a model cluster that is cast in a defect of crystal surface acting as a transient center of electron trap. This picture works well in **7** where the unpaired electron is exclusively localized in O using the 4*a′* orbital, as shown in Figure 4(b); indeed, (1) the spin density is +0.97 for O as shown in Figure 3, which dictates a completely localized spin, (2) the value of $\langle s^2 \rangle$ is 0.761 in the UHF calculation, which is very close to the exact value of 0.75 and hence supports the relevance of the electron configuration shown in Figure 4(b), and (3) the weight of the electron configuration is 0.936 in the CISD calculation with which the argument of Figure 4(b) is clearly reinforced. Moreover, the 7*a′* orbital in Figure 4(b) has the character of Si–Si σ bond with an orbital energy of -6.499 eV and therefore represents that of the conduction band in n-doped Si. However, the electron transfer from this 7*a′* orbital to the 4*a′* orbital with an orbital energy of -11.54 eV will result in the formation of the doubly negatively charged ion O^{2-}, which is strictly

inhibited by the experimental fact that the second electron affinity of O should be negative because of the resultant large electron-electron repulsion. On the other hand, no matter how transient the lifetime of the species **10** or **5** is, the excess electron in these species has strong interaction with the conduction band of Si as demonstrated by the distribution of charge and spin density in Figure 3. Thus, we can further assume that with the lapse of sufficient time, the excess electron should be released even from **10** or **5** .

3.4. Reactivity of Oxidized Si with Oxygen Anion

We have investigated the reactivity of O^- with Si that is partially oxidized on the surface using the following consecutive reactions:

$$SiH_{4-n}(OH)_n + O^- \rightarrow [SiH_{4-n}(OH)_nO]^-$$
$$\rightarrow SiH_{3-n}(OH)_{n+1}^-$$
$$\rightarrow SiH_{3-n}(OH)_{n+1}.$$

The reaction energies are summarized in Table 5 and energy diagrams and geometries are shown in Figure 6. In all cases, the stable penta-coordinated complexes are found. The stabilization energy increases as the number of n (n=0-4) increases. This tendency may serve as the driving force for layer-by-layer oxidation of H-Si(111) using O^- as a reactive species. The stabilization energy is enhanced if it releases the excess electron, which is a natural extension from the situation in preceding subsections. The most stable product up to n=3 is the neutral species $SiH_{3-n}(OH)_{n+1}$. The reaction energy increases as the number of n (n=0-3) increases.

Further investigation including the effects of surface strain in H-Si(111) is necessary in order to study a real material under oxidation. A preliminary attempt toward this investigation may be found in section 3.5.

3.5. Cage Model

For the H-Si(111) surface we have adopted a local cage model $Si_{10}H_{16}$ whose optimized geometry in T_d symmetry at HF/6-31G* level is shown in Figure 7. The total energy is shown in Table 6 and vibrational frequencies are shown in Table 7. The Si–Si

Table 5: Reaction Energies in $SiH_{4-n}(OH)_n + O^-$ System (First Row : CISD(full)/6-31+G** // HF/6-31+G**; Second Row : HF/6-31+G** (kcal/mol))

	n=0	n=1	n=2	n=3	n=4
$SiH_{4-n}(OH)_n + O^-$	0.0	0.0	0.0	0.0	0.0
	0.0	*0.0*	*0.0*	*0.0*	*0.0*
$\rightarrow [SiH_{4-n}(OH)_nO]^-$	-74.728	-85.384	-91.011	-92.380	-93.996
(axial)	*-31.266*	*-39.837*	*-44.470*	*-45.141*	*-47.058*
$\rightarrow [SiH_{4-n}(OH)_nO]^-$	-75.954	-88.209	-95.058	-96.608	-98.319
(equatorial)	*-31.044*	*-41.397*	*-47.380*	*-48.158*	*-50.175*
$\rightarrow [SiH_{3-n}(OH)_{n+1}]^-$	-112.889	-123.472	-132.260	-132.553	–
	-57.958	*-68.500*	*-77.390*	*-78.194*	–
$\rightarrow SiH_{3-n}(OH)_{n+1}$	-141.347	-148.800	-150.549	-151.131	–
	-93.121	*-100.276*	*-102.759*	*-103.743*	–

(a)

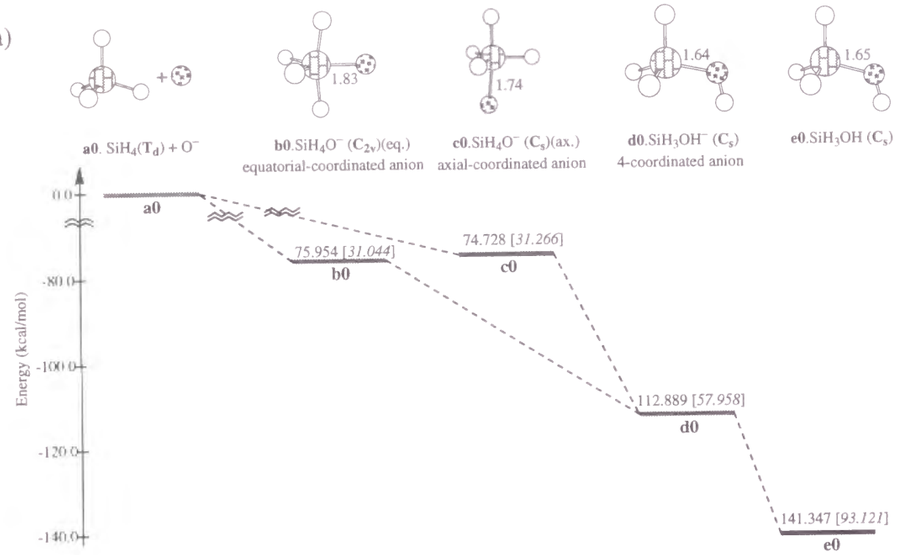

(b)

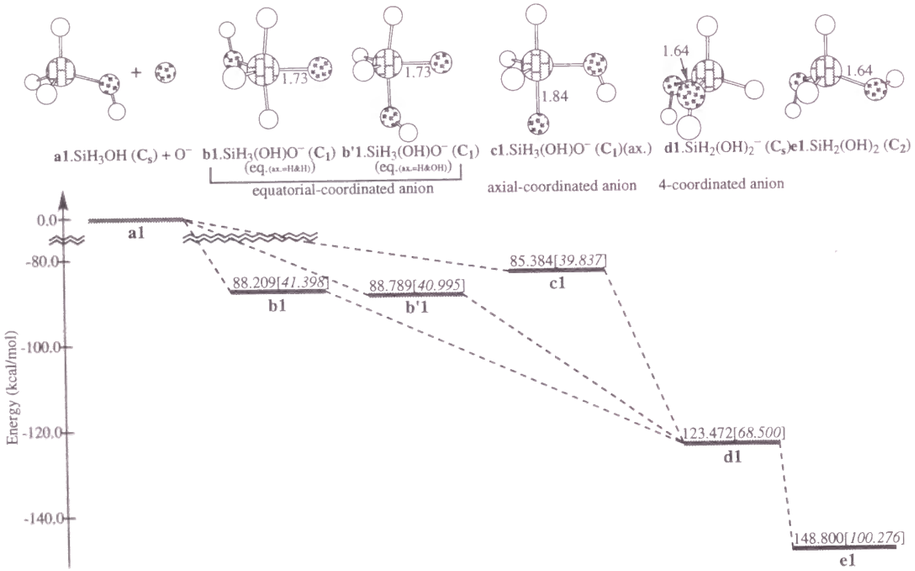

Figure 6. Energy diagrams in $SiH_{4-n}(OH)_n + O^-$ systems at the CISD(full)+QC/6-31+G** level [the HF/6-31+G** level] in kcal/mol: (a)-(e) corresponds to n=0-4, respectively.

(c)

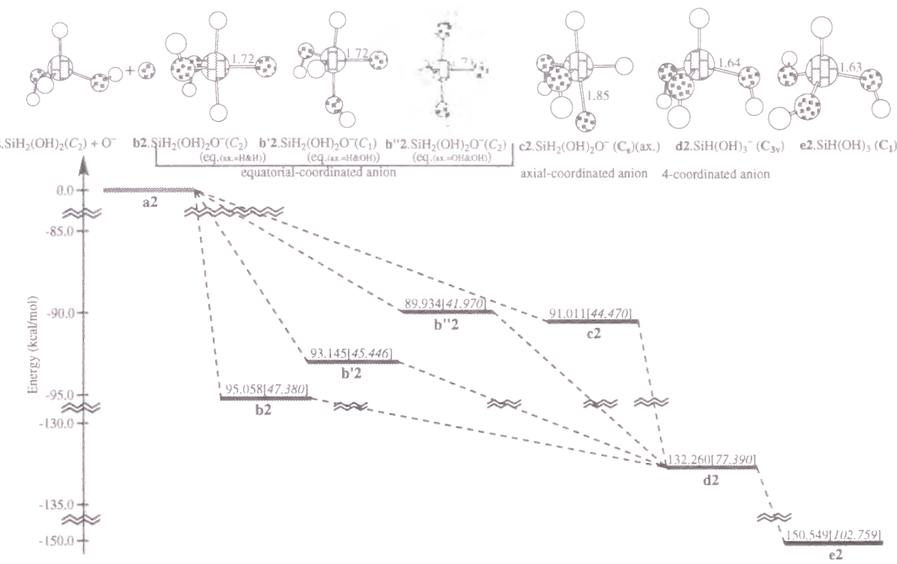

(d)

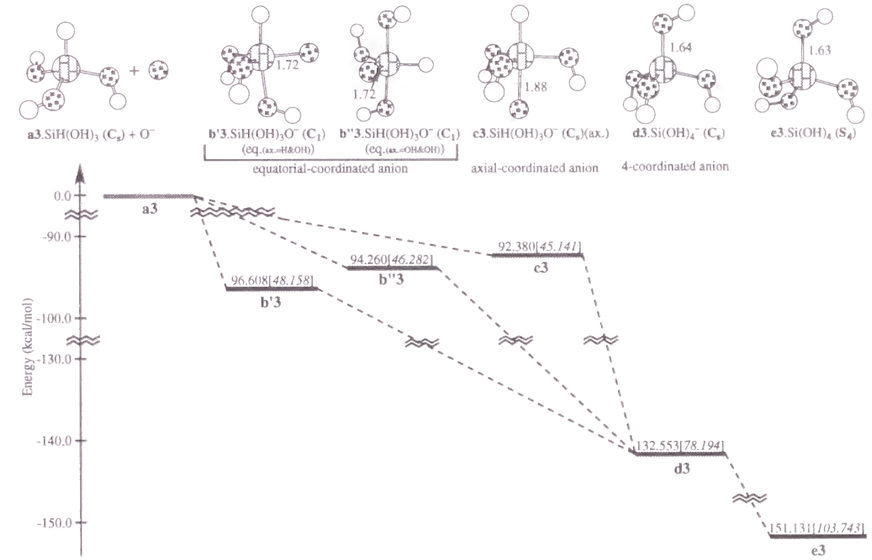

Figure 6. *(Continued from the previous page.)*

(c)

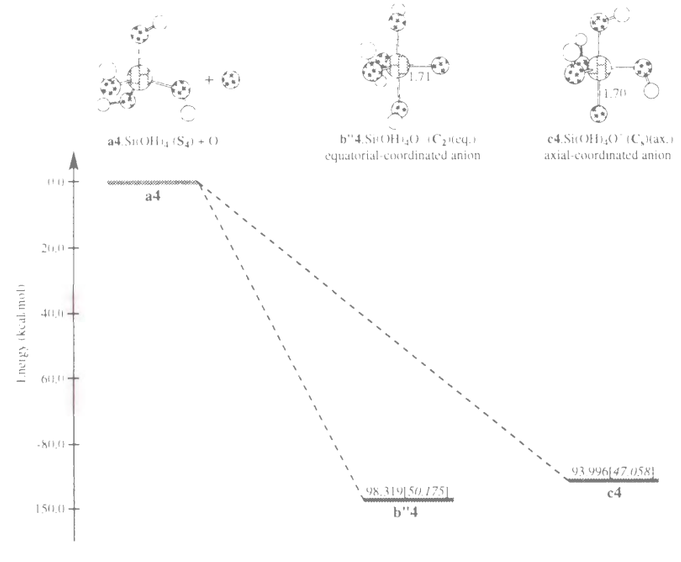

Figure 6. *(Continued from the previous page.)*

Table 6: Total Energies at the Hartree-Fock and MP2(fc) Levels in au

systems		HF	MP2(fc)//HF
Cage model $Si_{10}H_{16}$[a]	(T_d)	-2898.53000	-2899.33663
O^- in Cage (Si-O 2.3Å fixed)[b]	(C_{3v})	-2973.32690	-2974.92525

[a]Using 6-31G* basis set.

[b]Using the 6-31G* basis set for Si and H atoms and the 6-31+G* basis set for O atom.

Table 7: Vibrational Frequencies of Cage Model at the HF/6-31G* Level

harmonic vibrationsl frequencies (cm^{-1})	ZPE[a]
80(t_1), 111(e), 123(t_2), 202(t_2), 329(a_1), 347(a_1), 367(t_2), 417(t_1), 437(e), 456(t_2),511(t_1), 533(t_2), 626(t_1), 636(a_2), 698(t_1), 713(e), 747(t_2), 756(t_1), 798(e), 847(t_2), 1006(e), 1012(t_2), 1026(a_1), 2326(a_1), 2327(t_2), 2341(e), 2345(t_2), 2345(t_1), 2352(t_2),2359(a_1)	86.60

[a]ZPE scaled by 0.89.

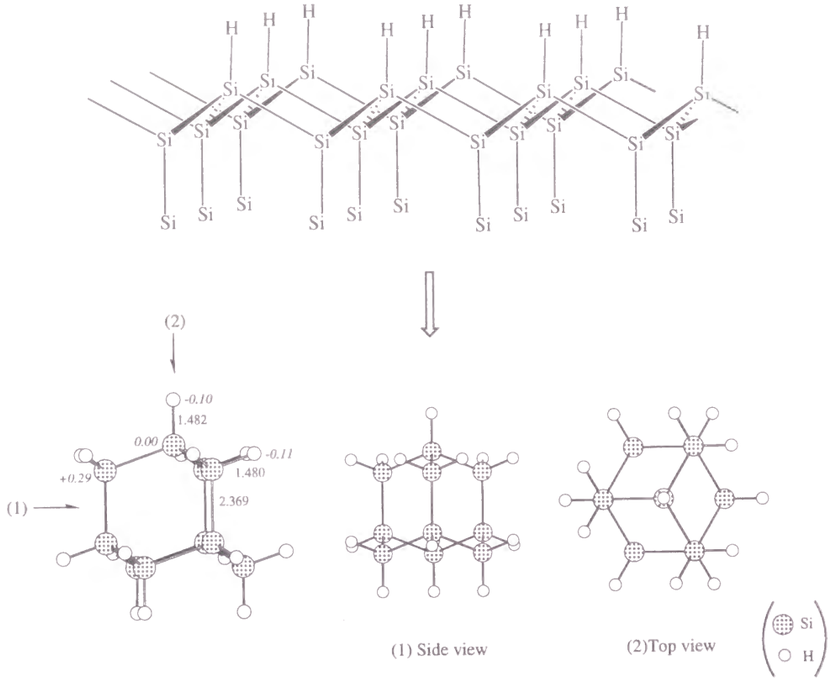

Figure 7. Optimized geometry of a local cage model $Si_{10}H_{16}$ of H-Si(111) surface. Bond length is given in Å and bond angle in degree. Mulliken atomic charges are given in italics.

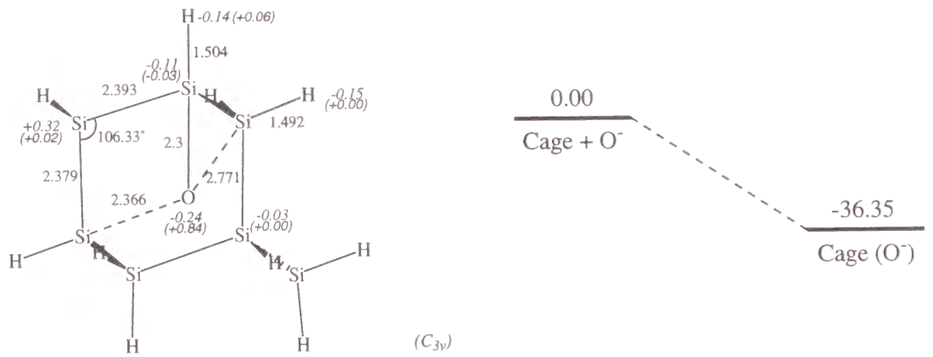

Figure 8. Stabilization of O^- in the cage model. (a) Optimized geometry of the cage model with Si-O bond length fixed at 2.3Å along the C_3 axis of the cage model. Bond length is given in Å and bond angle in degree. Mulliken atomic charges are given in italics. The spin densities are in parentheses. (b) Energy diagram at the MP2(fc)//HF level (kcal/mol).

bond length is 2.369Å and the Si–H bond terminating the Si surface is 1.482Å long. The Si–H bond length is larger than that of silane molecule SiH_4 (1.475Å at HF/6-31G*). This is because neighboring Si atoms donate electron in Si–H bond whose antibonding orbital component is mixed in occupied orbitals. Therefore the surface-terminating Si–H bond is weaker than the basic Si–H bond, which is also proven in Table 2 where the a_1 mode corresponding to Si–H stretching is 2359cm^{-1} (2100cm^{-1} if scaled by 0.89) while it is 2393cm^{-1} (2130cm^{-1} if scaled by 0.89; the experimental value is 2175 cm^{-1}) in silane molecule. This tendency can be extrapolated to the real H-Si(111) surface where FT-IR technique has revealed the fact that the surface-terminating Si–H stretching vibrational frequency is 2083.7 cm^{-1},[2] which is red-shifted from 2175 cm^{-1} of silane molecule.[44,45]

The hypervalency of Si is sufficiently strong to stabilize O^- in this cage, as shown in Figure 8(a). The electronic structure is $^2A'$. Both Si–Si and Si–H bonds are lengthened and Mulliken atomic charge shows that the excess electron is considerably transferred from O^- to the topmost Si. Irrespective of the large strain in the Si network of the cage and the delocalized excessive negative charge in it, the $Si_{10}H_{16}O^-$ cluster is more stable by 36.35kcal/mol than $Si_{10}H_{16} + O^-$, as shown in Figure 8(b). This result demonstrates that O^- can be included into Si bulk and diffuse through it. This is consistent with Jorgensen's observation [10], who studied the effect of an external electric field on silicon oxidation and concluded that oxygen ions are the predominant species diffusing through the growing film.

3.6. Extended Model of Periodic Boundary Condition

For an extended model of the oxidation of H-Si(111) surface by O^-, we adopted the supercell geometry system shown in Figure 9(a), (b). In the 2×2 surface unit cell, 4 layers of Si are contained and the vacuum region is 13.04 Å in size. An O^- anion approaches the H-Si(111) surface via reaction pathway (I) in Figure 1. The stabilization of the penta-coordinated reaction complex is unambiguously proven, as shown in Figure 9(c).

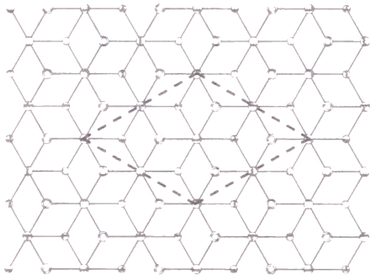

(a)

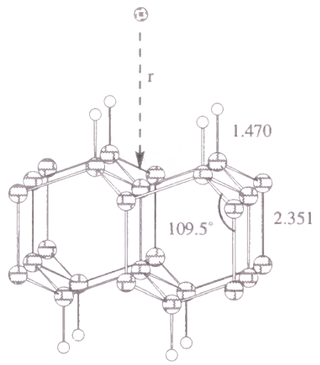

(b)

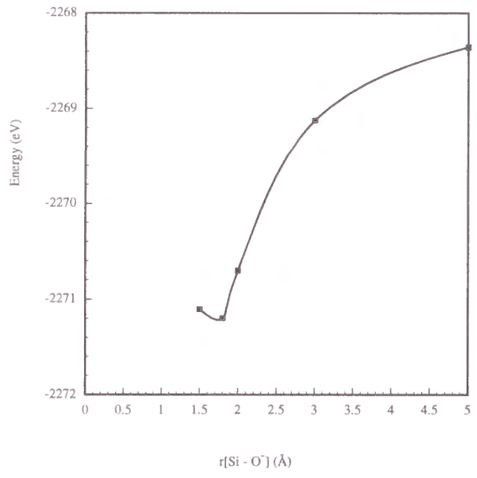

(c)

Figure 9. (a) Top view of the O^- absorbtion along the reaction pathway (I) on H-Si(111) surface under periodic boundary condition. Unit cell is indicated by dotted line. (b) Side view of the part of unit cell. Bond length is given in Å and bond angle in degree. r denotes the Si-O^- distance. (c) Potential energy curve of O^- absorption along the reaction pathway (I) on H-Si(111) surface.

4. Conclusion

We have investigated the oxidation mechanism of the H-Si(111) surface by O^- using *ab initio* molecular orbital method of quantum chemistry. We have found that the hypervalency of Si is fundamentally important to initiate and promote the oxidation. O^- can attack surface Si atoms to form penta-coordinated complexes, which should further lower the diffusion barrier for O^- transfer into the Si bulk. This has been proven using a local cage model of the H-Si(111) surface augmented by an extended model of periodic boundary condition. O^- should then be inserted into an Si–Si bond to form a local Si–O–Si structure. The reactivity of insertion arises from the unpaired radical electron in O^-. The stabilization energy is enhanced if the deformation energy in the local Si–O–Si structure is released. That the oxidized Si has a strong tendency to accept additional O^- is concluded using a series of cluster model calculations. Since the active species is a charged one, the external electric field will play an important role in controlling its reactivity, *e.g.*, charge-up of the material or the thickness of SiO_2 film.

References

(1) Takahagi, T.; Nagai, I.; Ishitani, A.; Kuroda, H.; Nagasawa, Y. *J. Appl. Phys.* **1988**, *64*, 3516.

(2) Higashi, G. S.; Chabal, Y. J.; Trucks, G. W.; Raghavachari, K. *Appl. Phys. Lett.* **1990**, *56*, 656.

(3) Higashi, G. S.; Becker, R. S.; Chabal, Y.; Becker, J. *Appl. Phys. Lett.* **1991**, *58*, 1656.

(4) Jakob, P.; Dumas, P.; Chabal, Y. J. *Appl. Phys. Lett.* **1991**, *59*, 2968.

(5) Watanabe, S.; Nakayama, N.; Ito, T. *Appl. Phys. Lett.* **1991**, *59*, 1458.

(6) Watanabe, S.; Shigeno, M.; Nakayama, N.; Ito, T. *Jpn. J. Appl. Phys.* **1991**, *30*, 3575.

(7) Watanabe, S.; Sugita, Y. *Surf. Sci.* **1995**, *327*, 1.

(8) Hattori, T. *CRC Crit. Rev. Solid State Mater. Sci.* **1995**, *20*, 339.

(9) Sakata, K.; Tachibana, A.; Zaima, S.; Yasuda, Y. *Jpn. J. Appl. Phys.* **1998**, *37*, 4962.

(10) Jorgensen, P. J. *J. Chem. Phys.* **1962**, *37*, 874.

(11) Tachibana, A.; Sakata, K.; Sato, T. *Ext. Abstr. (58th Autumn Meet,1997); Japan Society of Applied Physics, 2pD2* [in Japanese].

(12) DePuy, C. H.; Bierbaum, V. M.; Damrauer, R. *J. Am. Chem. Soc.* **1984**, *106*, 4051.

(13) Sheldon, J. C.; Hayes, R. N.; Bowie, J. H.; Depuy, C. H. *J. Chem Soc., Perkin Trans. 2* **1987**, 275.

(14) Gordon, M. S.; Davis, L. P.; Burggraf, L. W.; Dammrauer, R. *J. Am. Chem. Soc.* **1986**, *108,* 7889.

(15) Davis, L. P.; Burggraf, L. W.; Gordon, M. S. *J. Am. Chem. Soc.* **1988**, *110*, 3056.

(16) Gordon, M. S.; Carroll, M. T.; Davis, L. P.; Burggraf, L. W. *Comput. Mater. Sci.* **1993**, *1*, 161.

(17) Frisch, M. J.; Trucks, G. W.; Schlegel, H. B.; Gill, P. M. W.; Johnson, B. G.; Robb, M. A.; Cheeseman, J. R.; Keith, T.; Petersson, G. A.; Montgomery, J. A.; Raghavachari, K.; Al-Laham, M. A.; Zakrzewski, V. G.; Ortiz, J. V.; Foresman, J. B.; Peng, C. Y.; Ayala, P. A.; Chen, W.; Wong, M. W.; Andres, J. L.; Replogle, E. S.; Gomperts, R.; Martin, R. L.; Fox, D. J.; Binkley, J. S.; Defrees, D. J.; Baker, J.; Stewart, J. P.; Head-Gordon, M. ; Gonzalez, C.; Pople, J. A. *Gaussian 94*, *Revision B.3*; Gaussian, Inc.: Pittsburgh, PA, 1995.

(18) Hehre, W. J.; Radom, L.; Schleyer, P. v. R.; Pople, J. A. *Ab initio Molecular Orbital Theory*; Wiley: New York, 1986.

(19) Møller, C.; Plesset, M. S. *Phys. Rev.* **1934**, *46* , 618.

(20) Binkey, J. S.; Pople, J. A. *Int. J. Quantum Chem.* **1975**, *9*, 229.

(21) Pople, J. A.; Binkley, J. S.; Seeger, R. *Int. J. Quantum Chem. Symp.* **1976**, *10*, 1.

(22) Pople, J. A.; Binkley, J. S.; Krishnan, R. *Int. J. Quantum Chem. Symp.* **1977**, *11*, 149.

(23) Schlegel, H. B. *J. Phys. Chem.* **1988**, *92,* 3075.

(24) Mulliken, R. S. *J. Chem. Phys.* **1955**, *23*, 1833.

(25) Payne, M. C.; Teter, M. P.; Allan, D. C.; Aris, T. A.; Joannopoulos, J. D. *Rev. Mod. Phys.* **1992**, *61*, 1045.

(26) Perdew, J. P.; Zunger, A. *Phys. Rev. B* **1981**, *23*, 5048.

(27) Kleinman, L.; Bylander, D. M. *Phys. Rev. Lett.* **1982**, *48*, 1425.

(28) Lin, J. S.; Qteish, A.; Payne, M. C.; Haine, V. *Phys. Rev. B* **1993**, *47*, 4174.

(29) Hotop, H.; Lineberger, W. C. *J. Phys. Chem. Ref. Data* **1975**, *4*, 539.

(30) Curtiss, L. A.; Carpenter, J. E.; Raghavachari, K.; Pople, J. A. *J. Chem. Phys.* **1992**, *96*, 9030.

(31) Curtiss, L. A.; Raghavachari, K.; Pople, J. A. *J. Chem. Phys.* **1993**, *98*, 1293.

(32) Lauderdale, W. J.; Stanton, J. F.; Gauss, J.; Watts, J. D.; Bartlett, R. J. *J. Chem. Phys.* **1992**, *97*, 6606.

(33) Curtiss, L. A.; Nicholas, J. B.; Iton, L. E. *Chem. Phys. Lett.* **1991**, *184*, 215.

(34) Sauer, J.; Ahlrichs, R. *J. Chem. Phys.* **1990**, *93*, 2575.

(35) Apeloig, Y. *The Chemistry of Organic Silicon Compounds*, Patai, S., Rappoport, Z., Eds.; Wiley: New York, 1986.

(36) Nicholas, J. B.; Feyereisen, M. *J. Chem. Phys.* **1995**, *103*, 8031.

(37) O'Keeffe, M.; Gibbs, G. V. *J. Chem. Phys.* **1984**, *81*, 876.

(38) Ferrari, A. M.; Ugliengo, P.; Garrone, E. *J. Phys. Chem.* **1993**, *97*, 2671.

(39) Csonka, G. I.; Réffy, J. *Chem. Phys. Lett.* **1994**, *229*, 191.

(40) Luke, B. T. *J. Phys. Chem.* **1993**, *97*, 7505.

(41) Nicholas, J. B.; Winans, R. E.; Harrison, R. J.; Iton, L. E.; Curtiss, L. A.; Hopfinger, A. J. *J. Phys. Chem.* **1992**, *96*, 7958.

(42) Shambayati, S.; Blake, J. F.; Wierschke, S. G.; Jorgensen, W. L.; Schreiber, S. L. *J. Am. Chem. Soc.* **1990**, *112*, 691.

(43) Grigoras, S.; Lane, T. H. *J. Comp. Chem.* **1987**, *8* , 84.

(44) Smith, A. L.; Angelotti, N. C. *Spectrochim. Acta* **1959**, *15*, 412.

(45) Lucovski, G. *Solid State Commun.* **1979**, *29* , 571.

Chapter 6:

Quantum Chemical Study on Aluminum Selective CVD Reaction Mechanism

1. Introduction

Aluminum (Al) selective chemical vapor deposition (CVD) on the silicon (Si) surface has received much attention as promising technology for ultralarge-scale integration (ULSI) metallization.[1] Clever choice of the molecular precursor of Al as well as the substrate surface should play an important role in initiating selective nucleation of Al. One of the recent key issues in this field of research has shown that the best possible selectivity is achieved by the combination of dimethylaluminum hydride (DMAlH) as the Al precursor and hydrogen (H)-terminated Si as the substrate surface.[2-5]

The reaction kinetics of the Al-selective CVD on the H-terminated Si has been studied as a function of temperature using the *in-situ* Fourier transform infrared (FTIR) attenuated total reflection (ATR) technique.[6] Then, the variations in the FTIR-ATR desorption intensity of Al–H, Si–H and CH_3–Al bands have concluded the following facts:

(1) DMAlH gas is physisorbed on the H-terminated Si surface at 10 min, 1 Torr and room temperature. No desorption of any kind is observed in this low temperature regime.

(2) As temperature is raised, H atom exclusively from DMAlH is desorbed below 150 ˚C.

(3) If the temperature is raised further, H atom from the H-terminated Si surface and CH_3 group from DMAlH are desorbed simultaneously over around 150 ˚C.

In this paper, we have devised model reaction species and reaction paths and studied this interesting temperature-dependent reaction mechanism in terms of *ab initio* molecular orbital (MO) theory of quantum chemistry.

2. Methods of Calculation

MO calculations were performed with the GAUSSIAN94 program package.[7] The geometries were optimized by the analytical energy gradient method at Hartree-Fock (HF)

self consistent field (SCF) level and second-order Møller-Plesset (MP) perturbation theory[8,9] which includes correlation for all electrons, using the standard 6-31G** basis set (denoted as HF/6-31G** and MP2(full)/6-31G**).[10] Theoretical harmonic vibrational frequencies were obtained from analytical second derivatives calculated at MP2(full)/6-31G** level to verify each equilibrium structure as a true energy minimum or a saddle point. Zero-point vibrational energies (ZPE) were then scaled by a factor of 0.94.[11] To obtain higher correlation energies, single point calculations of single and double substituted configuration interaction (CISD)[12] including unlinked cluster quadruple corrections (QC)[13] were carried out on the MP2(full)/6-31G** geometries (denoted as CISD+QC(full)/6-31G**//MP2(full)/6-31G**).[11] The Mulliken atomic charge[14] was calculated using SCF density at MP2(full)/6-31G** level optimized geometry.

3. Results and Discussion

Model reaction paths and total energies of reactant and product species are listed in Tables 1 and 2. The transition state (TS) of the *n*th reaction path is denoted as **TS*n***. For the first and second reaction paths, the **TS1** and **TS2** are shown in Figure 1. The reaction energies are summarized in Table 1. The MO energy levels of the selected molecular species are shown in Figure 2 and the MO patterns in Figure 3. The energy diagrams are collected in Figure 4.

3.1. Optimized Structures

According to our calculation for alane (AlH_3), Al–H bond length is 1.582Å at HF level and 1.577Å at MP2 level. Electron correlation tends to shorten the Al–H bond. Aggregates of AlH_3 and its alkyl substitution products will polymerize at low temperature making strong charge transfer complexes[15] in a similar way borane (BH_3) does.[16-22] Theoretically, AlH_3 is also predicted to form Al–Al bond leaving hydrogen (H_2).[19-25] The resultant Al_2H_4 has several geometrical isomers[26,27], and we use a conventional D_{2d}

Table 1: Reaction Energies (kcal/mol)[a]

reaction		activation energy	heat of reaction
$AlH_3 + AlH_3 \rightarrow H_2AlAlH_2 + H_2$	(1)	25.29(27.16)	-0.08(1.39)
$AlH_3 + SiH_4 \rightarrow AlH_2(SiH_3) + H_2$	(2)	30.89(31.07)	0.80(1.14)
$AlH_3 + AlH_2(CH_3) \rightarrow H_2AlAlH_2 + CH_4$	(3)	34.91(34.32)	-4.26(-1.70)
$AlH_2(CH_3) + SiH_4 \rightarrow AlH_2(SiH_3) + CH_4$	(4)	38.49(36.47)	-3.38(-1.94)
$AlH_2(CH_3) + AlH_2(CH_3) \rightarrow H_2AlAlH_2 + CH_3CH_3$	(5)	84.18(83.79)	7.19(9.96)
$AlH_2(CH_3) + H_2 \rightarrow AlH_3 + CH_4$	(6)	34.25(33.62)	-4.18(-3.08)

[a]At the CISD(full)+QC/6-31G**//MP2(full)/6-31G** level including ZPE(scaled) corrections.
At the MP2(full)/6-31G** level including ZPE(scaled) corrections in parentheses.

Table 2: Total Energies(au)

species	HF/6-31G**[a]	MP2(full) /6-31G**[b]	CISD+QC(full) /6-31G**[b]
1H_2	-1.13133	-1.15766	-1.16514
2CH_4	-40.20170	-40.36986	-40.39258
3SiH_4	-291.23084	-291.34986	-291.37821
4CH_3CH_3	-79.23824	-79.55371	-79.59025
5AlH_3	-243.61899	-243.69917	-243.72073
6Al_2H_4	-486.09547	-486.23750	-486.27548
7$AlH_2(CH_3)$	-282.67013	-282.90120	-282.93625
8$AlH_2(SiH_3)$	-533.70499	-533.88689	-533.92987
TS1	-487.17203[c]	-487.35725	-487.40335
TS2	-534.77663	-535.00097	-535.05117
TS3	-526.20977[d]	-526.54795	-526.60363
TS4	-573.81646	-574.19403	-574.25420
TS5	-565.17307[c]	-565.67187	-565.74135
TS6	-283.73835	-284.01059	-284.05212

[a]At HF/6-31G** optimized geometries. [b]At MP2(full)/6-31G** optimized geometries.
[c]Optimized in C_1 symmetry. [d]Optimized in another C_s symmetry.

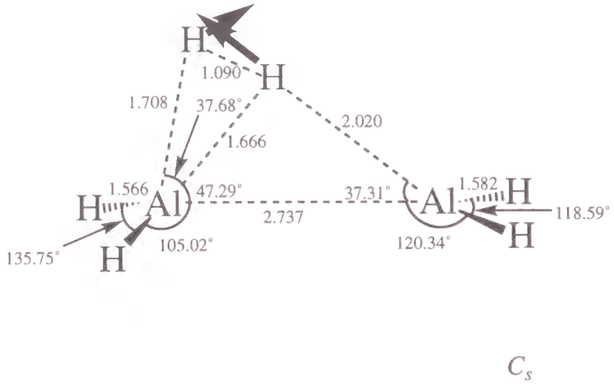

C_s

TS1

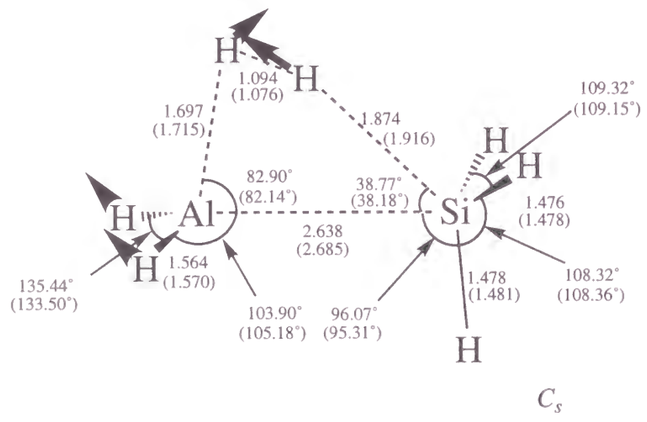

C_s

TS2

Figure 1. Optimized geometries at MP2(full)/6-31G** level. Bond lengths are in angstroms and bond angles and dihedral angles are in degrees. HF/6-31G** level optimized data are in parentheses.

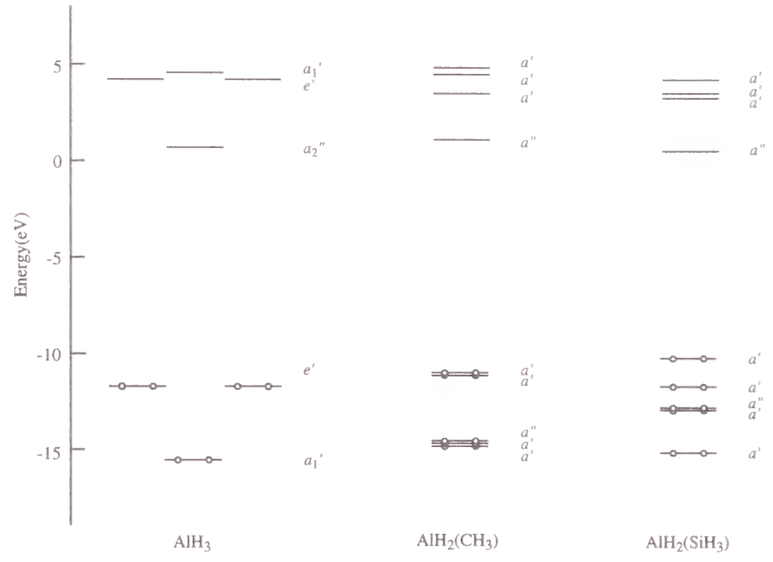

Figure 2. MO energy diagrams of AlH_3, $AlH_2(CH_3)$, and $AlH_2(SiH_3)$ at HF/6-31G** level on the MP2(full)/6-31G** level geometries.

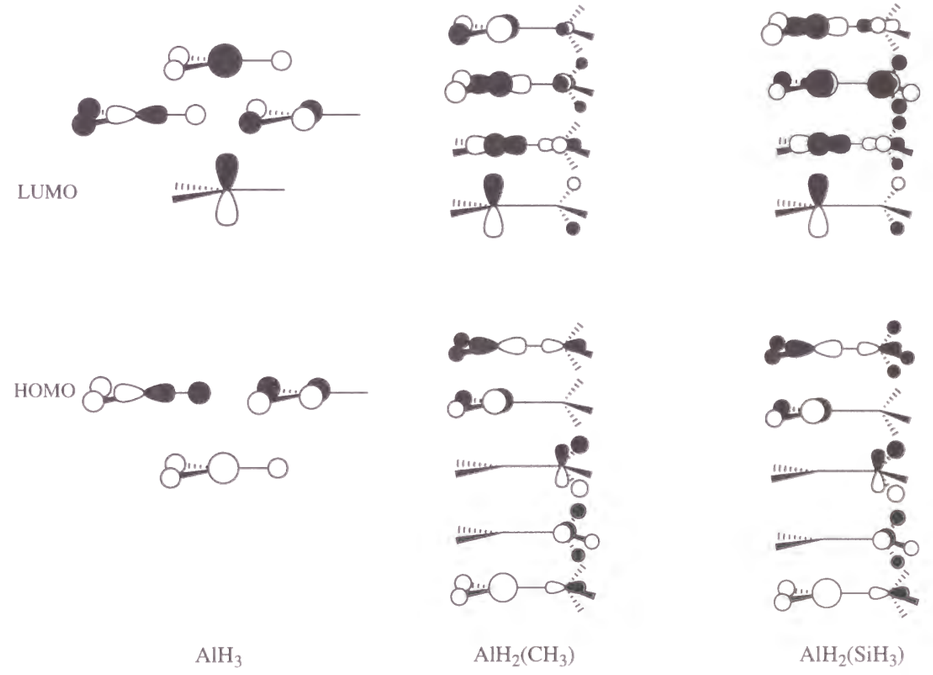

Figure 3. MO patterns of each energy levels.

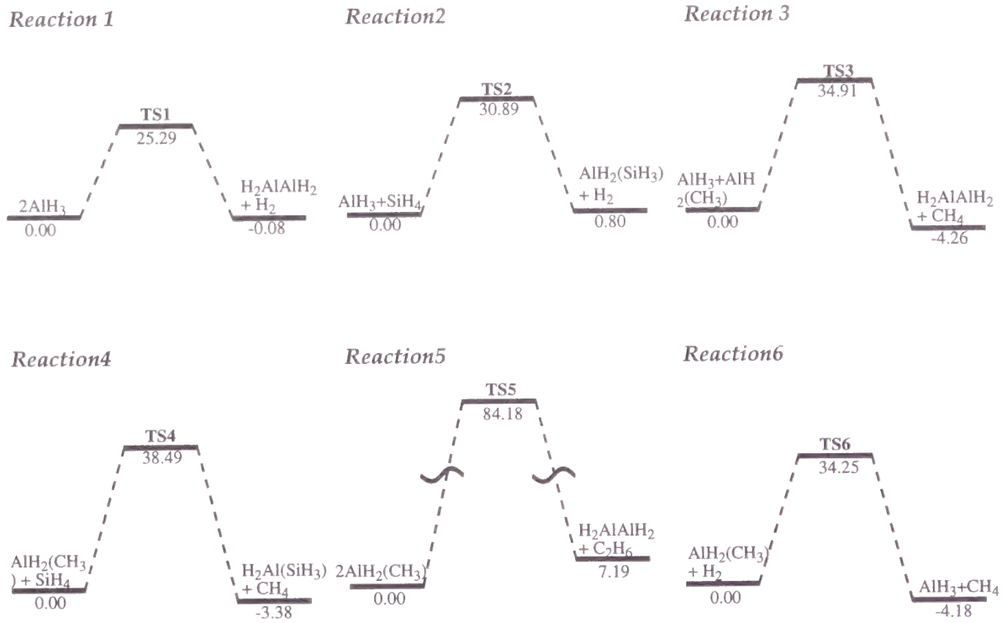

Figure 4. Energy diagrams of each reactions in kcal/mol. Relative energies are calculated by using total energies at CISD(full)+QC/6-31G**//MP2(full)/6-31G** level corrected with ZPEs.

form of AlH_2-AlH_2 here in this paper. In the AlH_2AlH_2, Al–Al bond length is 2.585Å and Al–H bond length is 1.587Å. AlAlH bond angle is 122.02° at MP2/6-31G** level, which nearly accords with Schleyer's HF/6-31G* level calculation.[27] The internal rotation energy barrier around the Al–Al bond is 1.5kcal/mol at MP4/6-31G**//HF/6-31G*+ZPE level by Schleyer *et al.* and 1.81kcal/mol at MP2/6-31G**+ZPE level by our calculation, which shows that the Al–Al bond is nearly free for rotation. We further optimized structures $AlH_2(CH_3)$ and $AlH_2(SiH_3)$ at C_S symmetry.[28-30] Al–C bond length is 1.960Å at MP2 level (1.971Å at HF level), while Al–Si bond length is 2.452Å (2.478Å at HF level).

3.2. Reactivity of DMAlH on the H-Terminated Si Surface

The Al in AlH_3 is calculated to be highly positively charged (+0.60) and the H on the terminated Si surface is assumed to be highly negatively charged, judging from the electronegativity difference. Actually, using silane (SiH_4) as a local model of the H-terminated Si in this case provides the value of -0.17 for the charge of H attached to Si. Because of the electrostatic effect, we may then assume that AlH_3 can easily be physisorbed on the H-terminated Si surface at room temperature. On the surface, the physisorped AlH_3 may first react with another AlH_3 to form the Al–Al bond prior to Al–Si bond formation. We assume reaction (1) in Table 1 as the model of this elementary process (i), while reaction (2) in Table 1 is the model of the elementary process (ii) to form the Al–Si bond.

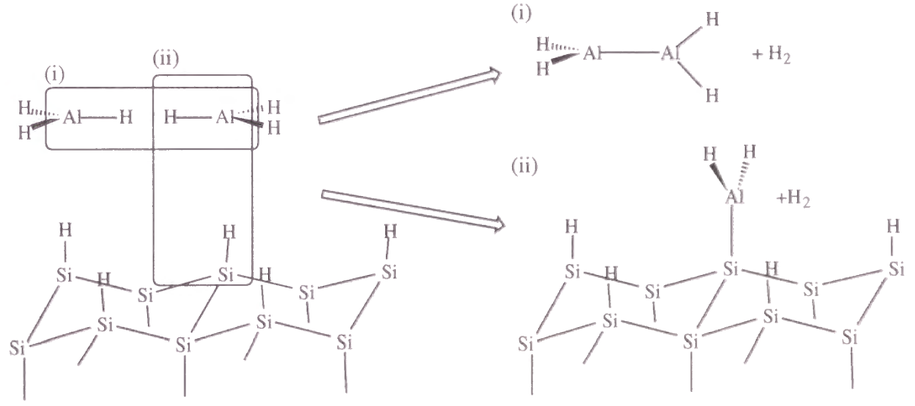

For reaction (1), the symmetry of the **TS1** is optimized to be C_1 at HF/6-31G** level, but C_S at MP2/6-31G** level, as shown in Figure 1. The activation energy of this reaction is 25.29kcal/mol at CISD+QC level including ZPE and heat of reaction nearly zero. This reaction is a combination of the elimination of H_2 and the succeeding internal rotation of Al–Al bond.

For reaction (2), the symmetry of the **TS2** is optimized to be C_S as shown in Figure 1. The barrier height is 45.93kcal/mol at HF/6-31G** level, 31.07kcal/mol at MP2/6-31G** level including ZPE, 30.89kcal/mol at CISD+QC/6-31G** level including ZPE. The LUMO of AlH_3 has very low orbital energy as shown in Figure 2. This means that AlH_3 works as a good electron acceptor in a similar manner BH_3 does.[31,32] According to the orbital patterns shown in Figure 3, the orbital interaction scheme below guides the course of this chemical reaction. Subsidiary back donation of charge is less active in this path.

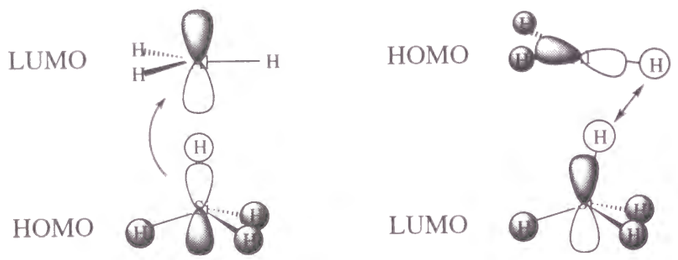

The barrier height of reaction (1) is lower than that of reaction (2) by 5.60kcal/mol at CISD level. It follows that the elementary process (i) can more easily occur than the elementary process (ii) at sufficiently low temperature regime. This qualitatively agrees quite well with the experimental fact that is observed below 150 °C .[6]

But in high temperature regime, the reactivity for the Al–Al bond formation is comparable with the Al–Si bond formation, so that both processes (i) and (ii) can occur competitively. Moreover, the Al as deposited on Si is terminated by H. Therefore, the following elementary process (i)' can also occur.

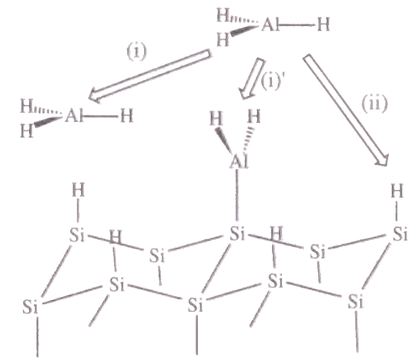

Evidently, the elementary process (i)' provides bump of nucleation. This may be a stumbling block for getting excellent morphology of the Al surface. If we can inhibit the elementary process (i)', then we may acquire perfect layer-by-layer nucleation, a defect-free Al surface as deposited. This may be achieved partly by using DMAlH in place of AlH_3, as will be shown below.

Now, in the reaction system composed of DMAlH and H-terminated Si, two new elementary processes (iii) and (iv) should occur.

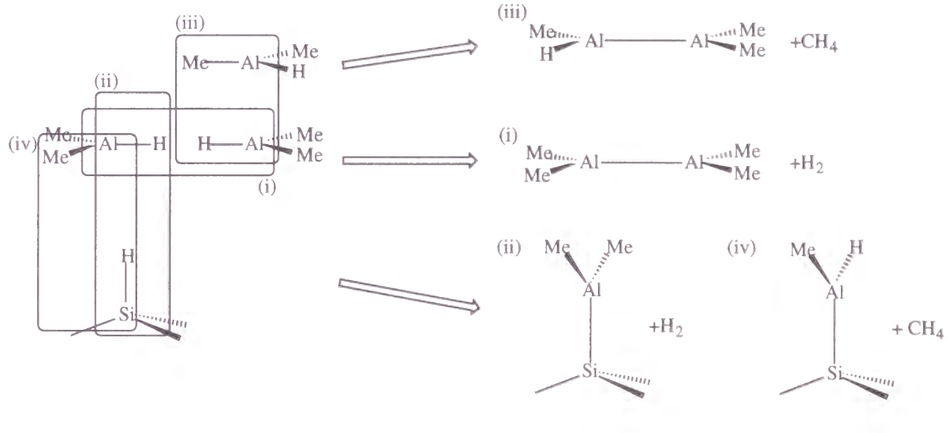

For the elementary process (iii), we assume reaction (3). The barrier height is 34.91kcal/mol at CISD +ZPE level, which is 9.62kcal/mol higher than reaction (1).

For the elementary process (iv), we assume reaction (4). The barrier height is 38.49kcal/mol at CISD+QC +ZPE level, which is 7.6kcal/mol higher than reaction (2). Additionally, the formation of C_2H_6 is examined by assuming reaction (5). The

activation energy is 84.18kcal/mol at CISD +ZPE level, so it rarely occurs actually. Namely, methyl group reacts only with H.

These higher activation energies for the elementary processes (iii) and (iv) tell us that the elementary processes (i) and (ii) are still dominant over and above (iii) and (iv) in this reaction system. But in high temperature regime, all the elementary processes (i)-(iv) are likely to occur. This corresponds to the experimental fact that is observed over around 150 °C.[6]

Moreover, the Al as deposited on Si is protected by methyl group and then the elementary process (i)' is rather inhibited. Therefore, a good morphology of the Al surface will result in this reaction system.

Furthermore, we can consider the following elementary processes.

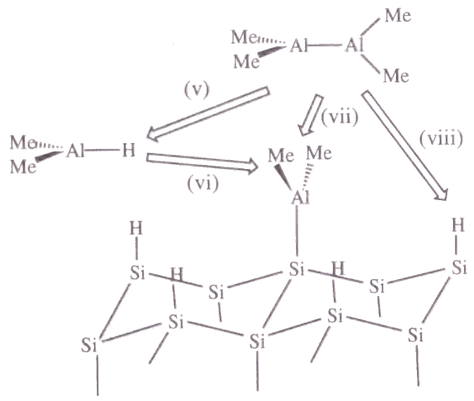

Each process has correspondence with the model reaction discussed above: that is, (v) with reaction (3), (vi) with reaction (3), (vii) with reaction (5), and (viii) with reaction (4). Clearly, the most probable processes are (v) and (vi) followed by (viii).

3.3. The Role of H_2 Carrier Gas

Finally, we discuss the role of H_2 carrier gas.[2] What we have found so far is that the Al as deposited on Si is terminated by methyl group using DMAlH as the molecular precursor. Then, the H_2 carrier gas can play an active role to transform the methyl-terminated Al surface into the H-terminated Al surface that is more reactive. This will be shown as follows, using model reaction (6).

The activation energy of reaction (6) is 51.67kcal/mol at HF level, 33.62kcal/mol at MP2 level including ZPE, 34.25kcal/mol at CISD+QC level including ZPE. The LUMO of AlH_2CH_3 has very low orbital energy as shown in Figure 2. According to the orbital patterns shown in Figure 3, the orbital interaction scheme below guides the course of this chemical reaction.

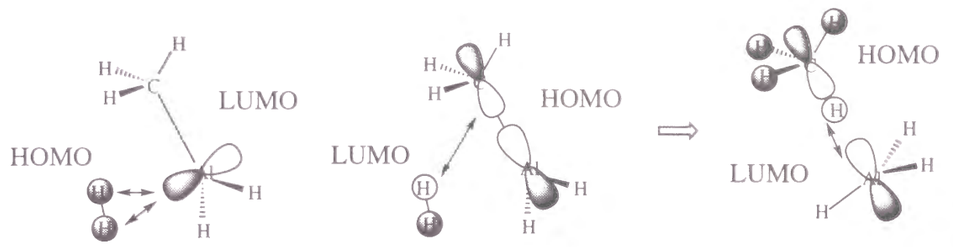

There occurs charge transfer from HOMO of H_2 to LUMO of AlH_2CH_3. Also, back-donation of charge from AlH_2CH_3 to H_2 may occur through interaction between HOMO of AlH_2CH_3 and LUMO of H_2. The latter interaction makes cleavage of Al–C bond and formation of Al–H bond. This completes the transformation of the methyl-terminated Al surface into the H-terminated Al surface. This function of H_2 also acts against intact DMAlH molecule. The whole idea of the active role of H_2 is shown below.

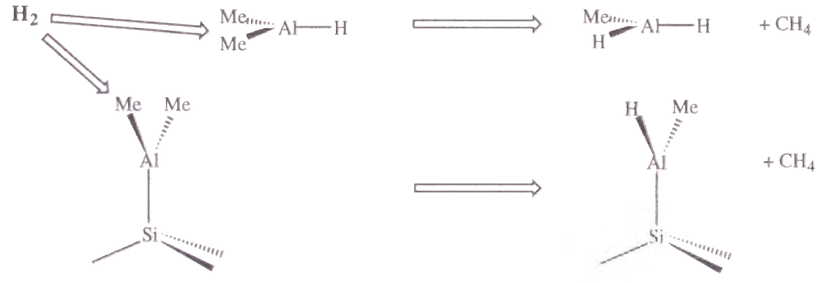

4. Conclusion

We have studied the reaction mechanism of the Al selective CVD processes in the system of DMAlH over H-terminated Si in terms of *ab initio* MO theory of quantum chemistry. Various elementary chemical reaction processes have been identified to account for the temperature-dependent reaction mechanism. We have also revealed that

methyl group suppresses the reactivity of DMAlH with the substrate surface. This reactivity suppression has been recovered by H_2 carrier gas. These results are qualitatively in good agreement with the experimental observations.[6]

In a real CVD system, the situation should be more complex. For example, even in a gas phase, a reaction intermediate may collide with an intact DMAlH molecule or stick to the surface. Defects and impurities on the substrate surface may also change the reactivity. Much work should be done in order to fully understand these new and extremely exciting phenomena.

References

(1) Simmonds, M. G.; Gladfelter, W. L. *The Chemistry of Metal CVD*, Kodas, T. T., Hampden-Smith, M. J., Eds.; VCH: New York, 1994; Chapter 2.

(2) Tsubouchi, K.; Masu, K. *J. Vac. Sci. Technol. A* **1992**, *10*, 856.

(3) Kawamoto, H.; Sakaue, H.; Takehiro, S.; Horiike, Y. *Appl. Phys. Lett.* **1990**, *57*, L1220.

(4) Kawamoto, H.; Sakaue, H.; Takehiro, S.; Horiike, Y. *Jpn. J. Appl. Phys.* **1990**, *11*, 2657.

(5) Tsubouchi, K.; Masu, K.; Shigeeda, N.; Matano, T.; Hiura, Y.; Mikoshiba, N. *Appl. Phys. Lett.* **1990**, *57*, 1221.

(6) Kawamura, K.; Ishizuka, S.; Sakaue, H.; Horiike, Y. *Technical Digest of Inter. Workshop on Science and Technology for Surface Reaction Process*: Tokyo, 1992;pp 91.

(7) Frisch, M. J.; Trucks, G. W.; Schlegel, H. B.; Gill, P. M. W.; Johnson, B. G.; Robb, M. A.; Cheeseman, J. R.; Keith, T.; Petersson, G. A.; Montgomery, J. A.; Raghavachari, K.; Al-Laham, M. A.; Zakrzewski, V. G.; Ortiz, J. V.; Foresman, J. B.; Peng, C. Y.; Ayala, P. A.; Chen, W.; Wong, M. W.; Andres, J. L.; Replogle, E. S.; Gomperts, R.; Martin, R. L.; Fox, D. J.; Binkley, J. S.; Defrees, D. J.; Baker, J.; Stewart, J. P.; Head-Gordon, M.; Gonzalez, C.; Pople, J. A.*Gaussian 94*, *Revision B.3*; Gaussian, Inc.: Pittsburgh, PA, 1995.

(8) Møller, C.; Plesset, M. S. *Phys. Rev.* **1934**, *46*, 618.

(9) Binkey, J. S.; Pople, J. A. *Int. J. Quantum Chem.* **1975**, *9*, 229.

(10) Hehre, W.; Radom, L.; Schleyer, P. v. R.; Pople, J. A. *Ab initio Molecular Orbital Theory*; Wiley: New York, 1986.

(11) Pople, J. A.; Scott, A. P.; Wong, M. W.; Radom, L. *Israel J. Chem.* **1993**, *33*, 345.

(12) Pople, J. A.; Binkley, J. S.; Seeger, R. *Int. J. Quantum Chem. Symp.* **1976**, *10*, 1.

(13) Pople, J. A.; Binkley, J. S.; Krishnan, R. *Int. J. Quantum Chem. Symp.* **1977**, *11*, 149.

(14) Mulliken, R. S. *J. Chem. Phys.* **1955**, *23*, 1833.

(15) Wiberg, E.; Amberger, E. *Hydrides of the Elements of Main Groups I-IV*; Elsevier: Amsterdam, 1971; pp 785.

(16) Gimarc, B. M. *J. Am. Chem. Soc.* **1973**, *95*, 1417.

(17) DeFrees, D. J.; Raghavachari, K.; Schelegel, H. B.; Pople, J. A.; Schleyer, P. v. R. *J. Phys. Chem.* **1987**, *92*, 1857.

(18) Page, M.; Adams, G. F.; Binkley, J. S.; Melius, C. F. *J. Phys. Chem.* **1987**, *91*, 2675.

(19) Duke, B. J.; Liang, C.; Schaefer, H. F. *J. Am. Chem. Soc.* **1991**, *113*, 2884.

(20) Bock, C. W.; Trachtman, M.; Murphy, C.; Muschert, B.; Mains, G.J. *J. Phys. Chem.* **1991**, *95*, 2339.

(21) Schen, M.; Schaefer, H. F. *J. Chem. Phys.* **1992**, *96*, 2868.

(22) Barone, V.; Orlandini, L.; Adamo, C. *J. Phys. Chem.* **1994**, *98*, 13185.

(23) Lammertsma, K.; Leszcyznski, J. *J. Phys. Chem.* **1990**, *94*, 2806.

(24) Rendell, A.; Lee, T. J.; Komornicki, A. *Chem. Phys. Lett.* **1991**, *178*, 462.

(25) McKee, M. L. *J. Phys. Chem.* **1991**, *95* , 6519.

(26) Zakzhevskii, V. G.; Charkin, O. P. *Chem. Phys. Lett.* **1982**, *90*, 117.

(27) Lammertsma, K.; Günter, O. F.; Drewes, R. M.; Reed, A. E.; Schleyer, P. v. R. *Inorg. Chem.* **1989**, *28*, 313.

(28) Wiberg, K. B.; Nakaji, D. J. *J. Am. Chem. Soc.* **1993**, *115*, 10058.

(29) Luke, B. T.; Pople, J. A.; Krogh-Jespersen, M.-B.; Apeloig, Y.; Karni, M.; Chandrasekhar, J.; Schleyer, P. v. R. *J. Am. Chem. Soc.* **1986**, *108*, 270.

(30) Hiraoka, Y.; Mashita, M.; Tada, T.; Yoshimura, R. *J. Crystal Growth* **1993**, *128*, 494.

(31) Geanangel, R. A. *J. Inorg. Nucl. Chem.* **1972**, *34*, 1083.

(32) Pearson, R. G. *Symmetry Rules for Chemical Reactions*; Wiley: NewYork, 1976.

Chapter 7:

Quantum Chemical Study on p-Doping Effect of F-Terminated Silicon Surface Reaction with Silane

1. Introduction

The atomic scale control of various silicon (Si) interface structures has been the most fundamentally important subject in the present and future ultralarge-scale integration (ULSI) technology.[1-3] In particular, the thermal chemical vapor deposition (CVD) processes have played an important role for the basic technology toward fabrication of new Si semiconductor devices. However, the elementary reaction mechanism has not been completely clarified so far in various CVD processes of the variety of source gases with the variety of reaction surfaces.

Thus, Ohmi *et al.* have devised ultra clean gas supplying system and applied it to the very basic study of the deposition of SiH_4 and Si_2H_6 gases on the surface of fluorine (F)-terminated Si (F-Si)[4] together with its p-doping effect[5] as well as on the variety of Si surfaces.[6] Then, the following experimental facts have been concluded:[5,6]

(1) For the deposition of SiH_4 on F-Si surface, the catalytic activity of the F-Si surface is maintained even after the deposition of SiH_4. Namely, the F atom is situated on top of the Si surface during the deposition process.

(2) On the other hand, for p-doped F-Si surface, the F atom is immersed under the Si polymer as deposited.

In this paper, we have devised model reaction species and reaction paths and studied the local electronic property pertaining to this interesting reaction mechanism in terms of *ab initio* molecular orbital (MO) theory of quantum chemistry.

2. Methods of Calculation

MO calculations were performed with the GAUSSIAN94 program package.[7] The geometries were optimized by the analytical energy gradient method at Hartree-Fock (HF) level and second-order Møller-Plesset (MP) perturbation theory[8,9] which includes correlation for all electrons, using the standard 6-31G** basis set (denoted as HF/6-31G** and MP2(full)/6-31G**).[10] In HF calculation, the spin-restricted HF (RHF)

method was used for closed-shell singlet states, the spin-unrestricted HF (UHF) method was used for open-shell doublet states. Theoretical harmonic vibrational frequencies were obtained from analytical second derivatives calculated at MP2(full)/6-31G** level. Zero-point vibrational energies(ZPE) were then scaled by a factor of 0.94.[11] To obtain higher correlation energies, single point calculations of single and double substituted configuration interaction (CISD)[12] including unlinked cluster quadruple corrections (QC)[13] were carried out on the MP2(full)/6-31G** geometries (denoted as CISD +QC(full)/6-31G**//MP2(full)/6-31G**).

3. Results and Discussion

Following our preceding works[14-16], we use molecular cationic species for local models of p-doped Si. Model reaction paths and total energies of reactant and product species are listed in Tables 1 and 2. The transition state (TS) of the *n*th reaction path is denoted as **TS*n***. The **TS1** and **TS2** are shown in Figure 1. Reaction energies are summarized in Table 1. The energy diagrams and the stability of the local structure are demonstrated in Figure 2.

3.1. Optimized Structures

Some of the model species are found in our preceding works.[14,16] SiH_4^+ has several geometrical isomers due to Jahn-Teller distortions.[17-20] We use a conventional C_{3v} structure of SiH_4^+ here in this paper. $SiH_3SiH_3^+$ is thought to be a reaction complex between SiH_3 and SiH_3^+, and is optimized to have symmetry of D_{3d}, the same as the neutral SiH_3SiH_3.[21] For the optimized geometry of $SiH_3SiH_3^+$, the Si–Si bond length is 2.658Å at MP2/6-31G** level, which is longer than that of neutral SiH_3SiH_3 by 0.32Å, showing the Si–Si bond in the p-doped Si is weakened. These data are in accord with the theoretical results published by Curtiss *et al.*[21] Moreover, the energy barrier of internal rotation around the Si–Si bond in $SiH_3SiH_3^+$ is only 1kcal/mol at the MP2/6-31G* level.[22] Judging from the data presented above, the local structure is considered

Table 1: Reaction Energies (kcal/mol)

reaction	heat of reaction /activation energy
staggerred-SiH_3SiH_3 + SiH_3F	0.0(0.0)
→*staggerred*-SiH_3SiH_3+ SiH_3F (1)	/65.34(60.46)
staggerred-SiH_3SiH_2F+ SiH_3F	-9.73(-9.17)
→*staggerred*-SiH_3SiH_3+ SiH_2F_2 (2)	/63.58(57.10)
$SiH_3SiH_3^+$ + SiH_3F	-12.56(-13.75)
→*eclipsed*-SiH_3-F-SiH_3^+ + SiH_3 (3)	/ –
$SiF_3SiH_3^+$ + SiH_3F	-28.39(-26.72)
→*eclipsed*-SiH_3-F-SiH_3^+ + SiF_3 (4)	/ –
SiH_4^+ + SiH_3F	-42.05(-43.92)
→*eclipsed*-SiH_3-F-SiH_3^+ + H (5)	/ –
SiH_3F^+ + SiH_4	-44.99(-46.72)
→*eclipsed*-SiH_3-F-SiH_3^+ + H (6)	/ –

At CISD(full)+QC/6-31G**//MP2(full)/6-31G** level including ZPE(scaled).
At MP2(full)/6-31G** level including ZPE(scaled) in parentheses.

Table 2: Total Energies(au)

species	HF/6-31G**	MP2(full) /6-31G**	CISD+QC(full) /6-31G**
H	-0.49823		
F	-99.36496	-99.48904	-99.49970
SiH_3	-290.61058	-290.70870	-290.73346
SiH_3^+	-290.33399	-290.42414	-290.44707
SiF_3	-587.38123	-587.98395	-587.98848
SiF_3^+	-587.05619	-587.66450	-587.66555
SiH_4	-291.23084	-291.34986	-291.37821
SiH_4^+	-290.83793	-290.93132	-290.95518
$FSiH_3$	-390.15284	-390.43837	-390.46031
$FSiH_3^+$	-389.74980	-390.01509	-390.03232
SiH_2F_2	-489.08483	-489.53890	-489.55427
SiF_4	-686.94984	-687.74066	-687.74322
H_3SiSiH_3	-581.31357	-581.53462	-581.58311
$H_3SiSiH_3^+$	-580.99307	-581.19069	-581.23823
$H_2FSiSiH_3$	-680.23306	-680.62065	-680.66167
F_3SiSiH_3	-878.10035	-878.82603	-878.85121
$F_3SiSiH_3^+$	-877.73500	-878.44422	-878.46697
$H_3Si\text{-}F\text{-}SiH_3$			
staggered	-680.68058	-681.09283	-681.13520
eclipsed	-680.68057	-681.09284	-681.13521
$H_3Si\text{-}F\text{-}SiH_3^+$			
staggered	-680.55884	-680.94190	-680.98472
eclipsed	-680.55886	-680.94195	-680.98477
$H_3Si\text{-}F\text{-}SiH_3^+..H$			
staggered	-681.05774	-681.44117	-681.48408
eclipsed	-681.05777	-681.44123	-681.48413
$H_3Si\text{-}F\text{-}SiH_3^+..SiH_3$			
staggered	-971.17441	-971.66448	-971.72910
eclipsed	-971.07444	-971.66454	-971.72916
$H_3Si\text{-}F\text{-}SiH_3^+..SiF_3$			
staggered	-1267.93520	-1268.92820	
eclipsed	-1267.93518	-1268.92813	
TS1	-971.34491	-971.87852	-971.94117
TS2	-1070.26551	-1070.96987	-1071.02251

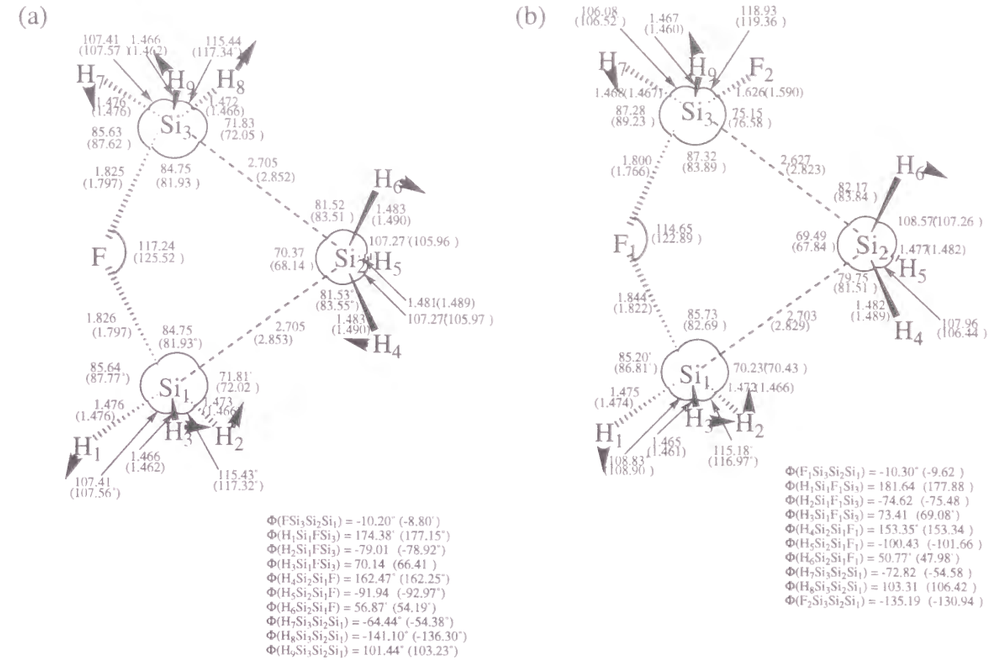

Figure 1. Optimized geometries at MP2(full)/6-31G** level: (a) **TS1** and (b) **TS2**. Bond lengths and bond angles are given in angstroms and degrees, respectively. HF/6-31G** level values are in parentheses.

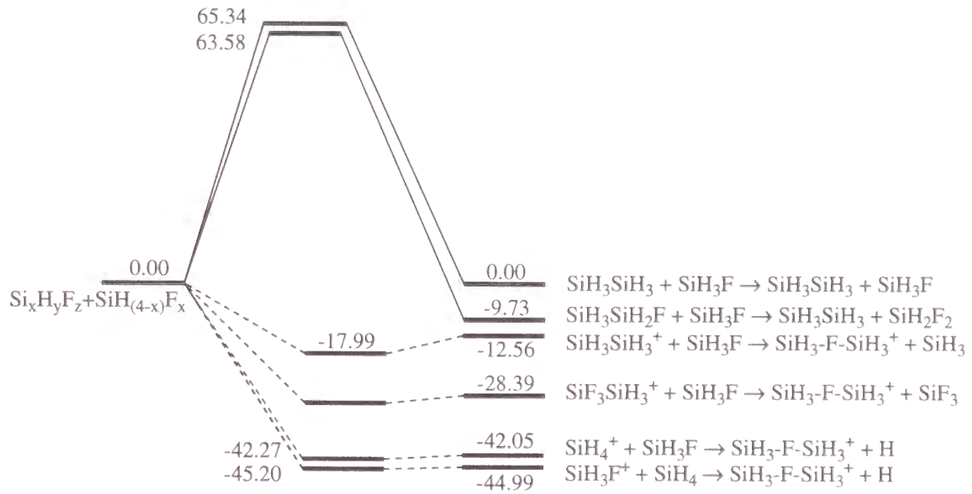

Figure 2. Relative energy diagrams at CISD(full)+QC/6-31G**//MP2(full)/6-31G** level including ZPE(scaled).

rather flexible in the p-doped Si. The tendency is valid also for the p-doped F-Si. Indeed, for the optimized geometry of $SiF_3SiH_3^+$, the Si–Si bond length is 2.312Å, which is longer than that of the neutral SiF_3SiH_3 by 0.29Å.

3.2. *Reaction of Two Neutral Silicon Compounds*

We consider the following neutral molecule reactions (1) and (2):

$$staggered\text{-}SiH_3SiH_3 + SiH_3F \rightarrow staggered\text{-}SiH_3SiH_3 + SiH_3F \quad (1)$$

$$staggered\text{-}SiH_3SiH_2F + SiH_3F \rightarrow staggered\text{-}SiH_3SiH_3 + SiH_2F_2 \quad (2)$$

The optimized geometries of **TS1** and **TS2** have symmetry of C_1, as shown in Figure 1. There were no marked differences between the HF optimized geometries and the MP2 optimized geometries, except slight difference in bond length between Si and F.

In reaction (1), the activation energy is 65.34kcal/mol at CISD+QC level including ZPE. The heat of the reaction is zero. In reaction (2), the activation energy is 63.58kcal/mol and the heat of reaction is -9.73kcal/mol at CISD+QC level.

We observe no tendency for F atoms to be immersed into the bulk of Si. This is confirmed also for the models of larger systems.[16] Namely, for the F-Si surface, the most probable position where an F atom can be situated is on top of the surface, trapped by the dangling bond of Si.

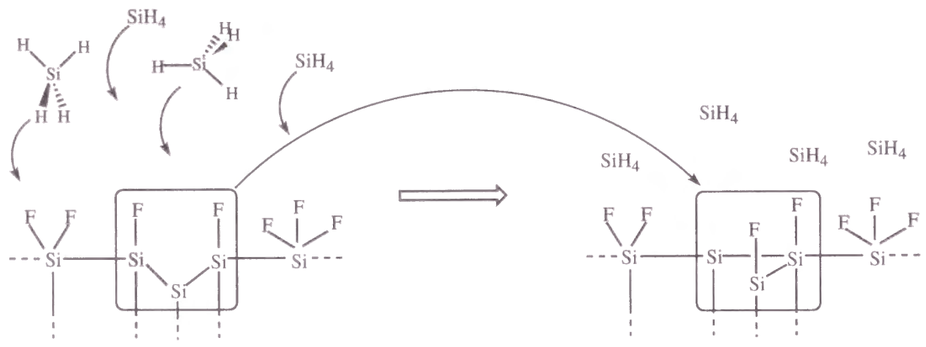

This "floating" reaction mechanism of F will be proved from a different viewpoint in the following discussions.

3.3. *Reaction of Cation and Neutral Silicon Compounds*

We consider the following reaction (3):

$$SiH_3SiH_3^+ + SiH_3F \rightarrow eclipsed\text{-}SiH_3\text{-}F\text{-}SiH_3^+ + SiH_3 \quad (3)$$

In reaction (3), the product SiH_3-F-SiH_3^+ is optimized in either staggered or eclipsed form both at linear configuration of Si–F–Si. Examining the normal vibrational modes of SiH_3-F-SiH_3^+, the staggered form has three imaginary frequencies ($2 \times 58i$, $20i$cm^{-1}) and eclipsed form has two ($2 \times 57i$cm^{-1}). These results agree with the theoretical work of Palafox.[23] There is no significant energy difference between these two alternative forms, which shows that the SiH_3 group is nearly free for rotation. Indeed, for the staggered form, one of the imaginary frequency mode whose symmetry species is A_{1u} corresponds to SiH_3 group internal rotation. For the residual imaginary frequency modes, the E_u mode in staggered form and E' mode in eclipsed form correspond to degenerate Si–F–Si rocking mode.[24] Aside from these imaginary frequency vibrational modes, what is most important here is that the $(Si–F–Si)^+$ configuration is stable against the Si–F–Si configuration decomposition mode whose symmetry species is A_2''. Namely, the F-bridged structure $(Si–F–Si)^+$ is considerably stabilized in the bulk of Si. This observation has also been found in our preceding study on the p-doping effect on chemical etching of Si.[14,15]

We have further optimized $SiH_3..H_3Si$-F-SiH_3^+ complex in C_{3v} symmetry, which keeps linearity of Si_1–F–Si_2–Si_3 configuration. For the optimized complex, the staggered form has three imaginary frequencies and the eclipsed form has two imaginary frequencies, which have the same trends in the case of H_3Si-F-SiH_3^+. The Si_2–Si_3 bond length is 2.755Å at HF/6-31G** level and 3.14Å at MP2/6-31G** level. From the viewpoint of the S_N2 type reaction, the relative energy is -17.99kcal/mol for $SiH_3..SiH_3$-F-SiH_3^+ complex and -12.56kcal/mol for SiH_3 + SiH_3-F-SiH_3^+ at CISD+QC level. As is apparent, this reaction has no activation energy and is exothermic.

Then, we have examined the stability of the F-bridged structure $(Si–F–Si)^+$ for various model reactions as follows.

The reaction (4):

$$SiF_3SiH_3^+ + SiH_3F \rightarrow \textit{eclipsed}\text{-}SiH_3\text{-}F\text{-}SiH_3^+ + SiF_3 \quad (4)$$

As compared with the reaction(3), the relative energy is more exothermic by 15.83kcal/mol because the SiH_3 group is here substituted by the SiF_3 group.

The reactions (5) and (6):

$$SiH_4^+ + SiH_3F \rightarrow \textit{eclipsed}\text{-}SiH_3\text{-}F\text{-}SiH_3^+ + H \quad (5)$$

$$SiH_3F^+ + SiH_4 \rightarrow \textit{eclipsed}\text{-}SiH_3\text{-}F\text{-}SiH_3^+ + H \quad (6)$$

The relative energy is -42.05kcal/mol for the reaction (5) and -44.99kcal/mol for the reaction (6) at CISD+QC level.

In Figure 2 are collected the reaction energy diagrams. The reaction (6) is just corresponding to the situation when SiH_4 is decomposed on the p-doped F-Si, which shows maximum exothermicity.

To conclude, upon SiH_4 decomposition, the terminating F atoms are immersed into the bulk by making $(Si–F–Si)^+$ bonds because the reactions are exothermic and bonds are stable.

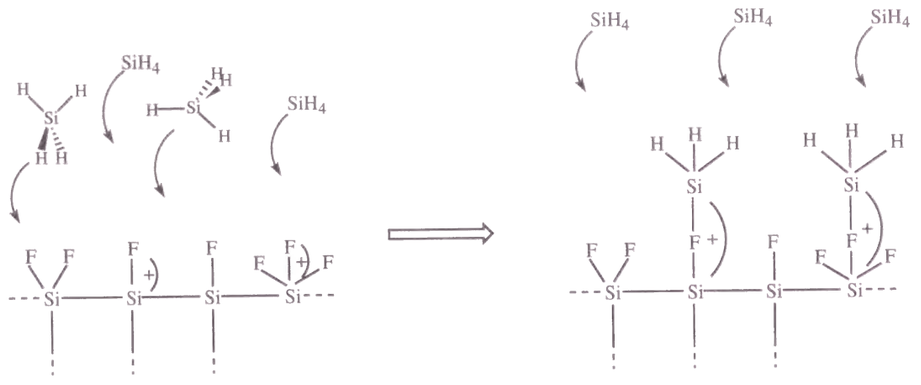

3.5. Stability of $(Si–F–Si)^+$ Bond

In this section, we study the stability of $SiH_3\text{-}F\text{-}SiH_3^+$ in terms of the Bader-Pearson's theory of the second-order Jahn-Teller effect.[25-27]

We assume that the electronic ground state is nondegenerate. When a molecule is distorted from local maximum or minimum along the ith normal coordinate Q_i, then using second-order perturbation theory, the electronic energy E for the ground state becomes

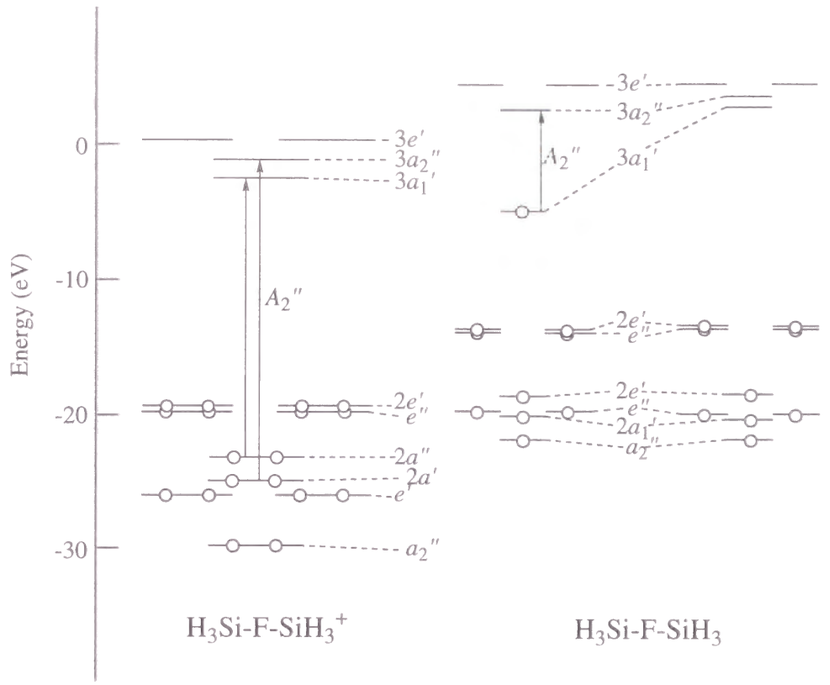

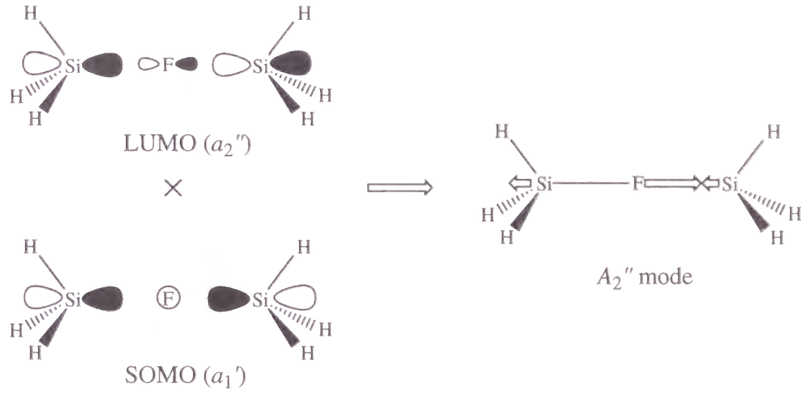

Figure 3. MO energy level diagram of eclipsed $H_3Si\text{-}F\text{-}SiH_3^+$ and eclipsed $H_3Si\text{-}F\text{-}SiH_3$ at HF/6-31G** level and A_2'' vibrational mode.

$$E = E_0 + \frac{1}{2} f_i Q_i^2$$

with the force constant

$$f_i = \left\langle \psi_0 \left| \frac{\partial^2 H}{\partial Q_i^2} \right| \psi_0 \right\rangle + 2 \sum_{k \neq 0} \frac{\left| \left\langle \psi_0 \left| \frac{\partial H}{\partial Q_i} \right| \psi_k \right\rangle \right|^2}{E_0 - E_k}$$

where Ψ_0 is the ground state wave function and E_k is the kth excited state energy of the Hamiltonian H.

For the force constant f_i, the second term gives negative contribution, which is brought about by mixing an excited state wave function Ψ_k into the ground state wave function Ψ_0. Because of the denominator $E_0 - E_k$, lowest excited state contributes most for f_i. The matrix element $\left\langle \psi_0 \left| \frac{\partial H}{\partial Q_i} \right| \psi_k \right\rangle$ will be nonzero only if the symmetry rule is fulfilled:

$$\Gamma_{\psi_0} \times \Gamma_{\psi_k} \subset \Gamma_{Q_i}$$

In Figure 3 are shown the MO energy level diagrams of eclipsed H_3Si-F-SiH_3 and H_3Si-F-SiH_3^+ at HF/6-31G** level. The lowest energy excitation in neutral H_3Si-F-SiH_3 is from singly occupied MO (SOMO) $3a_1'$ to lowest unoccupied MO (LUMO) $3a_2''$. It gives the transition density of the A_2'' symmetry, which corresponds to decomposition into SiH_4 and $FSiH_3$. The results of frequency analysis at MP2(full)/6-31G** level actually give an imaginary frequency for the A_2'' mode ($150i\text{cm}^{-1}$). On the other hand, for H_3Si-F-SiH_3^+, the A_2'' transition corresponds to a much larger excitation energy, which fails to bring about the imaginary frequency. Indeed, the corresponding A_2'' mode has positive frequency (629cm^{-1}) from our numerical frequency analysis.

Thus the stability of the F-bridged structure $(Si–F–Si)^+$ is proved for the p-doped Si in contrast with the F-floating reaction mechanism for the undoped Si.

4. Conclusion

In this study, we have studied the deposition of SiH_4 on the surface of Si with p-doping effect using *ab initio* molecular orbital calculations. We have calculated the local model of reaction sites and proved that $(Si–F–Si)^+$ bond formation is exothermic with no barrier of activation energy. The stability of the $(Si–F–Si)^+$ bond structure in contrast with the unstable neutral Si–F–Si structure is proved in terms of the second-order Jahn-Teller effect.

We have thus clarified the tendency of F that is immersed into the bulk for chemical bonding in between a pair of Si for the p-doped case. This high stability of the F-bridged structure $(Si–F–Si)^+$ in constant with the neutral F-floating reaction mechanism agrees qualitatively well with the experimental observation.

References

(1) Yu, H.-N.; Osburn, C. M.; Critchlow, D. L. *IEEE J. Solid State Circuits* **1979**, *SC-14*, 240.

(2) Ohmi, T. *Technical Digest, 1989 International Electron Devices Meeting*; Washington, D.C., 1989; pp 49-52.

(3) Ohmi, T.; Shibata, T. *Automated Integrated Circuits Manufacturing,* PV91-5; The Electrochemical Society: Pennington, NJ, 1991; pp 3-64.

(4) Kikuyama, H.; Miki, N.; Saka, K.; Takano, J.; Kawanabe, I.; Miyashita, M.; Ohmi, T. *IEEE Trans. Semicond. Manuf.* **1991**, *4(1)*, 26-35.

(5) Ohmi, T., private communication.

(6) Ohmi, T.; Nakamura, M.; Ohki, A.; Kawada, K.; Hirao, K; Watanabe, T. *ULSI Ultra Clean Technology Workshop No. 15, Proceedings,* 1991; pp 125-156.

(7) Frisch, M. J.; Trucks, G. W.; Schlegel, H.B.; Gill, P. M. W.; Johnson, B. G.; Robb, M. A.; Cheeseman, J. R.; Keith, T.; Petersson, G. A.; Montgomery, J. A.;

Raghavachari, K.; Al-Laham, M. A.; Zakrzewski, V. G.; Ortiz, J. V.; Foresman, J. B.; Peng, C. Y.; Ayala, P. A.; Chen, W.; Wong, M. W.; Andres, J. L.; Replogle, E. S.; Gomperts, R.; Martin, R. L.; Fox, D. J.; Binkley, J. S.; Defrees, D. J.; Baker, J.; Stewart, J. P.; Head-Gordon, M.; Gonzalez, C. ; Pople, J. A. *Gaussian 94, Revision B.3*; Gaussian, Inc.: Pittsburgh, PA, 1995.

(8) Møller, C.; Plesset, M. S. *Phys. Rev.* **1934**, *46*, 618.

(9) Binkey, J. S.; Pople, J. A. *Int. J. Quantum Chem.* **1975**, *9*, 229.

(10) Hehre, W.; Radom, L.; Schleyer, P. v. R.; Pople, J. A. *Ab initio Molecular Orbital Theory*; Wiley: New York, 1986

(11) Pople, J. A.; Scott, A. P.; Wong, M. W.; Radom, L. *Israel J. Chem.* **1993**, *33*, 345.

(12) Pople, J. A.; Binkley, J. S.; Seeger, R. *Int. J. Quantum Chem. Symp.* **1976**, *10*, 1.

(13) Pople, J. A.; Binkley, J. S.; Krishnan, R. *Int. J. Quantum Chem. Symp.* **1977**, *11*, 149.

(14) Tachibana, A.; Kawauchi, S.; Yamabe, T. *J. Phys. Chem.* **1991**, *95*, 2471.

(15) Tachibana, A.; Kawauchi, S.; Yamabe, T.; Fukui, K. *Molecules in Natural Science and Medicine*; Maksić, Z. B., Maksić, M. E., Eds.; Ellis Horwood: New York, 1991; pp 375-393.

(16) Tachibana, A.; Kurosaki, Y.; Kawauchi, S.; Yamabe, T. *Trends Inorg. Chem.* **1993**, *3*, 553.

(17) Pople, J. A.; Curtiss, L. A. *J. Phys. Chem.* **1987**, *91*, 155.

(18) Curtiss, L. A.; Pople, J. A. *Chem. Phys. Lett.* **1988**, *144*, 38.

(19) Kudo, T.; Nagase, S. *Chem. Phys.* **1988**, *122*, 233.

(20) Frey, R.; Davidson, E. R. *J. Chem. Phys.* **1988**, *89*, 4227.

(21) Curtiss, L. A.; Raghavachari, K.; Deutsch, P. W.; Pople, J. A. *J. Chem. Phys.* **1991**, *95*, 2433.

(22) Clark, T. *J. Am. Chem. Soc.* **1988**, *110*, 1672.

(23) Palafox, M. A. *Int. J. Quantum Chem.* **1994**, *50*, 69.

(24) Ignacio, E. W.; Schlegel, H. B.; Bicerano, J. *Chem. Phys. Lett.* **1986**, *127*, 367.

(25) Bader, R. F. W. *Mol. Phys.* **1960**, *3*, 137.

(26) Bader, R. F. W. *Can. J. Chem.* **1962**, *40*, 1164.

(27) Pearson, R. G. *Symmetry Rules for Chemical Reactions*; Wiley: New York, 1976.

Chapter 8:

Quantum Chemical Study on the Reaction between GeF_4 and Si_2H_6

1. Introduction

Recently low-pressure chemical vapor deposition (LPCVD) for low-temperature growth of group IV (Si, Ge) semiconductor films attracts much attention because of the feasibility of depositing a uniform large-area film. Fabrication of high-quality poly-Si or poly-SiGe becomes indispensable for the application of LPCVD to thin film transistors (TFTs) and solar cells.

Hanna *et al.* have proposed a novel technique for low-temperature film growth in thermal CVD, called 'reactive thermal CVD'.[1–5] In this technique, germanium tetrafluoride GeF_4 as a Ge source and disilane Si_2H_6 as an activator for germanium tetrafluoride were used. They applied this technique to fabrication of the hetero-epitaxial and polycrystalline Ge thin films at temperature lower than 400°C[1,2] and high crystallinity poly-$Si_{0.95}Ge_{0.05}$ thin films at 450°C.[5] This technique appears to be useful to produce high-quality large-area thin films, but little is known about this reaction mechanism. Their experiments showed that the film deposition proceeded in the case of the combination of GeF_4 and Si_2H_6 at the temperature 300-450°C, although it did not proceed in the case of the combination of GeF_4 and SiH_4 at the same temperature.[1] They also suggested that these reactions proceed in two parts, namely, in the gas near the surface and on the surface of the hot substrate. Therefore, both the gas phase reaction and the surface reaction must be investigated for a proper understanding of the deposition mechanism. Unfortunately the deposition mechanism seems subtle and is poorly understood yet; the quality of various depositing film depends sensitively on the experimental conditions, namely, the gas flow ratio, temperature, and substrates.

In this study we concentrate on the gas-phase reaction mechanism and make an effort to clarify why Si_2H_6 is more effective as an activator than SiH_4. We investigate the reactions of GeF_4 with two species of silane (Si_2H_6 and SiH_4) and compare the reactivities of Si_2H_6 and SiH_4. Although GeH_4, which is popularly used for the Ge film growth, is unstable, GeF_4 is stable thermally up to 1000°C in the moisture-free atmosphere. Therefore, the reaction between GeF_4 and silane should produce the Ge

active species of GeF_2 and GeF_3. Thus we examine reaction channels which produce GeF_2 and GeF_3 from GeF_4 activated by Si_2H_6 or SiH_4 in the following.

We assume that the reaction between Si_2H_6 and GeF_4 begins with formation of Si–Ge bond:

$$SiH_3SiH_3 + GeF_4 \rightarrow SiH_3GeF_3 + SiH_3F. \quad (1)$$

In the case of SiH_4, the corresponding reaction is

$$SiH_4 + GeF_4 \rightarrow SiH_3GeF_3 + HF\ . \quad (2)$$

From the result of our calculation, it has been found that the reaction (2) has a higher activation energy than the reaction (1) and the reaction is endothermic. On the other hand, the reaction (1) proceeds with exothermic reaction energy.

Next, we investigate the succeeding reactions to decompose the Si–Ge bond:

$$SiH_3GeF_3 \rightarrow SiH_3F + GeF_2 \quad (3)$$

$$SiH_3GeF_3 \rightarrow SiH_2 + GeF_3H \quad (4)$$

$$SiH_3GeF_3 \rightarrow SiH_3 + GeF_3. \quad (5)$$

We show that GeF_2 is easy to be produced through the reaction channel (1) → (3). On the other hand, the reaction channel (2) → (3) needs high activation energy.

2. Methods of Calculation

The quantum chemical calculations were carried out with the Gaussian98 program package.[6] Geometry optimization and vibrational analysis were performed by the density functional theory (DFT) using Becke's three-parameter hybrid method[7] with the Lee, Yang, and Parr correlation functional (B3LYP).[8] The electron correlation energy for each geometry was estimated with the coupled cluster calculation including single and double excitations with non-iterative inclusion of triple excitations (CCSD(t)).[9] Pople's 6-31G(d) basis sets for Si, F, and H atoms[10] and the 6-41(d) basis set for Ge atom proposed by Binning and Curtiss[11] were used. Zero-point energies obtained by the B3LYP level calculations were included in the activation energies and reaction energies. These methods are denoted by CCSD(t)//B3LYP(+ZPE).

3. Results and Discussion

The transition state (TS) and the complex of the *n*th reaction path are denoted by **TSn** and **CXn**, respectively. The optimized geometries of the reactant and product molecules are shown in Table 1. The structures of all the transition states and complexes are represented in Figure 1. The activation energies and the heat of reactions are summarized in Table 2. Energy diagram of the reaction between GeF_4 and Si_2H_6 and that of the reaction between GeF_4 and SiH_4 are shown in Figures 2(a) and (b), respectively.

3.1. Reaction 1

One of the reactants, GeF_4, has been studied theoretically from the interests in the edge inversion process[12], vibrational frequencies[13], and so on[14]. The Ge–F bond length is found to be 1.710Å in our study and it agrees well with the previous studies: the length reported by Dixon *et al.*[12] is 1.672Å, which was obtained by a Hartree-Fock calculation using the basis sets of (14s11p6d)/[10s8p3d] for Ge and (9s5p1d)/[3s2p1d] for F while the length reported by Shulz *et al.*[13] is 1.727Å, which was obtained with the MP2(fc) level calculation using the ECP for Ge and the 6-31+G* basis set for F.

The transition state **TS1** of this reaction is shown in Figure 1. The activation energy is 36.77kcal/mol and the reaction is exothermic by 17.67kcal/mol at the CCSD(t)//B3LYP (+ZPE) level. The comparison with the reaction (2) is made later. In the product SiH_3GeF_3, the Si–Ge bond length is 2.379Å. Some theoretical investigations have already been done for SiH_3GeH_3.[15–18] The Si–Ge bond length in SiH_3GeH_3 was reported to be 2.415Å by Grev *et al.*[15] and 2.374Å by Windus *et al.*[16] With a more precise calculation, Leszczyński *et al.* reported 2.372Å at the CISD/TZP(f,d) level.[17] Our calculation shows that the Si–Ge bond length in SiH_3GeH_3 is 2.376Å, which is not so different from the length in SiH_3GeF_3. Thus, we conclude that the Si–Ge bond length is not affected substantially by the substitution of H by F.

Table 1: Optimized Geometries[a]

species	symmetry	geomerical parameters
HF	$C_{\infty v}$	r(HF)=0.934
F_2	$D_{\infty h}$	r(FF)=1.404
$^1SiH_2$	C_{2v}	r(SiH)=1.530, θ(HSiH)=91.18
SiH_3	C_{3v}	r(SiH)=1.489, θ(HSiH)=108.06
SiH_4	T_d	r(SiH)=1.486
SiH_3F	C_{3v}	r(SiF)=1.613, r(SiH)=1.485, θ(HSiF)=110.60
SiH_3SiH_3	D_{3h}	r(SiSi)=2.350, r(SiH)=1.489, θ(SiSiH)=110.60
$^1GeF_2$	C_{2v}	r(GeF)=1.757, θ(FGeF)=97.24
GeF_3	C_{3v}	r(GeF)=1.739, θ(FGeF)=112.82
GeF_3H	C_{3v}	r(GeH)=1.524, r(GeF)=1.723, θ(HGeF)=112.70
GeF_4	T_d	r(GeF)=1.710
SiH_3GeF_3	C_{3v}	r(GeSi)=2.379, r(GeF)=1.735, r(SiH)=1.481
		θ(SiGeF)=114.55, θ(GeSiH)=107.58

[a]Bond length (r) in Å, bond angle (θ) in degree.

Table 2: Reaction Energies at the CCSD(t)//B3LYP(+ZPE) Level in kcal/mol (B3LYP(+ZPE) Level in Parentheses)

reaction		activation energy	heat of reaction
$SiH_3SiH_3 + GeF_4 \rightarrow SiH_3GeF_3 + SiH_3F$	(1)	36.77 (33.84)	-17.67 (-21.53)
$SiH_4 + GeF_4 \rightarrow SiH_3GeF_3 + HF$	(2)	54.68 (48.64)	5.71 (3.29)[a]
			17.35 (16.57)
$SiH_3GeF_3 \rightarrow SiH_3F + GeF_2$	(3)	31.86 (29.99)	1.79 (-3.42)[a]
			14.59 (7.41)
$SiH_3GeF_3 \rightarrow SiH_2 + GeF_3H$	(4)	—	61.04 (61.75)
$SiH_3GeF_3 \rightarrow SiH_3 + GeF_3$	(5)	—	78.44 (75.66)

[a] Complex.

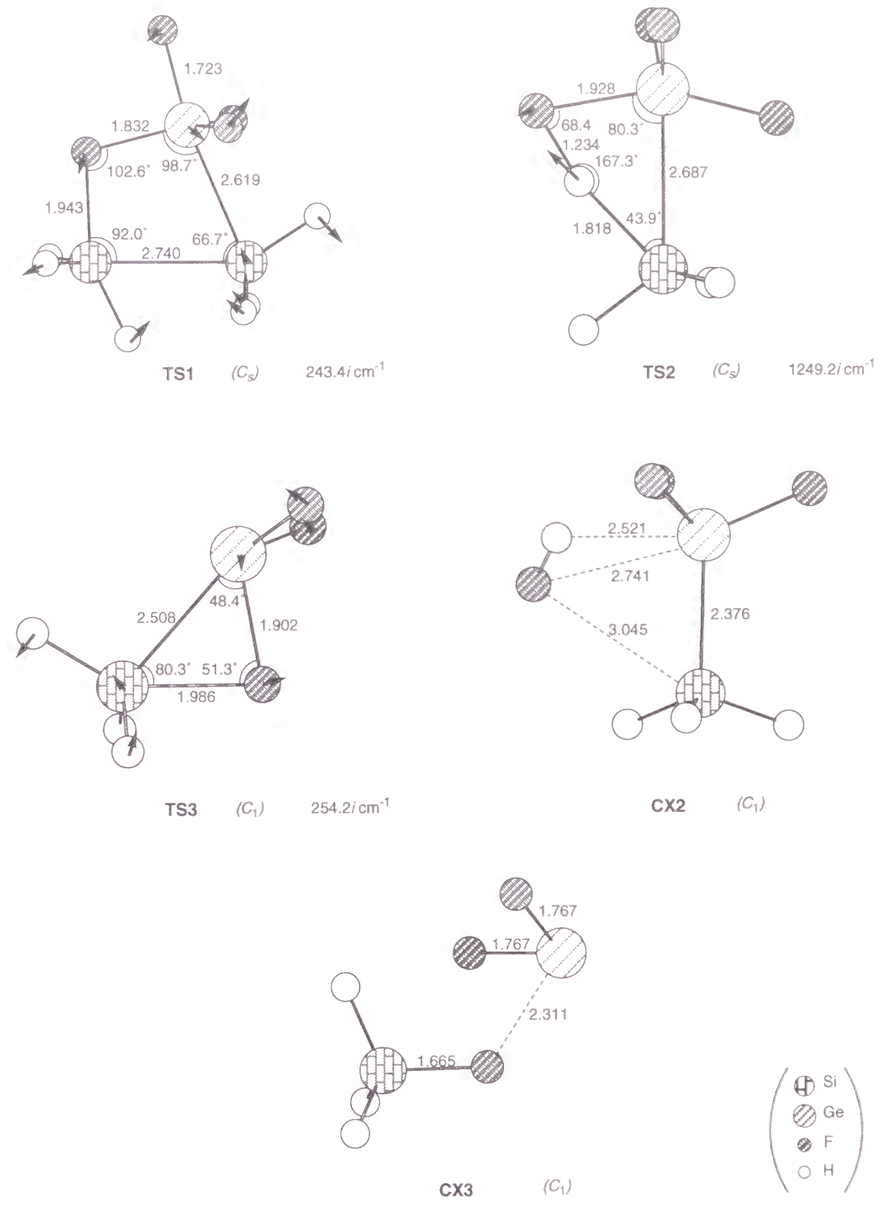

Figure 1. Optimized structures of transition states and complexes. Bond lengths are in Å, bond angles are in degrees.

(a)

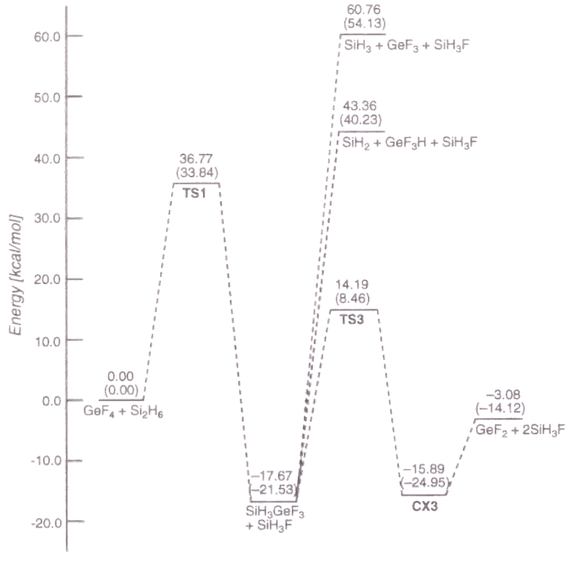

(b)

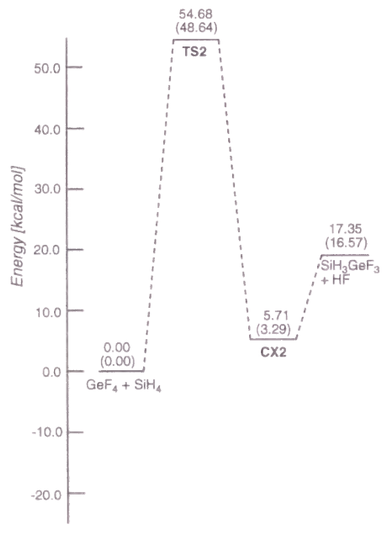

Figure 2. Energy diagrams (in kcal/mol) of the reactions of (a) $Si_2H_6 + GeF_4$ and (b) $SiH_4 + GeF_4$ at the CCSD(t)//B3LYP(+ZPE) level (B3LYP(+ZPE) level in parentheses).

3.2. Reaction 2

The transition state of the reaction (2), **TS2**, is shown in Figure 1. Compared with **TS1**, they have different structures although the Ge atom has the penta–coordinate structure in both of the two structures. The Si atom in Si_2H_6 approaches the Ge atom along the C_3 axis from the bottom of GeF_4 and the fluorine atom is located on equatrial site in **TS1** as shown in Figure 1. On the contrary, the Si atom in SiH_4 approaches the Ge atom along the C_2 axis of GeF_4 and the fluorine atom which is released from GeF_4 is located at the axial site in **TS2**. In Figure 3(a), the orbital energy diagram of the reactants calculated by the Hartree-Fock method is shown. It is clear that the energy levels of the occupied orbitals of GeF_4 are lower than those of silane. If Koopman's theorem is taken into account, this is the reason why the Ge–F bond is strong as explained later. One of the unoccupied triply degenerate orbitals $3t_{2z}$ can be expressed equivalently as linear combinations of three $3t_2$ orbitals as shown in Figure 3(b). These orbitals play an important role for electron delocalization from SiH_4 or Si_2H_6 to GeF_4. The $2a_1$ LUMO and the $3t_{2z}$ next-LUMO are responsible for the reaction with Si_2H_6, while the LUMO and the $3t_2$ orbital play dominant roles in the reaction with SiH_4. Certainly the orbital energies of the HOMOs and the next-HOMOs of Si_2H_6 are higher than those of the triply degenerate HOMOs of SiH_4, so electron delocalization from Si_2H_6 occurs more easily than that in the case of SiH_4. In Figures 4 (a) and (b), the HOMOs of **TS1** and **TS2** are shown. They share a similar feature in which the Ge atom orbital overlaps in–phase with the Si atom orbital. These orbitals are formed from the interaction between the occupied orbitals of silanes and the unoccupied orbitals of GeF_4.

The activation energy of the reaction (2) is 54.68kcal/mol and the reaction energy is 18.43kcal/mol endothermic at the CCSD(t)//B3LYP(+ZPE) level. The energetic difference between the reactions (1) and (2) is brought about by the orbital interactions as discussed above. Moreover, this tendency can be understood from a general fact that the Si–Si bond is weaker than the Si–H bond and that the Si–F bond is stronger than the H–F bond.

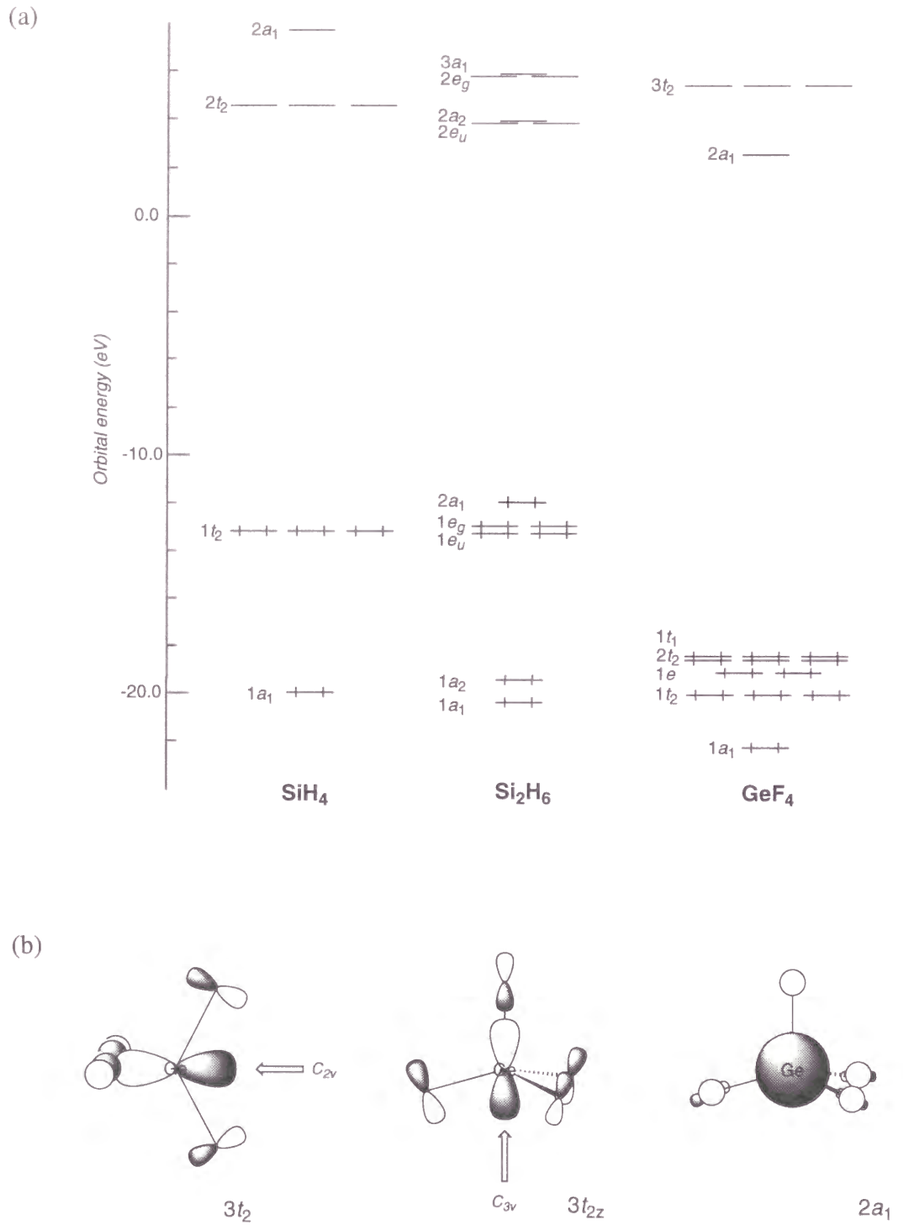

Figure 3. (a) Orbital energy diagrams of GeF_4, SiH_4, and Si_2H_6 at the Hartree-Fock level. Geometries optimized by B3LYP calculations were used. (b) $3t_2$, $3t_{2z}$ orbitals of the next-LUMO and the LUMO ($2a_1$).

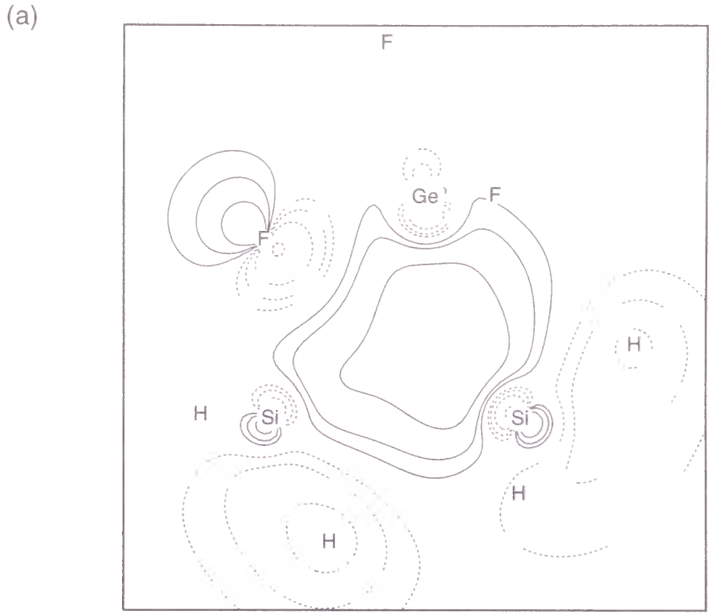

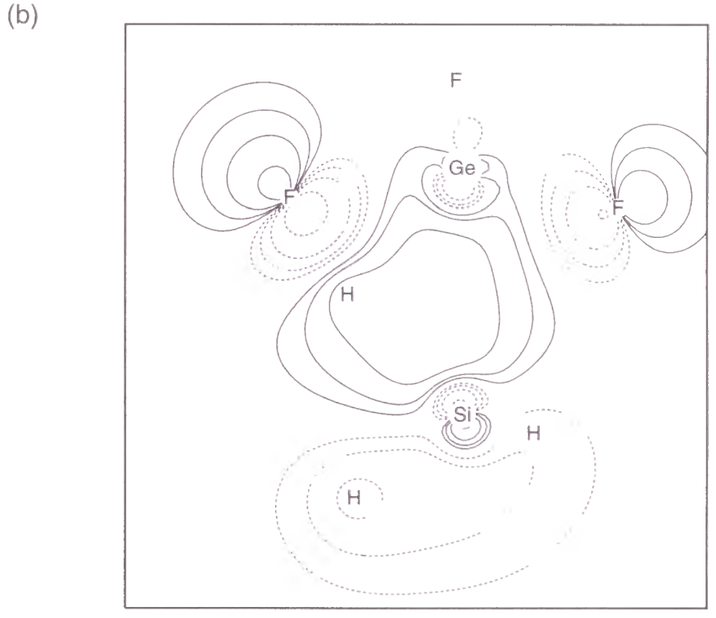

Figure 4. The contours of HOMO of (a) **TS1** and (b) **TS2** on the C_S mirror plane obtained by the Hartree-Fock calculations. Fot the geometries, see Figure 1.

The complex formed by SiH_3GeF_3 and hydrogen fluoride, **CX2**, is shown in Figure 1. The hydrogen- and fluorine-atomic charges are evaluated by the natural population analysis to be +0.565, -0.562, respectively, while these are ±0.535 in hydrogen fluoride molecule. The stronger polarization of the H–F bond in **CX2** was also confirmed by the calculation with the Hartree-Fock wave function (+0.604, –0.605 for H and F atom in the **CX2**, respectively, and ±0.560 in hydrogen fluoride molecule). Thus we see the hydrogen fluoride in **CX2** is highly polarized.

3.3. Reaction 3–5

The reaction (3) is the decomposition process of SiH_3GeF_3 into GeF_2 and SiH_3F. The B3LYP calculation unveils that **TS3** does not have any symmetry as shown in Figure 1. The activation energy is 31.86kcal/mol. This reaction proceeds to form the complex **CX3** and to decompose into $SiH_3F + GeF_2$ as shown in Figure 2(a). A recent density functional study showed that the Ge–F bond length of GeF_2 was about 1.747–1.794Å.[19] Our result (1.757Å) is consistent with that result. The other CASSCF and MRCI calculations showed that the ground state is singlet.[20]

The reaction (4) represents the decomposition of SiH_3GeF_3 into SiH_2 and GeF_3H. The reaction is endothermic by 61.04kcal/mol. The transition state of this reaction was found at the Hartree-Fock level calculation, but was not found at the B3LYP level. We may conclude that no energy barrier seems to exist on the way of the reaction.

The homolytic decomposition of the Si–Ge bond into $SiH_3 + GeF_3$ has the reaction energy of 78.44 kcal/mol. In SiH_3GeH_3, the bond dissociation energy is estimated to be 67.0 kcal/mol by the CCSD level calculation. Although the B3LYP level calculations show that the Si–Ge bond lengths are almost the same in SiH_3GeH_3 and SiH_3GeF_3 as noted above, the Ge–Si bond is strengthened by the substitution of H by F.

3.4. Comparison of Si_2H_6 and SiH_4 on the Reactions with GeF_4

Before we discuss the reaction between GeF_4 and silanes, we examine the stability of GeF_4, SiH_4, and Si_2H_6 in an isolated state. To find plausible mechanisms for the decomposition of GeF_4, we examine two reactions:

$$GeF_4 \rightarrow GeF_3 + F \quad (6)$$

$$GeF_4 \rightarrow GeF_2 + F_2 . \quad (7)$$

For comparison we also investigate the stability of GeH_4. The reaction energies of these decomposition processes are summarized in Table 3. The reaction energies of (6) and (7) are 130.16kcal/mol and 172.71kcal/mol, respectively, in our calculations at the CCSD(t) //B3LYP(+ZPE) level. In GeH_4, the Ge–H bond dissociation energy was estimated to be 84.0kcal/mol by CCSD//SCF calculations.[15] The other theoretical study by CCSD(t) level calculation showed that the activation energy of the decomposition reaction of GeH_4 into $GeH_2 + H_2$ is 59.0kcal/mol and that its reaction energy is 42.5kcal/mol.[21] The Dirac–Hartree–Fock calculation showed the similar reaction energy, 42.4kcal/mol.[22] Compared to GeH_4, the decomposition of GeF_4 needs a higher activation energy. Therefore, it is found that GeF_4 is more stable than GeH_4. Actually, it is known that GeF_4 is stable thermally up to 1000°C. On the other hand, the decomposition reactions of SiH_4 and Si_2H_6 have been studied precisely and the reported results are summarized in Table 4.[23–27] It is important to note that the decomposition energies exceed 50kcal/mol in both molecules.

Then we discuss the reaction channels of (a) GeF_4 and Si_2H_6 and of (b) GeF_4 and SiH_4 by connecting the reactions (1) with (3), and (2) with (3) as illustrated in Figures 2 (a) and (b). In the case of (b) GeF_4 and SiH_4, the initial reaction process (2) needs a high activation energy. The decomposition of silane into SiH_2 and H_2 has almost the same activation energy as shown in Table 4. Moreover, $SiH_3GeF_3 + HF$ is less stable than SiH_4 and GeF_4 because the reaction (2) has the endothermic reaction energy. Therefore, the entire reaction to produce $GeF_2 + SiHF_3 + HF$ needs a large amount of energy.

On the other hand, in the case of (a), the initial reaction (1) needs a lower activation energy than those of disilane decomposition reactions as shown in Table 4 and the

Table 3: Decomposition Energies of GeF_4 and GeH_4 (kcal/mol)

reaction		activation energy	heat of reaction	references
$GeF_4 \rightarrow GeF_3 + F$	(6)	–	130.16 (126.22)	*present study*[a]
$GeF_4 \rightarrow GeF_2 + F_2$	(7)	–	172.71 (159.36)	*present study*[a]
$GeH_4 \rightarrow GeH_3 + H$		–	84.0	Ref. 15[b]
$GeH_4 \rightarrow GeH_2 + H_2$		59.0	42.5	Ref. 21[c]
			42.4	Ref. 22[d]

[a]CCSD(t)//B3LYP(+ZPE) level. (B3LYP(+ZPE) level in parentheses.)
[b]CCSD calculation with DZP basis sets.
[c]CCSD(t) calculation with Hay-Wadt ECP.
[d]Dirac-Hartree-Fock calculation.

Table 4: Decomposition Energies of Si_2H_6 and SiH_4 (kcal/mol)

reaction	activation energy	heat of reaction	references
$SiH_3SiH_3 \rightarrow SiH_4 + SiH_2$	–	50.0	Ref. 24[a]
	56	56	Ref. 25[b]
$SiH_3SiH_3 \rightarrow SiH_3SiH + H_2$	55.5	53.4	Ref. 24[a]
	55	55	Ref. 25[b]
$SiH_3SiH_3 \rightarrow SiH_2SiH_2 + H_2$	86.1	47.0	Ref. 24[a]
	86	47	Ref. 25[b]
$SiH_3SiH_3 \rightarrow SiH_3 + SiH_3$	–	70.0	Ref. 24[a]
	76	76	Ref. 25[b]
$SiH_4 \rightarrow SiH_3 + H$	92	92	Ref. 26[c]
$SiH_4 \rightarrow SiH_2 + H_2$	60	57	Ref. 26[c]
	56.9	55.2	Ref. 27[d]

[a] MP4(SDTQ)/MC-311G**//MP2/6-31G** for heat of reaction and MP4(SDQ)/MP-311G**//MP2/6-31G** for activation energy.
[b] MP4(SDTQ)/6-31G*//HF/6-31G*.
[c] Gaussian–2 theory.
[d] MP4/MC-311++G(3df, 3pd)//MP2/MC-311G(2d,2p)(+ZPE).

reaction (1) is exothermic. Therefore this reaction is considered to be an important path. Furthermore, the most likely products of decomposition of SiH_3GeF_3 are SiH_3F and GeF_2. The products of this reaction have almost the same stability as $Si_2H_6 + GeF_4$. Hanna *et al.* observed epitaxial growth of Ge film on Si(100) substrate from GeF_4 and Si_2H_6 at 370°C.[1,2] In the case of Si epitaxial growth by $SiCl_4$ deposition, $SiCl_2$ is known to be the key molecule.[28] If Ge compounds have an analogous character, GeF_2 is also considered to be an important species for surface epitaxitial growth. A more important fact is that the GeF_2 was detected in gas phase although its origin is not yet clear.[2,29]

Moreover, our results suggest that other reaction processes in Figure 2(a) to produce SiH_2 and GeF_3H will be forwarded at high temperature. It is expected that these products influence the surface reaction. In fact, experiments also show the polycrystalline growth in higher temperature region (>400°C).[1,2]

4. Conclusion

To understand the reaction mechanism of low-temperature thermal chemical vapor deposition between GeF_4 and Si_2H_6, we investigated the gas–phase reaction between GeF_4 and Si_2H_6 and the reaction between GeF_4 and SiH_4 by *ab initio* quantum chemical techniques and compared those reactions. For the Si–Ge bond formation between GeF_4 and Si_2H_6, the activation energy is 36.77kcal/mol and the reaction is exothermic by 17.67kcal/mol at the CCSD(t)//B3LYP(+ZPE) level, while the activation energy is 54.68kcal/mol and the reaction is endothermic by 17.35kcal/mol in the case of SiH_4 and GeF_4. A study of orbital interactions also supported that the formation of the Si–Ge bond was easier in the case of Si_2H_6 than in that of SiH_4. One of the products of these reactions, SiH_3GeF_3, is easily decomposed into SiH_3F and GeF_2, which is considered to be one of key molecules for Ge film growth. This result gives us a clue to understand the experimental observation reported by Hanna *et al.*

References

(1) Yamamoto, M.; Hanna, J.; Miyauchi, M. *Appl. Phys. Lett.* **1993**, *63*, 2508.

(2) Yamamoto, M.; Takada, Y.; Hanna, J. *Appl. Phys. Lett.* **1994**, *64*, 3467.

(3) Hanna, J.; Ohuchi, T.; Yamamoto, M. *Mater. Res. Soc. Proc.* **1995**, *358*, 877.

(4) Hanna, J.; Ohuchi, T.; Yamamoto, M. *J. Non-Cryst. Solids* **1996**, *198-200*, 879.

(5) Shiota, K.; Inoue, D.; Minami, K.; Yamamoto, M.; Hanna, J. *Jpn. J. Appl. Phys.* **1997**, *36*, L989.

(6) Frisch, M. J.; Trucks, G. W.; Schlegel, H. B.; Scuseria, G. E.; Robb, M. A.; Cheeseman, J. R.; Zakrzewski, V. G.; Montgomery, J. A.; Stratmann, R. E.; Burant, J. C.; Dapprich, S.; Millam, J. M. ; Daniels, A. D.; Kudin, K. N.; Strain, M. C.; Farkas, O.; Tomasi, J.; Barone, V.; Cossi, M.; Cammi, R.; Mennucci, B.; Pomelli, C.; Adamo, C.; Clifford, S.; Ochterski, J.; Petersson, G. A.; Ayala, P. Y.; Cui, Q.; Morokuma, K.; Malick, D. K.; Rabuck, A. D.; Raghavachari, K.; Foresman, J. B.; Cioslowski, J.; Ortiz, J. V.; Stefanov, B. B.; Liu, G.; Liashenko, A.; Piskorz, P.; Komaromi, I.; Gomperts, R.; Martin, R. L.; Fox, D. L.; Keith, T.; Al-Laham, M. A.; Peng, C. Y.; Nanayakkara, A.; Gonzalez, C.; Challacombe, M.; Gill, P. M. W.; Johnson, B. G.; Chen, W.; Wong, M. W.; Andres, J. L.; Head-Gordon, M.; Replogle E. S.; Pople, J. A. *Gaussian 98 (Revision A.6)*; Gaussian, Inc.: Pittsburgh, PA, 1998.

(7) Becke, A. D. *J. Chem. Phys.* **1993**, *98*, 5648.

(8) Lee, C.; Yang, W.; Parr, R. G. *Phys. Rev. B* **1988**, *37*, 785.

(9) Pople, J. A.; Head-Gordon, M.; Raghavachari, K.; Trucks, G. W. *Chem. Phys. Lett.* **1989**, *164*, 185.

(10) Hehre, W. J.; Radom, L.; Schleyer, P. v. R.; Pople, J. A. *Ab initio Molecular Orbital Theory* ; Wiley: New York, 1986.

(11) Binning, R. C., Jr.; Curtiss, L. A. *J. Comp. Chem.* **1990**, *11*, 1206.

(12) Dixon, D. A.; Arduengo, A. J., III *J. Phys. Chem.* **1987**, *91*, 3195.

(13) Schulz, A.; Klapötke, T. M. *Spectrochim. Acta* **1995**, *51*, 905.

(14) Jolly, W. L.; Eyermann, C. J. *J. Phys. Chem.* **1982**, *86*, 4834.

(15) Grev, R. S.; Schaefer, H. F., III; Baines, K. M. *J. Am. Chem. Soc.* **1990**, *112*, 9458.

(16) Windus, T. L.; Gordon, M. S. *J. Am. Chem. Soc.* **1992**, *114*, 9559.

(17) Leszczyński, J.; Huang, J. Q.; Schreiner, P. R.; Vacek, G.; Kapp, J.; Schleyer, P. v. R.; Schaefer, H. F., III *Chem. Phys. Lett.* **1995**, *244*, 252.

(18) Schleyer, P. v. R.; Kanpp, M.; Hampel, F.; Bremer, M.; Mislow, K. *J. Am. Chem. Soc.* **1992**, *114*, 6751.

(19) Escalante, S.; Vargas, R.; Vela, A. *J. Phys. Chem. A* **1999**, *103*, 5590.

(20) Dai, D.; Al-Zahrani, M. M.; Balasubramanian, K. *J. Phys. Chem.* **1994**, *98*, 9233.

(21) Hein, T.; Thiel, W.; Lee, T. J. *J. Phys. Chem.* **1993**, *97*, 4381.

(22) Dyall, K. G. *J. Chem. Phys.* **1992**, *96*, 1210.

(23) In *The Chemistry of Organic Silicon Compounds*: Patai, S., Rappoport, Z. Eds.; Wiley: New York, 1989; Vol. 1, Chapter 2.

(24) Gordon, M. S.; Truong, T. N.; Bonderson, E. K. *J. Am. Chem. Soc.* **1986**, *108*, 1421.

(25) Ignacio, E. W.; Schlegel, H. B. *J. Phys. Chem.* **1992**, *96*, 1758.

(26) Su, M.-D.; Schlegel, H. B. *J. Phys. Chem.* **1993**, *97*, 9981.

(27) Gordon, M. S.; Gano, D. R.; Binkley, J. S.; Frisch, M. J. *J. Am. Chem. Soc.* **1986**, *108*, 2191.

(28) Ohshita, Y.; Ishitani, A.; Takada, T. *Phys. Rev. B* **1990**, *41*, 12720.

(29) Hanna, J., private communication.

General Conclusion

The development of quantum chemistry and the spread of its applications have provided us with clear understanding of complicated chemical phenomena abundantly. On the other hand, attempts to understand a variety of chemical phenomena give new insights into theoretical chemistry. Intimate connection of the two aspects is now indispensable to the development of chemistry.

In the field of quantum chemistry, there remains many subjects to be solved. One of these subjects is the establishment of more precise theory of chemical reactivity. Now, we can calculate easily the accurate wave function and its eigenvalue for a variety of reaction models and its reaction paths. However, it seems that these calculations do not make the most of the results to clarify chemical reactivity of molecules. We must construct a new view of chemical reactivity which is adapted to the present conditions.

The another subject to be solved is the establishment of a new view of chemical reactions under the macroscopic environment, such as surface reactions and the chemical reactions in solution. Toward these problems, especially in solution chemical reactions, some interesting methods, such as a hybrid between the quantum mechanical method and the molecular mechanical method or a combination of *ab initio* electronic structure theory and the statistical mechanics of molecular liquids, have to be explored. In material science which includes solid–state science and surface science, we must also develop a mesoscopic view which comprehends both the macroscopic and the microscopic regions. Fortunately, an application of the first–principle calculations using the Car–Parrinello's method to surface reactions is already attempted. The author assumes that its development gives closer connections between physics and chemistry, between which there is yet a gap.

This thesis summarizes the studies of chemical reactivity of molecules and some surface reactions which appear in manufacturing the silicon semiconductor devices by utilizing the molecular orbital theory and the density functional theory.

In Chapter 1, electron delocalization between NO_2^+ and substituted benzenes has been examined by the molecular orbital theory. It has been shown that the interacting

orbitals were localized around the reaction site By projecting a reference orbital function that has been chosen to specify the bond to be formed onto the MOs of the substituted benzenes, the local potential of the reaction site for electron donation has been estimated. The results were consistent with the experimental scale of the electron–donating and –withdrawing strength of substituent groups. It has been shown that the reactivity was governed by the local electronegativity and the local chemical hardness and also by the localizability of interaction on the reaction site.

In Chapter 2, the population analysis along the intrinsic reaction coordinate has been performed, taking the 1,3–dipole cycloaddition as an example. By calculating the derivatives of the Mulliken atomic charge and the Mayer's bond order with respect to the nuclear motion analytically, the decomposition of the derivatives into two components, the density derivative term and the overlap derivative term, was demonstrated. The density derivative term represents the effect of redistribution of electrons due to the nuclear motion. By using this method, the electronic character of asynchronous bond formation was revealed clearly.

In Chapter 3, the author has taken up the gas phase reaction between singlet oxygen (^1D) and silane. One of the methods to produce SiO_2 layer over the Si surface is the chemical vapor deposition (CVD) using oxygen gas and silane gas. Applying a quantum chemical method, a low energy reaction path has been found in addition to the excited-state reaction path. This agrees well with the experimental observation on the vibrational energy distribution of the product SiO found by laser-induced fluorescence.

In Chapter 4, cluster model reactions of the oxidation sites in hydrogen- and water-terminated Si dimers have been examined using *ab initio* molecular orbital calculations, to obtain a chemical insight into the bond in the Si surface network which the oxidant prefers to attack. First, the author focused on the basic reaction enthalpies of Si_2H_6 with O_2 and found that the Si–Si bond in the cluster was more easily oxidized than the terminal Si–H bond. A similar oxidation tendency was also found in the reaction of $SiH_3SiH_2(OH)$ with H. The transient reaction intermediate that possessed a terminal oxygen radical was fully transferred with low activation energy to the Si–Si bond, but with much higher activation

energy to the adjacent Si–H bond. These results demonstrated a facile Si–Si back-bond oxidation, which should provide a key to understand the microscopic character of the oxidation site on the Si surface.

In Chapter 5, the oxidation mechanism of the hydrogen–terminated Si(111) surface by an oxygen anion has been studied using *ab initio* molecular orbital method. The author has clarified the stability of an oxygen anion in a cage of silicon cluster. The oxygen anion attacks the Si atom to form a penta-coordinated complex, which should lower the diffusion barrier for the oxygen anion transfer in the Si bulk. The oxygen anion inserts then into the Si–Si bond to form a local Si–O–Si structure. The stabilization energy is enhanced if the deformation energy in the local Si–O–Si structure is released. The oxidized Si has a tendency to accept additional oxygens. This has been concluded using a series of cluster model calculations, assuming that the crystallographic strain is completely relaxed.

In Chapter 6, the author has discussed the reaction mechanism between dimethyl aluminum hydride and the Si surface terminated by hydrogen. The author has clarified that the Al–Al bond formation occurs prior to the Al–Si bond formation and that the methyl group has an effect to suppress the reactivity of Al and Si. Moreover, the H_2 carrier gas has been found to enhance the reactivity.

In Chapter 7, the author has performed a quantum chemical study of the deposition of SiH_4 on the surface of F–terminated Si to see the p–doping effect. It has been clarified that the fluorine atom immersed into the bulk had a tendency to insert into a pair of Si atoms and to form chemical bonds in the p–doped case. The high stability of the $(Si–F–Si)^+$ bonding structure makes a clear contrast to the unstable Si–F–Si antibonding structure and this conclusion agrees qualitatively well with the experimental observation.

In Chapter 8, the gas-phase reaction mechanism of the low-temperature thermal chemical vapor deposition between GeF_4 and Si_2H_6 has been studied by quantum chemical techniques. For the Si–Ge bond formation reaction between GeF_4 and Si_2H_6, the activation energy has been found to be 36.77kcal/mol and the reaction is exothermic by 17.67kcal/mol, while the activation energy is 54.68kcal/mol and the reaction is

endothermic by 18.43kcal/mol in the case of the reaction between GeF_4 and SiH_4 at the CCSD(t)//B3LYP(+ZPE) level. One of products in these reactions, SiH_3GeF_3, has been shown to be easily decomposed into SiH_3F and GeF_2.

Acknowledgment

This thesis is the summary of the author's studies from 1994 to 1999 at the Department of Molecular Engineering, Kyoto University.

The author cordially thanks Professor Hiroshi Fujimoto and Professor Akitomo Tachibana for their kind guidance, valuable suggestions, stimulating discussions, and continuing encouragement. He is also grateful to Mr. Tasuku Yano, Mr. Koichi Nakamura, Mr. Masahiro Fuju, Mr. Takahiro Sato, and Mr. Osamu Makino for their valuable discussions and suggestions. Acknowledgment is also made to Dr. Hiroyuki Fueno, Dr. Kiyoyuki Omoto, Mr. Tomohiro Suzuki, and Mr. Hajime Hirao for their suggestions and encouragement. The author also thanks the Kyoto University Venture Business Laboratory (KU-VBL) for supporting a part of his studies.

Finally, the author would like to express his gratitude to his parents Shigeru Sakata and Shigeko Sakata for their continuing encouragement.

List of Publications

Chapter 1. Hiroshi Fujimoto, Ken Sakata, and Kenichi Fukui
"Transient Bonds and Chemical Reactivity of Molecules,"
Int. J. Quantum Chem. **1996**, *60*, 401-408.

Chapter 2. Ken Sakata
"Population Analysis along the Intrinsic Reaction Coordinate: Application to 1,3-Dipole Cycloaddition,"
to be published.

Chapter 3. Akitomo Tachibana and Ken Sakata
"Quantum Chemical Study on Low Energy Reaction Path for $SiH_4 + O(^1D) \rightarrow SiO + 2H_2$,"
Appl. Surf. Sci. **1997**, *117/118*, 151-157.

Chapter 4. Ken Sakata, Akitomo Tachibana, Shigeaki Zaima, and Yukio Yasuda
"Quantum Chemical Study of the Oxidation Sites in Hydrogen- and Water- Terminated Si Dimers: Attempt to Understand the Si–Si Back-Bond Oxidation on the Si Surface,"
Jpn. J. Appl. Phys. **1998**, *37*, 4962-4973.

Chapter 5. Akitomo Tachibana, Ken Sakata, and Takahiro Sato
"Quantum Chemical Study on the Oxidation of Hydrogen-Terminated Silicon Surface by Oxygen Anions,"
Jpn. J. Appl. Phys. **1998**, *37*, 4493-4504.

Chapter 6. Akitomo Tachibana, Ken Sakata, and Kiyoyuki Omoto
"Quantum Chemical Study on Aluminum Selective CVD Reaction Mechanism,"
Appl. Surf. Sci. **1997**, *117/118*, 465-471.

Chapter 7. Akitomo Tachibana and Ken Sakata
"Quantum Chemical Study on p-Doping Effect of F-Terminated Silicon Surface Reaction with Silane,"
Appl. Surf. Sci. **1997**, *117/118*, 54-60.

Chapter 8. Ken Sakata and Akitomo Tachibana
"Quantum Chemical Study on the Reaction between GeF_4 and Si_2H_6,"
submitted.